Alma Mater Studiorum – Università di Bologna

DOTTORATO DI RICERCA IN

CHIMICA

Ciclo XXVI

Settore Concorsuale di afferenza: 03/B1

Settore Scientifico disciplinare: CHIM/03

CHARACTERIZATION OF OPTICAL TRANSDUCTION-BASED MOLECULAR SYSTEMS AND NANOPARTICLES FOR THE DEVELOPMENT OF CHEMICAL SENSORS

Presentata da: **Massimo Sgarzi**

Coordinatore Dottorato **Relatore**

Prof. Aldo Roda **Prof. Luca Prodi**

Esame finale anno 2014

Saranno cose già sentite
o scritte sopra un metro un po' stantio
ma intanto questo è mio.
E poi voi queste cose non le dite,
poi certo per chi non è abituato
pensare è sconsigliato,
poi è bene essere un poco diffidente
per chi è un po' differente.

Canzone di notte n.2

Francesco Guccini

Contents

Chapter 1: Introduction

1.1 Sensing

Each living being, once thrown in this world, has the necessity to communicate. Every organism possesses its own instruments to interact with the environment, and use them to survive. Sensory systems are the basis of this interaction: perception is the main function which allow the organisms to acquire information about the state and the variations of its habitat, thanks to the action of senses such as sight, hearing, smell, taste and touch, and about the state of its own body by means of proprioception[1]. When dealing with animals, a sensory system consist of sensory receptors, neural pathways and parts of the brain involved in sensory perception: this is an example of *biological sensor*, i.e. a micro- or macroscopic device that interact reversibly with a biological analyte with signal transduction. The extraordinary efficiency of these natural devices has inspired the creation of artificial ones. Generally speaking a *sensor* is a device that interact with matter or energy and yields a measurable signal in response. With the increasing importance that nanotechnologies have in everyday life, it is not difficult to realize that also a single molecule, if properly designed, can be a device able to perform useful functions: such a chemical species is called *chemosensor*, that is a molecule of abiotic origin that signals the presence of matter or energy. *Signal transduction* is the mechanism by which an interaction of a sensor with an analyte yields a measurable form of energy[2].
We can make a parallel between *signal transduction* and *communication*: in both cases we have an input signal (the message leaving from the transmitter) which, by means of the transfer of the information carried in the signal, is received and processed providing an output signal (the message is received and interpreted by the receiver, who responds accordingly to the collected information). In order to have a real information exchange it is necessary that the ability to correctly interpret the message exists between the transmitter and the receiver, that is the capability of assigning the correct meaning to a certain piece of information has to occur. This is possible only if a common background is present, a series of factors which allows decoding the transmitted message[3]. Similarly, when dealing with the design of a chemosensor, we need to take into account this communication requirement between its three components: the *receptor unit*, the *spacer* and the *signalling unit*. A *luminescent chemosensor* (*Figure 1.1*) communicates a variation of the physico-chemical properties of the receptor unit with a luminescence output signal. By analysing the system in more detail, the chemosensor acts itself like a *transducer*, a translator between what happens at the nanoscopic level and the operator who performs the experiment: the communication logic which intrinsically permeates the chemosensor is the same with which it communicates with the operator, acting as “magnifying glass” for phenomena otherwise invisible to the human eye. It is light itself that represents the common background allowing the operator to contact the studied system and, since we deal with light every moment of our life, the use of light as an output signal is particularly efficient and easy to interpret.

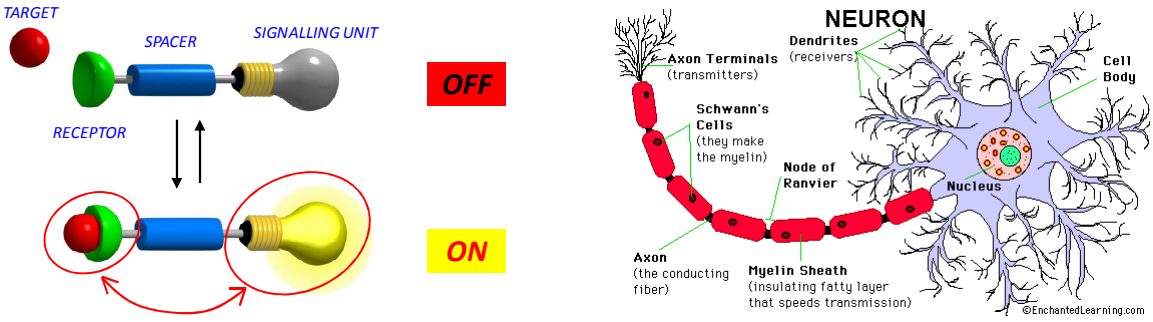

Figure 1.1: comparison between a an OFF-ON luminescent chemosensor (left) and a neuron (right).

As well as biological sensors are important for life, chemical sensors can be designed in order to improve the quality of our lives by creating species not present in Nature. The progresses of science and technology have made life easier (for those who can afford them) but at the same time we see the emergence of problems such as pollution and diseases related to it. It is widely known that the effects of pollutants is not confined in the places where they are produced but they diffuse globally: a typical example is the "ozone hole" caused by chlorofluorocarbons, which were used mainly as refrigerants and were later discovered to be able to deplete the ozone layer in the stratosphere, which protect us from solar ultraviolet radiation. So on one hand we have to proceed with caution when introducing waste materials in the atmosphere, in water or in the soil, on the other hand we need a constant and diffuse monitoring of the situation and an accurate scientific analysis of collected data[4]. Hence it appears clear that we need specific and sensitive chemosensor for each analyte we want to assess and whose concentration we want to monitor. The same logic can be applied not only to environmental issues but also to process control, food and beverage analysis and medical diagnosis. The development of chemical sensors can completely change the paradigm of chemical analysis: time and cost are the limiting factors for the application of classical analysis, which consists in collecting, transporting and pre-treating the sample, and subsequently in using expensive and non user-friendly instrumentation. Chemical sensors bypass these restrictions and can cover a large field of applications, resulting the best choice for real-time and real-space measurements. The design of these chemical sensors needs the contribution of specialists in different disciplines, such as chemistry, physics, biology, engineering: chemists are involved in the development of the "active part" of the device, that is the one in contact with the analyte to assess, thus they are responsible for the selectivity and the sensibility of the whole device. An important contribution to tackle this task is provided by supramolecular chemistry, and in particular by supramolecular photochemistry[5].

1.2 Supramolecular chemistry

Jean-Marie Lehn, who shared the Nobel Prize in 1987 with Donald J. Cram and Charles J. Pedersen, wrote that "beyond the molecule, supramolecular chemistry aims at developing highly complex chemical systems from components interacting by non-covalent intermolecular forces"[6]. This definition encompasses not only host-guest systems but also molecular devices and machines, molecular recognition, self-assembly and self-organization.

The simplest supermolecule we can imagine is a host-guest complex: a "host" molecule possessing convergent binding sites (e.g. Lewis basic donor atoms, hydrogen bond donors, etc.) binds another one, called "guest" which possesses divergent binding sites (e.g. a spherical Lewis acidic metal cation or hydrogen bond acceptor anion). The nature of non-covalent forces which make the host and the guest interact is varied but the common feature of the resulting complex is always a "complementary stereoelectronic arrangement of binding sites in host and guest"[7]. When dealing with the host design, the complementarity with the guest is very important: its size, geometry, charge density and "hardness" have to be taken into account so that the guest fits the space created by the host following the "lock and key" principle, postulated in 1894 by Hermann Emil Fischer[8]. An example of a biological host-guest complex is shown in *Figure 1.2*.In principle the feature that distinguishes a supermolecule from a "large molecule" is the possibility to split the supermolecule into individual molecular subunits (components) capable of a separate existence. The properties of a supermolecule will not generally be a simple superimposition of those of the components, but depend on the inter-components interactions, such as electron or energy transfer or complexation by two or more components. These new properties are the object of study of supramolecular photochemistry.[9]

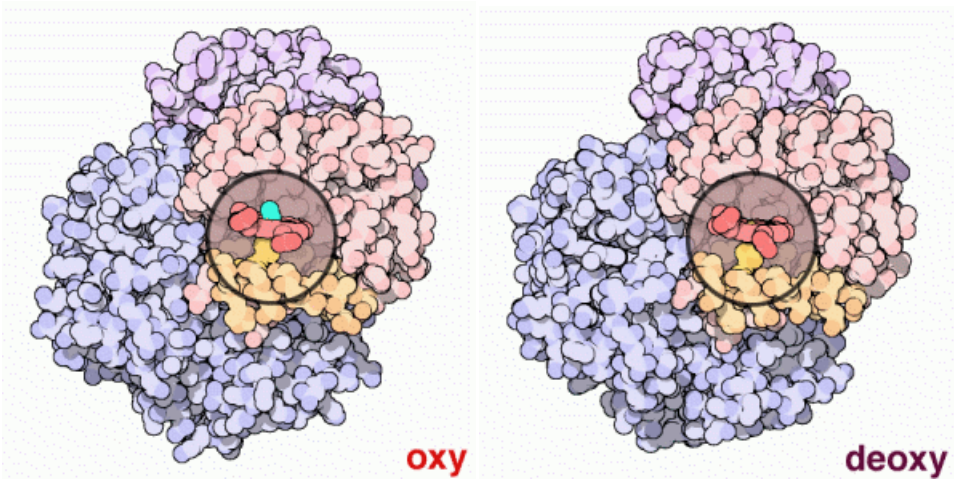

Figure 1.2: oxyhaemoglobin (left) and deoxyhaemoglobin (right) as an example of host-guest complex. The presence of oxygen modifies the conformation of the whole haemoglobin.

The "host-guest" concepts concerns the receptor unit of a chemosensor, whose definition, described in *Paragraph 1.3*, contemplates further functions the supermolecule can have, because the different states at the receptor unit are then communicated to the signalling moiety.

1.3 Chemosensors

A *chemical sensor* is "a device that transforms chemical information, ranging from the concentration of a specific sample component to total composition analysis, into an analytically useful signal."[10]. The use of chemical sensors for analytical purposes provides several advantages with respect to classical analysis, such as low cost, portability, possibility to perform real-time and real-space measurements[2]. The role of the chemist is to design the "sensitive" part of the sensor, the one in contact with the analyte and responsible for the signal transduction, that is the *chemosensor*. As already said in *Paragraph 1.1* a chemosensor is "a molecule of abiotic origin that signals the presence of matter or energy"[2], and it is the most important component because it determines the selectivity and the sensitivity of the whole sensor.
The main components of a chemosensor are:

- the *receptor unit*, responsible for the selective analyte binding;
- the *signalling unit*, whose physico-chemical properties change upon complexation;
- the *spacer*, which controls the geometry of the system and modulates the electronic interaction between the receptor and the fluorophore.

1.3.1 Fluorescent chemosensors

Between the several kinds of chemosensors, fluorescent ones present many advantages. Fluorescence is a very sensitive, low cost and rapid method for a wide range of clinical, biological and environmental applications and it offers a submicrometer spatial and submillisecond temporal resolution. Moreover it is possible to finely tune the photophysical properties of the chemosensor in order to maximize the efficiency of the system. One of the most important goal of fluorescence sensing is non-invasive monitoring of clinically relevant species and physiological parameters. In principle every change in photophysical properties of a fluorescent chemosensor can be related to changes in the analyte concentration, such as

intensity of the emitted light, excited state lifetime and anisotropy. The most direct sensing method is fluorescence intensity variation, but in some case it is not the best solution, because of its dependence of chemosensor concentration. When dealing for example with fluorescence microscopy it is useful to use ratiometric fluorescent chemosensor, which display shifts in wavelength in the emission spectrum upon analyte complexation. The presence of two emission bands gives two fluorescence values whose ratio is independent of the chemosensor concentration. Also anisotropy measurements have a ratiometric nature (see *Paragraph 2.6*). Moreover fluorescence lifetimes can be use for sensing. The advantages in using fluorescent chemosensors resides in their sensitivity (the detection is possible until to the single molecule) and low cost, in the ease of performing measurements, and in the possibility to tune a wide number of parameters in order to optimize the signal.

1.4 Fluorescent chemosensor design

A chemosensor can be built via a modular, supramolecular approach, that is by linking together its three components in a proper way: it is necessary to choose a selective receptor for the analyte to assess, to select a convenient fluorophore, to put an efficient intercomponent process in action in order to associate recognition to signalling[11].
Dealing with the design of the receptor, sensing application require the existence of receptors (hosts) that associate with analyte (guests) selectively and reversibly.
The mechanisms by which these fluorescent chemosensors generally work are mainly three:

- photoinduced electron transfer (PET),
- photoinduced charge transfer (PCT),
- excimer formation or disappearance.

Each class has subclasses, distinguished by the type of complexation agent:

- chelators,
- podands,
- coronands,
- cryptands,
- calixarenes[12].

Intensity measurements are the most common and relates to a variation of the intensity of the emitted light caused by the analyte binding. The complexation of a metal ion we want to assess can produce an increase of fluorescence intensity, and in this case we speak about “chelation enhanced fluorescence” effect (*CHEF effect*): non-redox active, closed shell metal ions such as Zn^{2+}, Cd^{2+}, Al^{3+} generally cause a CHEF effect. When a decrease of the fluorescence intensity is detected we have a “chelation enhanced quenching” effect (*CHEQ effect*): metal ions such as Cu^{2+}, Hg^{2+}, Ni^{2+} produce this effect. A variation of intensity can be caused also by enhancing or inhibiting PET: we can observe PET when an amine group is linked but not conjugate with an aromatic moiety, whose fluorescence is quenched; upon protonation or complexation of the amine an increase in the emitted light occurs resulting in a CHEF effect.
If the chemosensors possess two emission bands that vary their intensities upon the analyte complexation we obtain a ratiometric system: the ratio between the two signal is independent of the chemosensor concentration. Systems that comprise an energy transfer donor and acceptor have ratiometric nature: the donor emission decreases while the acceptor emission band rises.

A third ratiometric system is represented by induced excimer formation or dissociation: the complexation can induce two identical fluorophores to approach and form excimers, and vice versa.
Another method which overcomes some drawbacks of intensity measurements is lifetime detection. The instrumentation used is more sophisticated but the advantage is that lifetime is independent of the chemosensor concentration[2].

1.4.1 PET chemosensors

These chemosensors contain an electron accepting fluorophore and an electron donating receptor. In *Figure 1.3* the MO diagram is shown, in the case of free and bound chemosensor, an anthracene-derivatized aza-18-crown-6 ether, the first and simplest coronand chemosensor, whose quantum yield increases from 0.003 to 0.14 upon binding of K^+ in methanol[13]. In this case the anthracene is the electron acceptor, while the tertiary amine acts as an electron donor. When the receptor is free, the selective excitation of fluorophore is not followed by the emission of light because of the quenching exerted by the lone pair of the tertiary amine. In fact the HOMO of the receptor is higher in energy with respect to the HOMO of the fluorophore, so an electron transfer can occur and an electron occupies the HOMO of the fluorophore, preventing its emission. When a cation is present, the lone pair of the amine is no more available for electron transfer because it is involved in the complexation, pushing the energy of the HOMO to lower energy than the fluorophore's one, so that the emission of the fluorophore occurs. As a result, the complexation leads to an enhancement of the emission intensity.

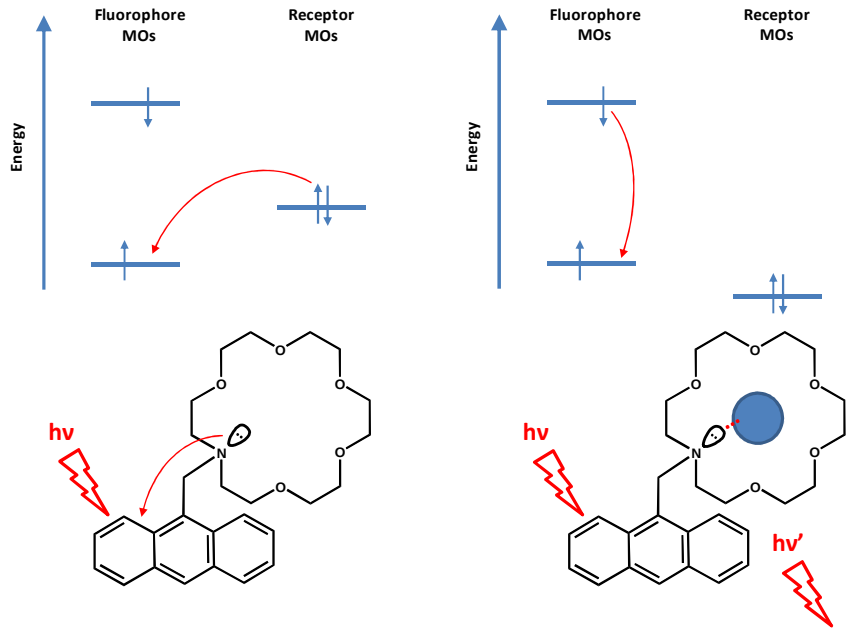

Figure 1.3: operating mechanism of a PET chemosensor, possessing a fluorophore as an electron acceptor and a receptor as an electron donor.

When dealing with transition metals, it is possible to have also the electron transfer from the fluorophore to the bound receptor with a luminescence quenching.[14,15]
Other examples of this kind of compounds exist (see *Figure 1.4*), such as cryptand-based[16], podand-based[17] and calixarene-based ones.[18]

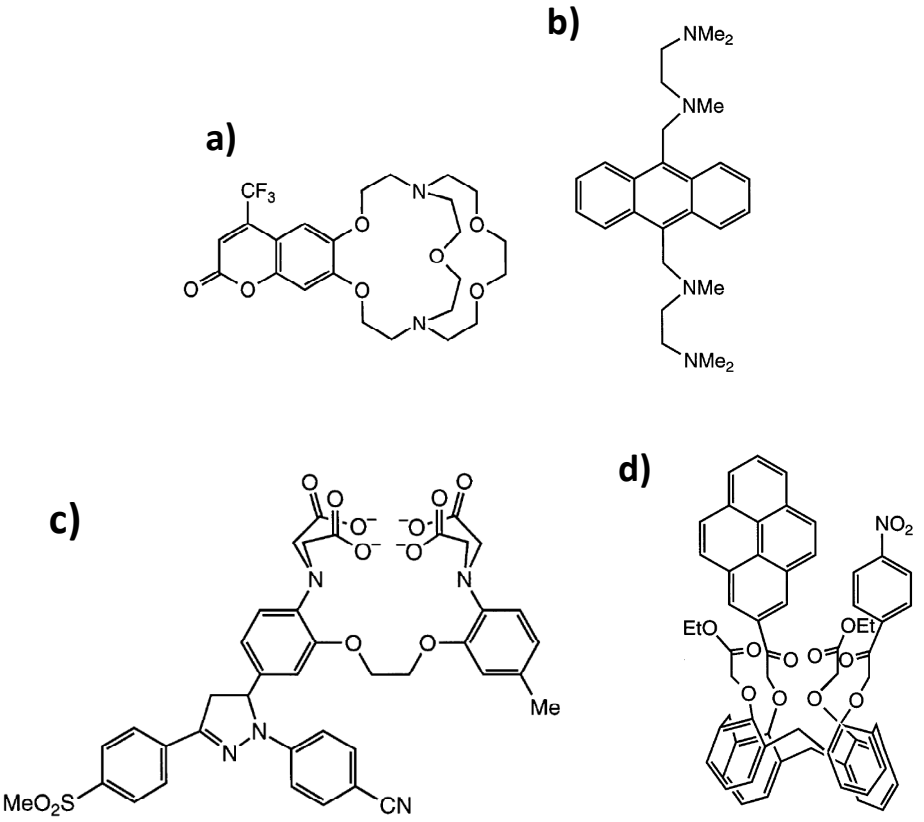

Figure 1.4: different kinds of PET chemosensors, based on cryptand (a), podand (b), chelator (c) and calixarene (d).

In some case these PET chemosensors may lead to the formation of excimers as a consequences of the complexation. Considering for example the compound shown in *Figure 1.5*, a diazacrown ether with two pendant pyrene groups, upon complexation it is possible to observe an increase in the fluorescence as a consequence of the reduction of PET processes involving the tertiary nitrogens. This chemosensor is ratiometric, because in the emission spectra the monomer and the excimer band are visible and vary their intensity as a function of the concentration of added metal ion. This compound showed a higher affinity toward K^+ and Ba^{2+} ions.

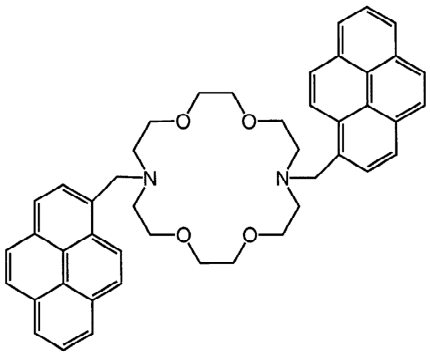

Figure 1.5: PET chemosensor which, upon complexation, forms excimers.

1.4.2 PCT chemosensors

Differently from PET chemosensors, PCT ones present conjugated electron donor and acceptor, between which intramolecular charge transfer occurs as a consequence of excitation by light. The interaction of a metal ion with the electron donor or acceptor causes variation in the photophysical properties of the chemosensor.[19] When an electron donor interacts with a cation it will decrease its electron donating character, thus reducing the conjugation of the system and generally providing an ipso- and ipochromic shift in the absorption spectrum. On the other hand if the cation interacts with the electron acceptor, it enhances the electron withdrawing character of the latter, enhancing the conjugation of the chemosensor and producing a batho- and hyperchromic shift in the absorption spectrum. Generally the behaviour in the emission spectra are similar to that observed in the absorption spectra, and moreover quantum yields and lifetimes changes are common.

The excited state of this kind of chemosensors possesses a larger dipole moment than that of the ground state. So if the cation interacts with the donor group, the excited state is more destabilized than the ground state and this produces a blue shift in the absorption and emission spectra. On the other hand if the cation interacts with the acceptor group, the excited state is more stabilized than the ground state, so that a red shift is observed (see *Figure 1.6*).[20]

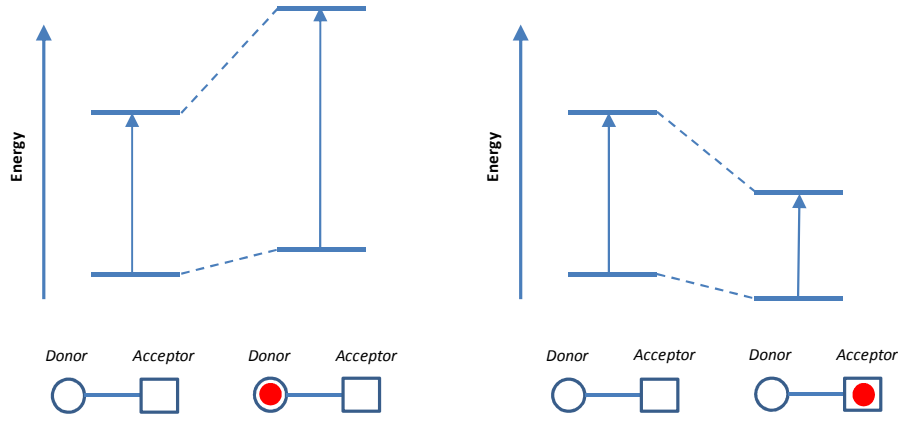

Figure 1.6: spectral variations of PCT chemosensors as a consequence of the interaction of a metal ion with the donor (left) or the acceptor (right) group.

Typical chemosensors whose donor group interacts with cations are azacrown conjugated to electron-withdrawing groups such as diphenyl[21], cyanophenyl[21], benzothiazolyl[22] and BODIPY groups[23] (*Figure 1.7*).

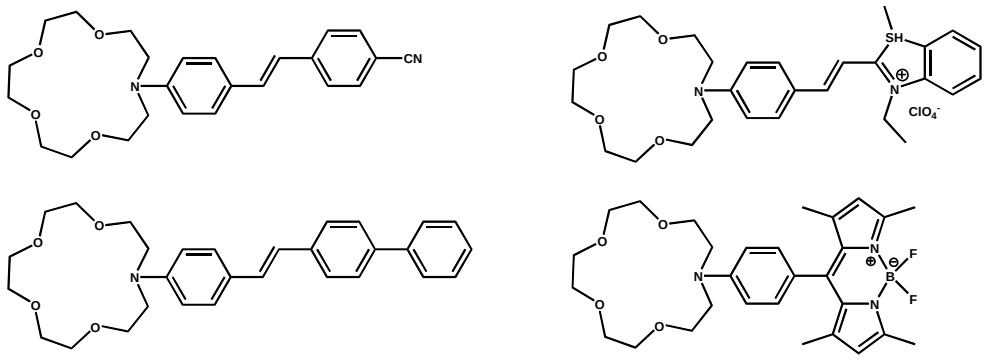

Figure 1.7: crown-based PCT chemosensors whose donor group (the azacrown) interacts with metal ions.

These compounds are not able to distinguish between metals of the same chemical family: the derivatization with external groups which can interact with the metal ion[24] (see *Figure 1.8*) considerably improves the selectivity.

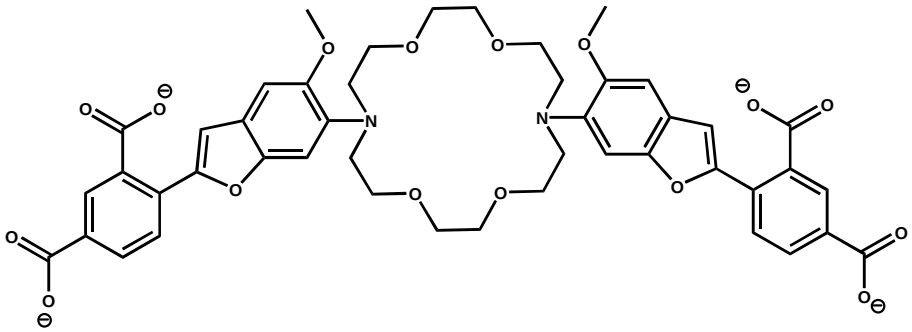

Figure 1.8: crown-based PCT chemosensors possessing two chelating "arms", used to detect intracellular K^+ ions.

1.4.2.1 Chelating PCT chemosensors

The most famous chelators of cytosolic Ca^{2+}, Indo-1 and Fura-2[25] (*Figure 1.9*), belong to this class of compounds: the fluorophore is a donor-acceptor molecule with an amino group as the electron-donating group which participates in the complexation, while the receptor belongs to the BAPTA family.

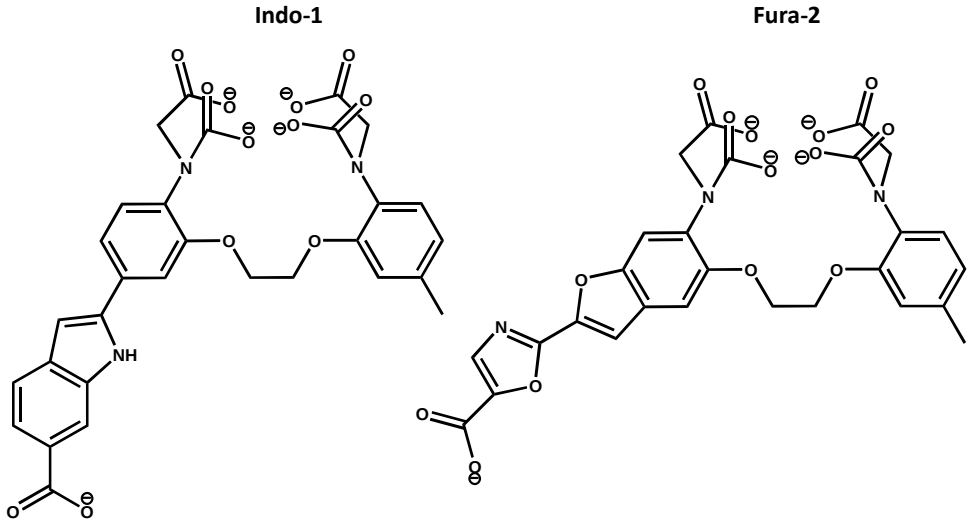

Figure 1.9: Indo-1 and Fura-2, well known cytosolic Ca^{2+} chelators.

Using the same fluorophore, but reducing the size of the binding site, it is possible to create Mg^{2+} selective chemosensors, such as Mag-Indo-1 and Mag-Fura-2 (*Figure 1.10*), with the drawback that they maintain a residual selectivity towards Ca^{2+} ions[26].

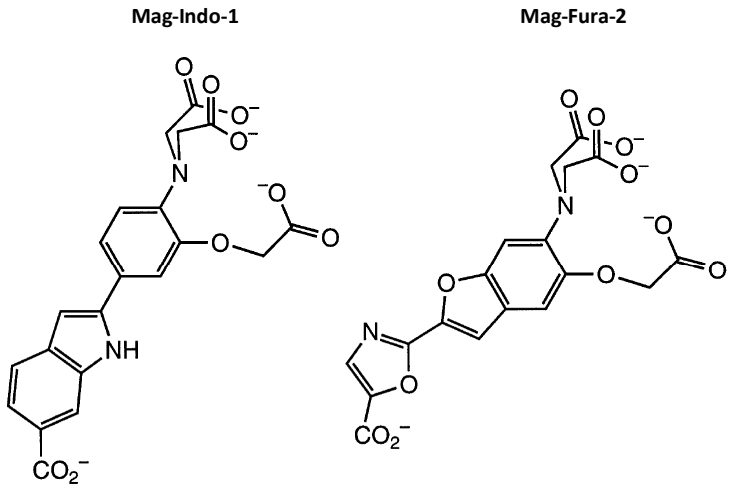

Figure 1.10: Mag-Indo-1 and Mag-Fura-2, Mg^{2+} fluorescent chemosensors for biological applications.

1.4.2.2 Cryptand-based PCT chemosensors

The PCT chemosensors shown so far are suitable for the complexation of alkaline-earth cations but not for alkali cations. The introduction of cryptand as a receptor in the structure of these chemosensors confers a high selectivity towards these ions. For example, if we want to detect free intracellular sodium concentration we can use the compound shown in *Figure 1.11*[27], where the indole derivative acts like the fluorophore.

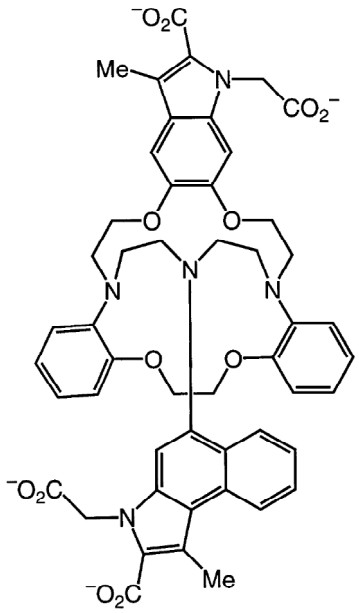

Figure 1.11: a cryptand-based fluorescent chemosensor for the detection of free intracellular Na^+ ions.

1.4.2.3 Calixarene-based PCT chemosensors

The chemosensor shown in *Figure 1.12* is selective to Li^+ ions[28]: the benzothiazole group is linked to the calix[4]arene and Li^+ ions is responsible for a complexation/deprotonation process involving the hydroxy groups of the calixarene. Also the methoxy groups participate to the ion complexation. No changes in the absorption and emission spectra were observed in the presence of Na^+ and K^+ ions.

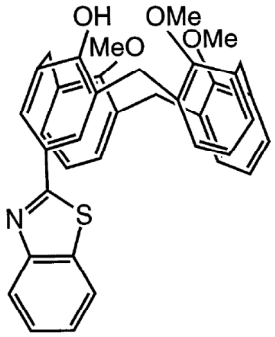

Figure 1.12: calix[4]arene derivatized with a benzothiazole, a PCT chemosensors selective to Li^+.

1.4.2.4 PCT chemosensors whose electron-acceptor group interacts with the cation

This class of chemosensor is not populated as the previous one, but there are some important examples, such as azacrowns derivatized with coumarins (see, for instance, *Figure 1.13*), whose carbonyl group is directly involved in the complexation of Li^+ ions. The factors which have to be taken into account for an efficient sensing with these compounds are the rigidity of the link between the fluorophore and the receptor and the rigidity and the size of the receptor itself.

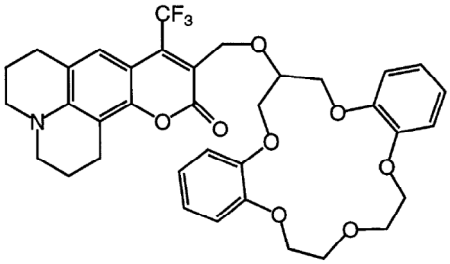

Figure 1.13: a PCT chemosensor selective to Ca^{2+} in ACN.

1.4.3 Excimer-based chemosensors

Aromatic molecules such as pyrene and anthracene can form excimers when a molecule in an excited state comes close to another one in the ground state in a shorter time than excited state lifetime. By analysing the emission spectrum, it is possible to observe two bands, the one of the monomer and the one of the excimer, which generally is red-shifted with respect to the former. If the two fluorophore are linked together by means of a cation receptor, the complexation can make the two species approach at the suitable distance to form excimers. This kind of chemosensors are then ratiometric, and the ratio of the intensities of these two bands correlates with the concentration of formed excimers, and as a consequence, of the bound cation. In some cases, conversely, the complexation can cause the excimer disruption.

1.4.3.1 Coronands

The bisanthraceno-crown ether shown in *Figure 1.14*[29-31] can complex Na^+ in methanol, with a decrease of the anthracene emission band and the rise of the excimer band, caused by the complexation induced approach of the two anthracenes. Every species complexes two Na^+ ions with a cooperative effect.

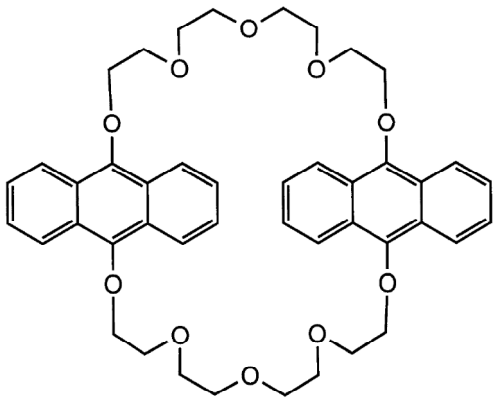

Figure 1.14: coronand-based chemosensor which forms excimers by Na^+ complexation.

1.4.3.2 Podands

An example of this class of compounds is shown in *Figure 1.15*[32]. It spontaneously forms excimers in ACN, whose formation is prevented in the presence of alkaline-earth cations. The stability constants toward Ca^{2+}, $Sr^{2+}$and Ba^{2+} are very high (10^6-10^7 M^{-1}) but it is not possible to discriminate between these ions, due to the conformational flexibility of the linking chain.

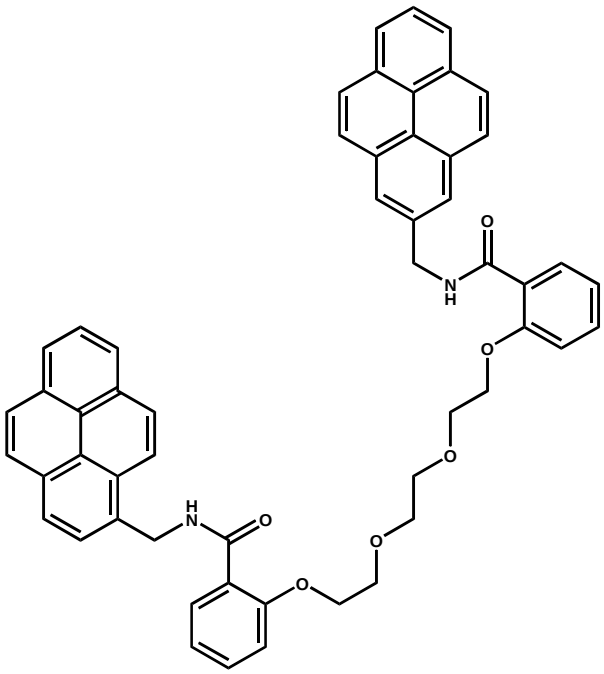

Figure 1.15: an excimer-forming podand selective to alkaline-earth cations.

1.4.3.3 Calixarenes

The chemosensor in *Figure 1.16*[33] is selective to alkaline ions: the excimers in the free form are disrupted when they complex these species.

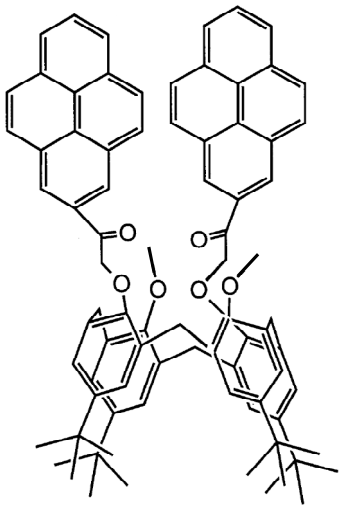

Figure 1.16: a calixarene-based chemosensor for alkali ions.

1.5 Nanochemistry

Nanochemistry deals with the synthesis and the study of chemical systems, called nanomaterials, which possess at least one dimension less than 100 nm and whose properties scale with size. When speaking about chemosensor design, nanochemistry plays an important role because it provides complex nanostructures which can act like scaffold for a great number of fluorophores, such as silica nanoparticles, or which are intrinsically strongly luminescent, such as QDs. So scientific community is spending many effort in studying these systems in order to obtain more efficient luminescent devices for different purposes, from biomedical to environmental applications.

There are two main approaches to the synthesis of these materials: "top down" and "bottom up" approaches. The first one concerns the most modern technique for producing electronic components, starting from the bulk material and going down to a smaller scale by removing matter. The second one produces nanostructures starting from molecules, which are assemble together in order to obtain a more complex system. Nature itself uses this second approach with extraordinary results: let us think to the innumerable molecular machines working inside living organisms, such as RNA polymerase for transcription, ribosomes for translation or DNA polymerase for DNA replication. Man can draw inspiration from Nature in order to build new kind of machines, such as molecular-based computers[34].

1.6 Nanoparticles

Nanoparticles are very small approximately spherical fragment of materials of radius in the approximate range 2-100 nm[8]. These systems are characterized by new and interesting properties which origins from their nanometric dimensions and this is the reason why many investments have been done for financing research projects on nanotechnology. It is out of doubt that nanotechnologies will have a strong impact on several fields of our lives and many publications attest the importance to scientifically approach this research topic.
The application of nanotechnology are nowadays still limited but many uses in industries already exist in different fields, such as electronics and optoelectronics, biomedicine, pharmacy, cosmetics, catalysis, material science. The use of nanoparticles is emerging in medical diagnosis and for drug delivery.

When dealing with luminescence-based methods, the use of more complex architectures like nanoparticles is useful to overcome typical limitations that can be experienced when conventional fluorophores are used, such as low (photo)stability and quantum yield, insolubility in water and unsuitability for physiological conditions. The word nanoparticle comprise a variety of very different systems, such as conjugated polymers, quantum dots, gold nanoparticles and silica nanoparticles doped with flurophores[35-37].
Regardless of their chemical nature, nanoparticles represent a protected environment where active species do not undergo luminescence quenching or degradation processes[38-40].

1.7 Luminescent silica nanoparticles

If we want to design an efficient photochemical device we need it to be (photo)stable, to have environment-independent photophysical properties and to be compatible with the milieu in use. Other useful characteristics are the ease and cheapness of synthesis and biocompatibility and non toxicity. Silica nanoparticles fulfil all these requirements:

- silica is photophysically inert, it is transparent to visible light and is not involved in energy and electron-transfer processes. Thus it is the species inside and/or outside the nanoparticles that confers its own photophysics to the whole system;
- silica is not toxic, and for this reason silica nanoparticles can be used for biological and environmental applications;
- each silica nanoparticle can contain a large number of photochemically active species, providing a system with very high molar absorption coefficient and, if the species are luminescent, very high quantum yields;
- the silica matrix protects the segregated material from external species or undesired photoreactions.

For many analytical applications the need to immobilize the chemosensor on a solid support exists in order to develop a device which can allow continuous measurements in the field. The modification of silica nanoparticles (SiNPs) can represent a method for immobilizing luminescent chemosensors. SiNPs used in this work are core-shell systems, in which a silica core is surrounded by a Pluronic® F127 polymeric shell. These nanoparticles can be loaded with fluorophores or chemosensors, which can be placed inside the core (dye-doped silica nanoparticles DDSNs) or outside in the shell. When different proper fluorophores are present inside the core and in the shell, energy transfer processes can occur.

When the nanoparticles contain two or more different fluorophores it is possible to boost or to minimize electronic excitation energy transfer processes by varying the single concentrations, obtaining in every case a ratiometric system for quantitative assessments[41-43]: the excitation at a single wavelength provides different emission signals, allowing the simultaneous detection of multiple targets[44,45]. So energy transfer processes can induce collective properties in luminescent silica nanoparticles, obtaining three main classes of systems:

- *antenna systems*, with an enhanced light sensitivity because of the higher cross section;
- *sensitized systems*, useful when it is not possible to directly excite the photoactive species;
- *light-energy up-conversion systems*, which are excitable with long wavelength radiation and exploit two photon absorption processes.

Within these three main classes, we are interested in the first, that allows to obtain signal amplification, with a consequent increase in sensitivity and a decrease in lower detection limits[46].
We can identify two kinds of possible multichromophoric nanostructures:

- the chemosensors are all segregated in the silica core (*Figure 1.17 (a)*);
- one or more chemosensors are in the silica core and one is on the surface of the nanoparticle, in the PEG shell (*Figure 1.17 (b)*).

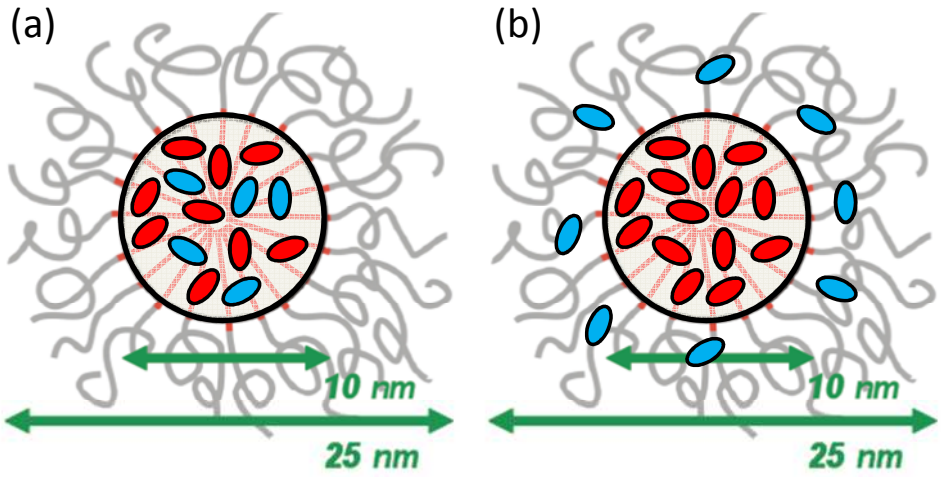

Figure 1.17: core-PEG shell silica nanoparticles (a) doped with two different fluorophores or (b) doped with one fluorophore and with the shell loaded with another fluorophore.

1.8 Aim of the work

This thesis work consists in the characterization of new molecular and nanoparticle-based system which can be used as sensitive materials for the construction of new optical transduction devices able to provide information about the concentration of analytes in solution. In particular two direction were taken. The first is to continue in the development of new chemosensors (see *Chapter 3*), that is the first step for the construction of reliable and efficient devices, and in particular the work will be focused on chemosensors for metal ions for biomedical and environmental applications. The second is to study more efficient and complex organized systems, such as derivatized silica nanoparticles, and the possibility to use them as efficient water-soluble chemosensors (*Chapter 4*). These system can potentially have higher sensitivity than molecular systems, and present many advantages, like the possibility to be ratiometric, higher Stokes shifts, a lower signal-to-noise ratio.

References

[1] U. Galimberti, *Enciclopedia di Psicologia*, Garzanti, Milano, **2005**

[2] A. W. Czarnik, *Supramolecular chemistry, fluorescence, and sensing*, in *Fluorescent chemosensors for ion and molecule recognition*, ACS Symposium Series 538, Washington, DC, USA, **1993**

[3] R. Jakobson, *Saggi di linguistica generale*, Feltrinelli, Milano, **1966**

[4] N. Armaroli, V. Balzani, *Energia per l'astronave Terra*, Zanichelli, Bologna, **2008**

[5] L. Prodi, M. Montalti, N. Zaccheroni, L. S. Dolci, *Probes and sensors for cations*, in *Topics in Fluorescence Spectroscopy, Volume 9, Advanced concepts in Fluorescence Sensing, Part A: Small Molecule Sensing*, C. D. Geddes and J. R. Lakowicz ed., New York, NY, USA, **2005**

[6] J.-M. Lehn, *Proc. Nat. Acad. Sci. USA*, **2002**, *99*, 4763

[7] E.-P. Kyba, R. C. Helgeson, K. Madan, G. W. Gokel, T. L. Tarnowski, S. S. Moore, D. J. Cram, *J. Am. Chem. Soc.*, **1977**, *99*, 2564

[8] J. W. Steed, J. L. Atwood, *Supramolecular chemistry*, 2nd edition, John Wiley & Sons Ltd, Chicester, UK, **2009**

[9] V. Balzani, F. Scandola, *Supramolecular Photochemistry*, Ellis Horwood, Chicester, England, **1991**

[10] A. Hulanicki, S. Geab, F. Ingman, *Pure Appl. Chem.*, **1991**, *63*, 1247

[11] L. Fabbrizzi, M. Licchelli, G. Rabaioli, A. Taglietti, *Coord. Chem. Rev.*, **2000**, *205*, 85

[12] B. Valeur, I. Leray, *Coor. Chem. Rev.*, **2000**, *205*, 3

[13] A.P. de Silva, S.A. de Silva, *J. Chem. Soc. Chem. Commun.*, **1986**, 1709

[14] L. Fabbrizzi, M. Lichelli, P. Pallavicini, D. Sacchi, A. Taglietti, *Analyst*, **1996**, *121*, 1763

[15] R. Bergonzi, L. Fabbrizzi, M. Lichelli, C. Mangano, *Coord. Chem. Rev.*, **1998**, *170*, 31

[16] K. Golchini, M. Mackovic-Basic, S.A. Gharib, D. Masilamani, M.E. Lucas, I. Kurtz, *Am. J. Physiol.*, **1990**, *258*, F438

[17] M.E. Huston, K.W. Haider, A.W. Czarnik, *J. Am. Chem. Soc.,* **1988**,*110*, 4460

[18] I. Aoki, T. Sakaki, S. Shinkai, *J. Chem. Soc. Chem. Commun.*, **1992**, 730

[19] B. Valeur, J. Bourson, J. Pouget, *Ion recognition detected by changes in photoinduced charge or energy transfer*, in A.W. Czarnik (Ed.), *Fluorescent Chemosensors for Ion and Molecule Recognition*, ACS Symposium Series 538, American Chemical Society, Washington, DC, **1993**

[20] H.-G. Löhr, F. Vögtle, *Acc. Chem. Res.*, **1985**, *18*, 65 and references therein

[21] J.F. Létard, R. Lapouyade, W. Rettig, *Pure Appl. Chem.*, **1993**, *65*, 1705

[22] E.N. Ushakov, S.P. Gromov, O.A. Fedorova, M.V. Alfimov, *Izv. Akad. Nauk, Ser. Khim.*, **1997**, 484 [Russ. Chem. Bull., 1997, 46, 463]

[23] M. Kollmannsberger, K. Rurack, U. Resch-Genger, J. Daub, *J. Phys. Chem.*, **1998**, *102*, 10211

[24] S.E. Kasner, M.B. Ganz, *Am. J. Physiol.*, **1992**, *262*, F462

[25] G. Grynkiewicz, M. Poenie, R.Y. Tsien, *J. Biol. Chem.*,**1985**, *260*, 3440

[26] R.P. Haugland, *Handbook of Fluorescent Probes and Research Chemicals*, Molecular Probes, Inc, Eugene, OR, USA, **1992**

[27] G.A. Smith, T.R. Hesketh, J.C. Metcalfe, *Biochem. J.*, **1988**, *250*, 227

[28] K. Iwamoto, K. Araki, H. Fujishima, S. Shinkai, *J. Chem. Soc. Perkin Trans.*, **1992**, *1*, 1885

[29] H. Bouas-Laurent, A. Castellan, M. Daney, J.-P. Desvergne, G. Guinand, P. Marsau, M.-H. Riffaud, *J. Am. Chem. Soc.*, **1986**, *108*, 315

[30] D. Marquis, J.-P. Desvergne, *Chem. Phys. Lett.*, **1994**, *230*, 131

[31] D. Marquis, J.-P. Desvergne, H. Bouas-Laurent, *J. Org. Chem.*, **1995**, *60*, 7984

[32] Y. Suzuki, T. Morozumi, H. Nakamura, M. Shimomura, T. Hayashita, R.A. Bartsch, *J. Phys. Chem.*, **1998**, *102*, 7910

[33] I. Aoki, H. Kawabata, K. Nakashima, S. Shinkai, *J. Chem. Soc. Chem. Commun.*, **1991**, 1771

[34] K. Sakamoto, H. Gouzu, K. Komiya, D. Kiga, S. Yokoyama, T. Yokomori, M. Hagiya, *Science*, **2000**, *288*, 1223

[35] S. M. Borisov, I. Klimant, *Analyst*, **2008**, *133*, 1302

[36] F. Mancin, P. Scrimin, P. Tecilla, U. Tonellato, *Coord. Chem. Rev.*, **2009**, *253*, 2150

[37] T. Doussineau T, A. Schulz, A. Lapresta-Fernandez, A. Moro, S. Körsten, S. Trupp, G. J. Mohr, *Chem. Eur. J.*, **2010**, *16*, 10290

[38] P. Teolato, E. Rampazzo, M. Arduini, F. Mancin, P. Tecilla, U. Tonellato, *Chem. Eur. J.*, **2007**, *13*, 2238

[39] X. Michalet, F.F. Pinaud, L.A. Bentolila, J.M. Tsay, S. Doose, J.J. Li, G. Sundaresan, A.M. Wu, S.S. Gambhir, S. Weiss, *Science*, **2005**, *307*, 538

[40] R. Gill, M. Zayats, I. Willner, *Angew. Chem. Int. Ed.*, **2008**, *47*, 7602

[41] T. Doussineau, S. Trupp, G.J. Mohr, *J. Colloid Interface Sci.*, **2009**, *339*, 266

[42] M. Arduini, F. Mancin, P. Tecilla, U. Tonellato, *Langmuir*, **2007**, *23*, 8632

[43] L. Wang L, M.B. O'Donoghue, W. Tan, *Nanomed.*, **2006**, *1*, 413

[44] L. Wang, W. Tan, *Nano Lett.*, **2006**, *6*, 84

[45] L. Wang, C.Y. Yang, W. Tan, *Nano Lett.*, **2005**, *5*, 37

[46] S. Zhu, T. Fischer, W. Wan, A.B. Descalzo, K. Rurack, *Luminescence amplification strategies integrated with microparticle and nanoparticle platforms*, in *Luminescence Applied in Sensor Science*, *Top. Curr. Chem.*, **2010**, 1

Giorno d'estate, giorno fatto di vuoto,
giorno di luce che non si spegnerà,
sembra d'andare in un paese remoto
chissà se in fondo c'è la felicità!

Giorno d’estate

Francesco Guccini

Chapter 2: Experimental section

2.1 Chemicals

All the DCHQs (see *Chapter 3*) were synthesized by professor Trombini's group, in the Department of Chemistry of the University of Bologna. DEAC and all kind of SiNPs were synthesized by professor Prodi's group, in the Department of Chemistry of the University of Bologna. Compound **1** (see *Chapter 4*) was synthesized following Chang's synthesis by professor Rizzarelli's group, in the Department of Chemical Sciences of the University of Catania. Compunds **L1**-**L3** (see *Chapter 4*) were synthesized by professor Lippolis's group, in the Department of Geological and Chemical Sciences of the University of Cagliari.

2.2 Electronic absorption spectra

For the acquisition of electronic absorption spectra a double beam spectrophometer *UV/Vis Perkin Elmer Lambda-45* was used, whose scheme is shown in *Figure 2.1*.

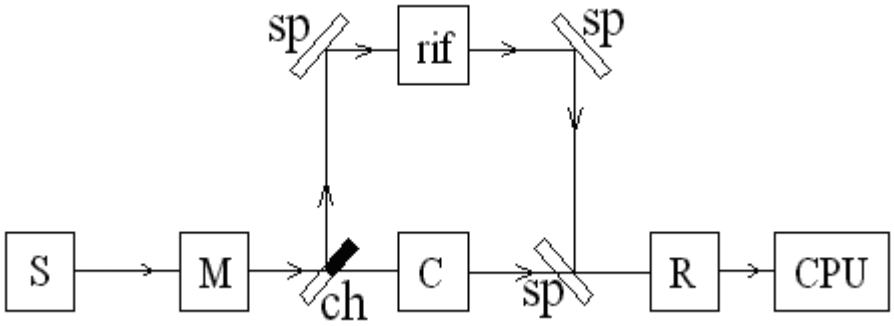

Figure 2.1: block diagram of *UV-vis Perkin Elmer Lambda-45* spectrophotometer.

The components of the spectrophotometer are:

- *source* (S): formed by two lamps, a tungsten filament lamp which works between 1100 nm and 320 nm and a deuterium lamp operating between 320 nm and 190 nm;
- *monochromator* (M): a diffraction lattice;
- *sample* (C): a solution of the sample contained in a cuvette, generally of quartz;
- *reference* (rif): the solvent, contained in a second cuvette;
- *detector* (R): a photomultiplier tube;
- *chopper* (ch), a mechanical device which allows the light to be alternatively transmitted through the sample and the reference, or to be suppressed in order to measure the dark current of the photomultiplier used as detector;
- *mirrors* (sp).

The amount of the absorbed light is provided by the difference of the intensity of incident light (I_0) and the intensity of transmitted light (I_t) and it is expressed as transmittance (T):

$$T = \frac{I_t}{I_0}$$

or as absorbance (A):

$$A = -log_{10}\, T = log_{10}\frac{I_0}{I_t}$$

By means of the spectrophotometer it is possible to measure the transmittance and calculate the absorbance of the solution containing the sample as a function of the wavelength and thus to identify the electronic transitions which lead the molecule from its ground state to different excited states. The instrument determines the absorbance of the sample subtracting from the "raw" value of absorbance the absorbance of the reference. From the registered spectra moreover it is possible to determine the probability of every transition by calculating the *molar absorption coefficient* ε, expressed in M^{-1} cm^{-1}, according to *Lambert-Beer law*:

$$A = \varepsilon c l$$

where A is the absorbance of the sample, c is the molar concentration of the sample, and l is the optical path length of the cuvette (usually 1 cm).

2.3 Emission and excitation spectra

The registration of the emission and excitation spectra was performer using a spectrofluorimeter *Perkin Elmer LS55* and a spectrofluorimeter *Fluorolog 3 ISA Jobin Yvon – Spex, Instruments S.A.*.
These instruments consist of:

- *source* (S): a xenon lamp, pulsed in the case of *Perkin Elmer LS55*, continuous-wave in the case of *Fluorolog 3*;
- two *monochromator*: M_{ex} for excitation light and M_{em} for emission light;
- two *photomultipliers*: R1, in order to correct the signal as a function of the emission spectrum of the lamp, and R2, for the detection of the emission signal of the analyte;
- *sample* (C): solution of the sample in a quartz fluorimeter cuvette;
- *chopper* (ch);
- *slit*: it determines the bandwith of the excitation and emission light.

The scheme of the instrument is shown in *Figure 2.2*.

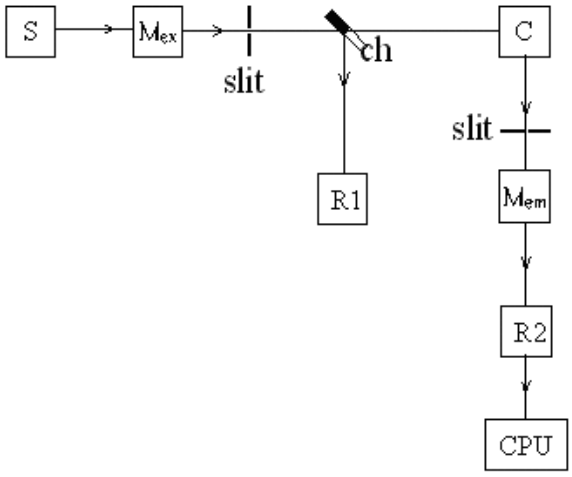

Figure 2.2: block scheme of a spectrofluorimeter.

In order to register an *emission spectrum* the excitation monochromator has to be positioned at a determined wavelength, which normally corresponds to the absorption maximum or lower wavelengths, and a scan with the emission monochromator is performed. Solutions having an absorbance lower than 0.1 at the excitation wavelength have to be used so that the relation between the emission intensity and the concentration is linear.

In order to register an *excitation spectrum* the emission monochromator is positioned at a fixed wavelength which generally corresponds to the emission maximum or higher wavelengths, while the excitation monocromator scans the spectrum region in which the sample absorbs. If we want to obtain a correct spectrum we need a solution of sample possessing an absorbance lower than 0.1 all over the wavelength range chosen to register the excitation spectrum. In this way the registered emission intensity is directly proportional to the absorbance value, and the obtained spectrum results proportional to the absorption one (this is strictly true if the species follows Kasha's rule).

In *Figure 2.3* the optical schemes of the two kind of measure are reported.

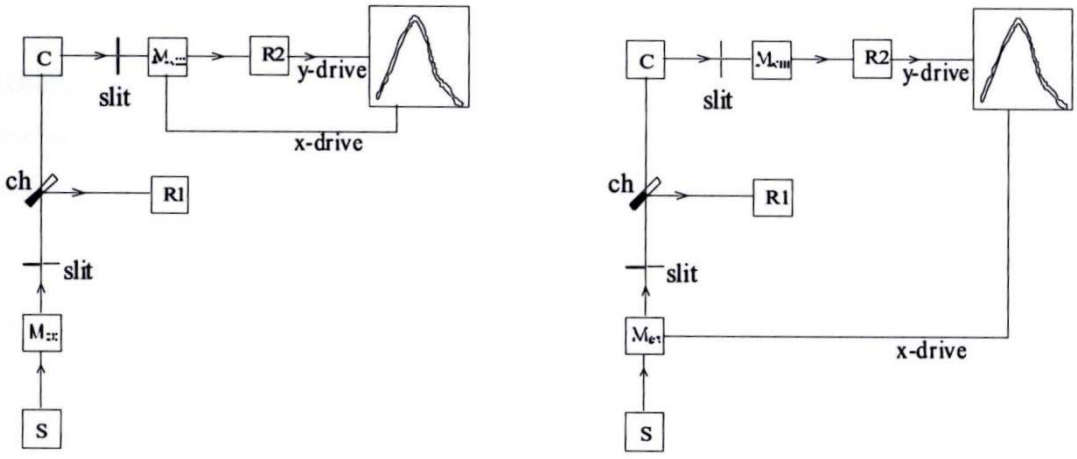

Figura 2.3: instrumental scheme for the registration of an emission spectrum (left) and an excitation spectrum (right).

2.4 Luminescence quantum yield assessment

A very used quantity in photophysics is the luminescence quantum yield Φ_l, defined as the ration between the number of emitted photons and the number of photons absorbed by a species in the same time and for a determined excitation wavelength:

$$\Phi_l = \frac{number\ of\ emitted\ photons}{number\ of\ absorbed\ photons}$$

For the assessment of luminescence quantum yield with a relative method we need a reference possessing a known Φ_l. The species used as a reference has to emit in the same spectral region in which the sample emits so that emission spectra are obtained in the same experimental conditions. For the assessment of Φ_l we adopted the following experimental procedure[1]: the absorption spectra of the sample and of the reference were registered and, when possible, isosbestic points were used as excitation wavelength for the registration of emission spectra. The following equation was used to determine the value of luminescence quantum yield:

$$\Phi_x = \Phi_r \frac{I_x\ A_r\ {n_x}^2}{I_r\ A_x\ {n_r}^2}$$

where Φ_x is the luminescence quantum yield of the sample, Φ_r the luminescence quantum yield of the reference, I_x the area of the emission spectrum of the sample and I_r the area of the emission spectrum of the reference, A_r the absorbance of the reference at the excitation wavelength, A_x the absorbance of the sample at the excitation wavelength, n_x the refractive index of the solvent of the sample, n_r the refractive index of the solvent of the reference.

2.5 Excited state lifetime measurements

Excited state lifetime measurements were performed using a spectrofluorimeter *Edinburgh Analytical Instruments FLS920*, equipped with a *time-correlated single-photon counting* device, which is able to measure lifetimes in a range between 0.5 ns and 30 μs. The *time-correlated single-photon counting* is based on the probability that a single photon emitted by a luminescent sample is collected by a proper high sensitivity detector: this probability is statistically correlated with the variation of the concentration of the excited states in solution.

The components are:

- *source* (S): a pulsed deuterium arc lamp (continuous emission spectrum) at circa 0.5 atm operating at a frequency of 50-100 kHz with pulses of about 1 ns or a pulsed laser;
- two *monochromators*: M_1 for excitation light and M_2 for emission light;
- two *photomultipliers*: D_{start}, start photomultiplier, and D_{stop}, stop photomultiplier;
- *sample* (C): solution containing the species to investigate in a quartz fluorimetere cuvette;
- *time-to-amplitude converter* (TAC);
- *multichannel analyser* (MCA);
- *computer* (CPU).

In *Figure 2.4* the block scheme of the instrument is shown.

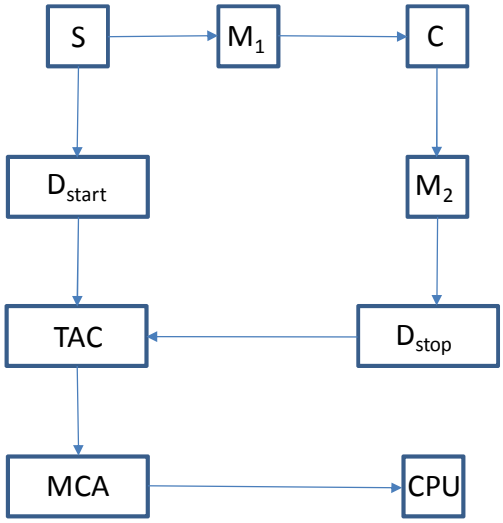

Figure 2.4: block scheme of a time-correlated single-photon counting device.

When the source emits a pulse, the start photomultiplier, which is connected to the lamp, sends a signal to the TAC, which in turn start a linear voltage ramp, blocked when the stop signal arrives. If the sample emits a photon after the excitation pulse, the stop photomultiplier detects the emitted photon and sends a stop signal to the TAC, which block the voltage ramp. The TAC acts like a chronometer which measures the time interval between the start signal, which corresponds to the excitation of the sample, and the stop signal, which corresponds to the emission of a photon from the sample: this time interval is converted in an electrical signal and then sent to MCA. The MCA counts the number of decay events occurring at each time interval and then accumulating together the counts at the same delay from excitation in the proper channel. For statistical reasons the frequency of the registered events does not to exceed 2% of the work frequency of the lamp. A reliable decay profile as a function of time is obtained only if the emitted photons in any instant have a probability to be monitored which depends only on the concentration of emitting excited states, that is only if all photons, regardless of the time at which they are emitted, have a finite probability to be detected. By operating with values higher than 2% the photons emitted immediatley after the flash have a higher probability to be detected than those emitted at longer times, causing the decay profile to undergo a shift toward shorter times[2]. The data obtained by the MCA are then sent to the computer which builds the decay profile, shown in *Figure 2.5*.

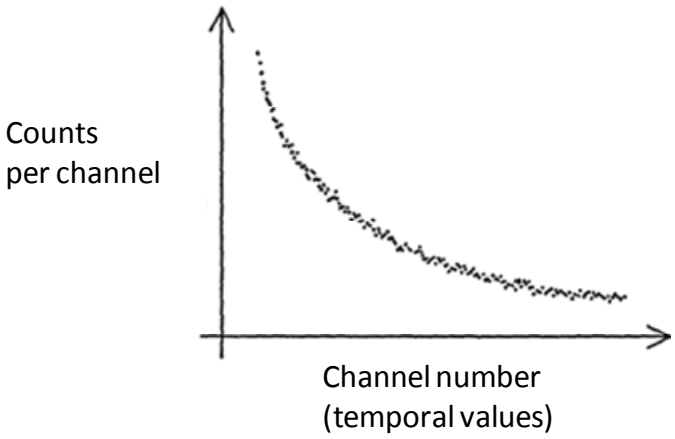

Figure 2.5: example of a (monoexponential) decay profile.

Mono and biexponential fitting were obtained by means of least squares analysis and their reliability is espressed from the factor χ^2, whose values has to approach 1 in order to have an accurate fitting.

2.6 Fluorescence anisotropy measurements

Fluorescence anisotropy measurements were performed using a spectrofluorimeter *Edinburgh Analytical Instruments FLS920***.**

These measurements are mainly used to study two phenomena: the rotation dynamics of a fluorophore in the space and excitation energy transfer processes. In particular it is possible to study the dynamics of deactivation processes and migration of energy in supramolecular systems.

Fluorescence anisotropy is a quantity that allows to measure the polarization of the light emitted from a sample excited by polarized light. For this purpose fluorimeters equipped with a couple of polarizers placed respectively between the excitation monochromator and the sample and between the latter and the emission moochromator. By performing the measurement at different wavelengths and by fixing the excitation wavelength the fluorescence anisotropy spectrum is obtained. The instrumental configuration is shown in *Figure 2.6*.

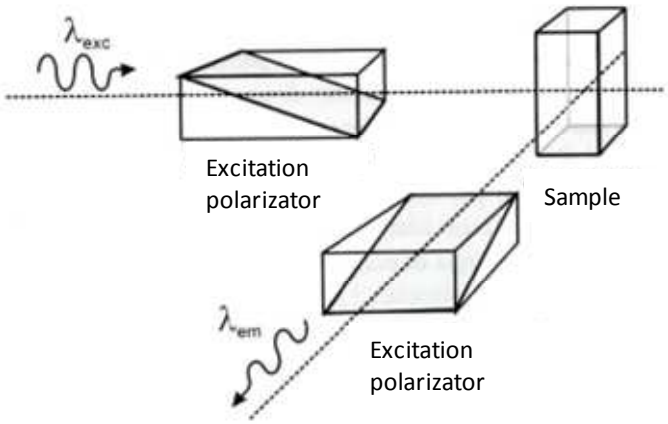

Figure 2.6: instrumental configuration used for fluorescence anisotropy measurements.

If we indicate with $\boldsymbol{I}_{\parallel}$ the intensity measured when the emission polarizer is vertical (and therefore parallel to the excitation one) and with $\boldsymbol{I}_{\perp}$ the one measured when the emission polarizer is horizontal (perpendicular to the excitation one), the fluorescence anisotropy $\boldsymbol{r}$ is defined as

$$r = \frac{I_{\parallel} - I_{\perp}}{I_{\parallel} + 2I_{\perp}}$$

Taking into account this definition, it would be necessary to register only two emission spectra, one with the polarizers parallel to each other, one with the perpendicular polarizers. Actually if we register only these two spectra for a sample with a known null anisotropy spectrum, we obtain anisotropy values different from zero. This is due to the fact that the system response is not independent of the polarization of the detected light. So we obtain different values if we register I_{VV} and I_{HH} and the same happens for I_{HV} and I_{VH}. The component that mainly determines this anisotropic behaviour is the emission monochromator, which possesses an intrinsically anisotropic structure. If we consider that

$$\frac{I_{VV}}{I_{VH}} = G\frac{I_{\parallel}}{I_{\perp}}$$

It is possible to calculate the anisotropy at each wavelength from I_{VV} and I_{VH}, once we know the value of the G factor for each wavelength:

$$r = \frac{I_{VV} - GI_{VH}}{I_{VV} + 2I_{VH}}$$

The G factor is a purely experimental parameter, that can be determined by registering emission spectra maintanining the excitation polarizer in horizontal position and varying the orientation of the emission one:

$$G = \frac{I_{HV}}{I_{HH}}$$

Therefore four emission spectra are acquired in the same experimental conditions, by combining the four possible orientations of the polarizers (I_{VV}, I_{HH}, I_{VH}, I_{HV}). These four spectra can be also directly usable for the fluorescence anisotropy calculation, using the following equation:

$$r = \frac{I_{VV}I_{HH} - I_{VH}I_{HV}}{I_{VV}\,I_{HH} + 2I_{VH}\,I_{HV}}$$

2.7 Dynamic Light Scattering: hydrodynamic diameter measurements of particles

Dynamic Light Scattering (DLS) measurements were performed using a *Malvern Instruments DLS ZetaSizer Nano-ZS* (*Figure 2.7)*. With this instrument it is possible to determine the dimension of particles having a diameter between 1 nm and 10 μm.

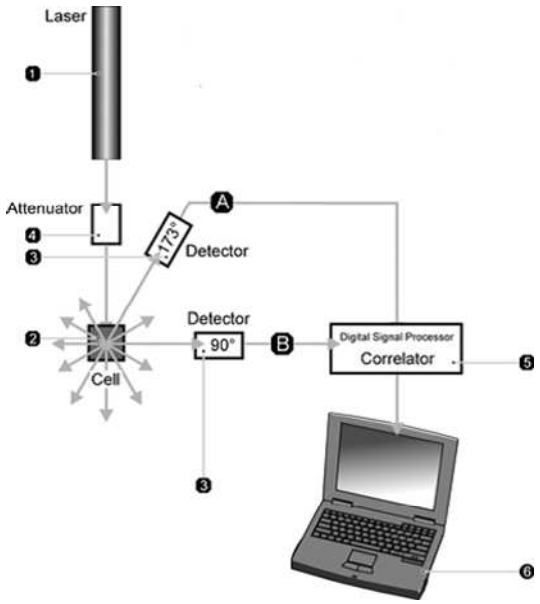

Figure 2.7: block scheme of a *Malvern Instruments DLS ZetaSizer Nano-ZS*.

Its components are:

- *Laser*: He-Ne laser (λ_{exc} = 633 nm), that lights the sample;
- *Cell*: it contains the sample;
- *Detector*: positioned at 173° or at 90° with respect to the incident laser beam, it registers the light scattered by the sample;
- *Attenuator*: it modulates the intensity of the laser beam;
- *Correlator*: it compares the output signals as a function of time;
- *Nano Software*: it translates the information, by providing the dimensions of the several populations of particles present in the sample.

The DLS technique allows the measurements of submicrometric particles. It exploits the study of Brownian motions to determine the hydrodynamic diameter of particles suspended in solution. The higher the dimensions, the lower the particle speed of displacement: as a consequence the smallest particles move more rapidly. It is necessary to know the viscosity and the temperature of the system for DLS measurements and in particular the system has to be kept at a constant temperature in order to avoid internal convection currents that can affect the measurements.
Stokes-Einstein equation defines the dimensions of a particle from its translational diffusion coefficient D

$$d(H) = \frac{kT}{3\pi\eta D}$$

where $d(H)$ is the hydrodynamic diameter espressed in m, k is Boltzmann constant in $J \cdot K^{-1}$, T is the absolute temperature, η is the viscosity in $Kg \cdot m^{-1} \cdot s^{-1}$ and D is the diffusion coefficient in $m^2 \cdot s^{-1}$.
The obtained diameter is a value referred to particles dispersed in a fluid, so it is reported as hydrodynamic diameter, which is defines as the diameter of a rigid sphere that diffuses at same speed of the particle. Its value is not only dependent of the particle dimensions, but also of the concentration and the kind of ions present in the dispersant. Some changes in the superficial structure are able to influence

the diffusion speed and as a consequence the hydrodynamic diameter of the particle: for example a polymeric shell covering a nanoparticle (*Figure 2.8*) can reduce the diffusion speed and thus enhancing its hydrodynamic diameter.

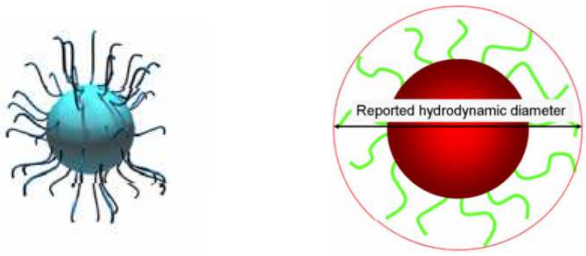

Figure 2.8: (left) particle with a polymeric shell; (right) hydrodynamic diameter measure.

The charge and the concentration of ions in the dispersant also influence the diffusion speed of the particle: an increase of the ionic strength causes a decrease of the hydrodynamic diameter. According to *Rayleigh approximation*, the light scattering of the particles irradiated by the laser is mainly isotropic if the particles have dimensions that are negligible with respect to the wavelength used (generally less than $\frac{\lambda}{10}$, about 60 nm if a He-Ne laser is used). With this hypothesis the scattered light intensity I becomes directly proportional to the sixth power of the particle diameter d and inversely proportional to the fourth power of the incident light wavelength λ:

$$I \propto d^6$$
$$I \propto \lambda^{-4}$$

The proportionality to d^6 specifies that the ratio between the scattering intensity of a particle having a diameter of 50 nm and that of one having a diameter of 5 nm is equal to 1 million. The proportionality to λ^{-4} indicates that a high scattering intensity is obtained using short wavelengths.
If we imagine that a stationary state is reached, we would observe a speckle pattern after the laser irradiation (*Figure 2.9 (a)*). The black zones are due to the effect of a destructive interference of scattered light of different particles (*Figure 2.9 (b)*). Observing the system from a dynamic point of view, that is considering that Brownian motion occurs, the single points of the pattern are in continuous motion.

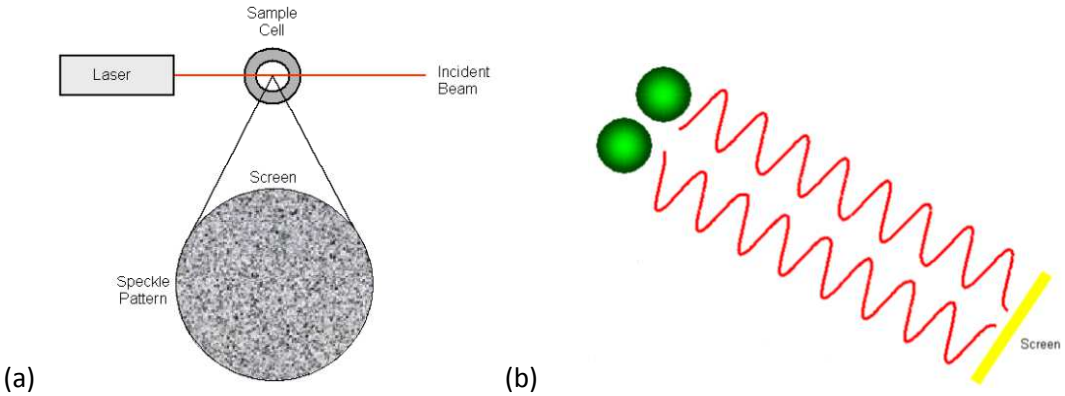

Figure 2.9: (a) sample speckle pattern; (b) effect of the destructive interference of two waves scattered by two particles.

The correlator is necessary to measure the frequency spectrum of these intensity fluctuations. It compares the signals by measuring their degree of similarity in a determined time range. For a random process, such as diffusion, it is not possible to correlate two signals that are temporally distant, that is when δt is in the order of milliseconds (*Figure 2.10*). On the other hand, if δt is in the order of microseconds to nanoseconds, it is possible to observe that the signal intensity at the time t is correlated with the signal in the subsequent instant t+δt.

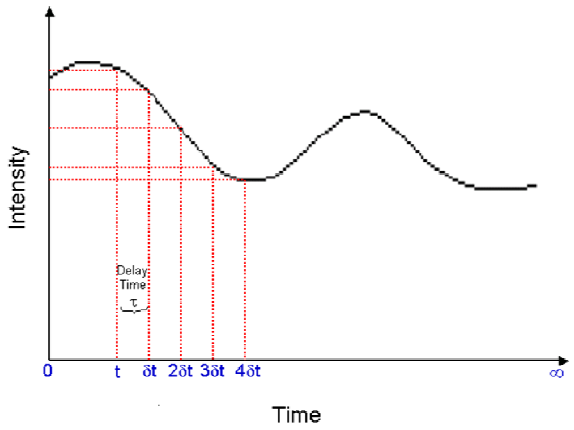

Figure 2.10: **I**ntensity fluctuations of the scattered light as a function of time (t = ∞ is equal to 1-10 ms).

If the particles are big, the signal slowly fluctuates and the correlation persists for a long time interval. On the other hand, if the particles are small they rapidly move and the correlation decreases more quickly. In *Figure 2.11* the differences in the shape of the correlogram as a function of particle dimensions is shown: the left correlogram represents a sample containing big particles and it is characterized by a slow decay; the right one relates to small particles and it is characterized by faster decay.

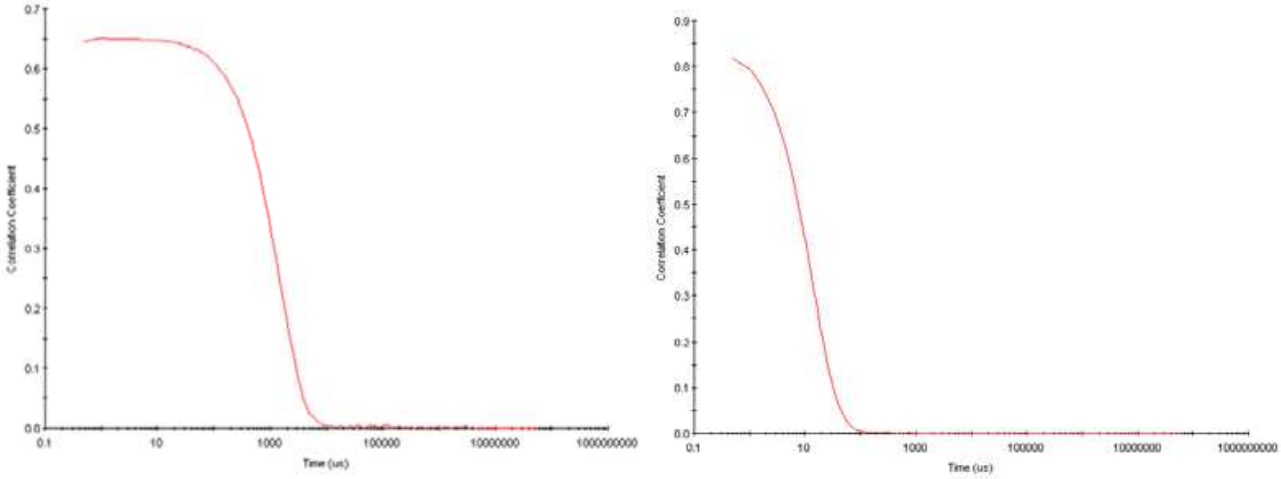

Figure 2.11: (left) correlogram of a sample containing big particles; (right) correlogram of a sample containing small particles.

The hydrodynamic diameter is obtained from the correlogram mainly by using two approaches:

- Monoexponential fitting of the correlation function in order to obtain the average dimension (*Z-average diameter*) and an estimate of the width of the distribution (*Polidispersity index, PDI*);
- Multiexponential fitting of the correlation function in order to obtain the particle size distribution.

The particle size distribution is obtained from the relative scattering intensity graph of the several particle size classes (*intensity size distribution*). It is also possible to obtain this distribution as a function of particle volume, or particle number. Let us consider, for example, a sample containing two populations of spherical particles having a diameter of 5 and 50 nm respectively and present in the same number (*Figure 2.12*). As far as the number of particle is concerned, the graph consists of two peaks, one at 5 nm and the other at 50 nm, with a 1:1 ratio. If we convert the number distribution in volume distribution, the two peaks ratio is 1:1000, because the volume of a sphere is equal to $\frac{4\pi}{3}\left(\frac{d}{2}\right)^3$. If we switch to intensity distribution, the ratio becomes equal to 1:10^6 according to Rayleigh approximation.

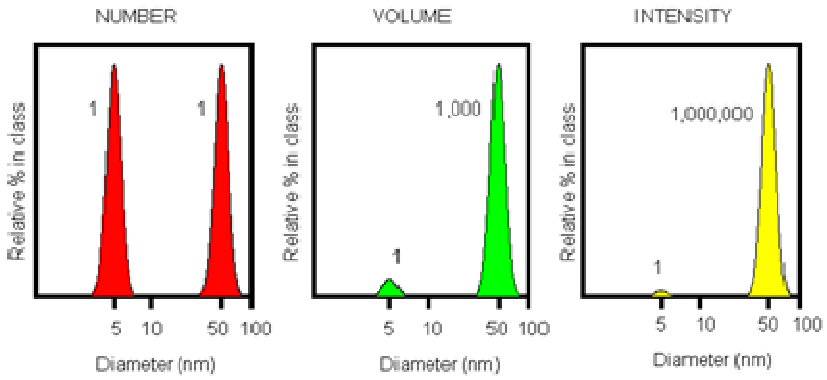

Figure 2.12: number, volume and intensity distribution of a sample containing spherical particles of 5 and 50 nm diameter in equal numbers.

Finally it is important to underline that sample absorbing and/or emitting at the analysis wavelength are not suitable for DLS technique.

References

[1] J. N. Demas, G. A. Crosby, *J. Phys. Chem.*, **1971**, *75*, 991

[2] L. Moggi, A. Juris, M. T. Gandolfi, *Manuale del Fotochimico, Tecniche e metodologie*, Bononia University Press, Bologna, **2006**

“Non c'è solo il vento”, diceva,
“anche la luce può portarti via,
se hai tempo da perdere
e dentro la giusta elettricità,
e se da sempre ti aspetti un miracolo.”

Ballando con una sconosciuta

Francesco Guccini

Chapter 3: Chemosensors for metal ion sensing

3.1 Magnesium sensing

3.1.1 Introduction

Magnesium ion, the most abundant divalent cation in cells, is required for many cell processes such as proliferation[1] and cell death.[2] It is involved in the regulation of hundreds of enzymes and molecules of different structure and function.[3] Most ATP in cells is bound to Mg^{2+} since $MgATP^{2-}$ is the active species in enzyme binding and the energy-producing form in active transport[4] and muscular contraction.[5] Thus, alteration in total or free magnesium can have significant consequences for cell metabolism and cell functions. Although the biochemistry of Mg^{2+} has been thoroughly studied in vitro, a full understanding of cellular magnesium homeostasis has not been achieved. Cytosolic Mg^{2+} concentration is regulated by plasma membrane and organelle transport and by intracellular binding. It is maintained far from electrochemical equilibrium by means of inward and outward transport mechanisms.[6] Cytosolic free Mg^{2+} levels are reported to be 0.2-1 mM depending on the tissue and/or the measurement techniques employed,[7] representing less than 10% of the total Mg^{2+}; the remainder is bound or sequestered in different cellular organelles. It has been presumed that cellular magnesium, in particular the free form, is kept constant at the level necessary for cellular metabolic demands and that, under physiological conditions, its concentration does not undergo drastic and rapid changes. In recent years, however, it has been demonstrated that sizable fluxes of Mg^{2+} can cross the plasma membrane in either direction following hormonal and non-hormonal stimuli, resulting in major changes in total and, to a lesser extent, free Mg^{2+} content[8]. Furthermore, *in vivo* NMR measurements have shown that concentrations of free Mg^{2+} change in human skeletal muscle under different metabolic conditions and that these changes can only partially be ascribed to redistribution of Mg^{2+} among the different equilibria within the cytosolic milieu.[7g,h,9] In this context, the need for a sensitive and reliable tool to measure concentrations and fluctuations of cellular Mg^{2+} becomes very stringent, since available techniques have serious limitations. Atomic absorption spectroscopy is very sensitive and accurate but requires volatilization of the sample and a relatively high number of cells, and it does not discriminate between free and bound forms. On the other hand, *in vivo* NMR spectroscopy allows an accurate measurement of cytosolic free Mg^{2+} but supplies no information on the total Mg^{2+} concentration and its distribution among cellular subcompartments. Electron probe microanalysis has been exploited to measure Mg^{2+} content in distinct cellular subcompartments in freeze-dried cryosections. This technique again does not provide information on free and bound Mg^{2+} and does not allow kinetic measurements of Mg^{2+} fluxes.[10]

Fluorescent probes, if properly designed, can offer a suitable solution. They are widely used to evaluate changes in intracellular metal ion concentrations. In particular, their application in fluorescence confocal imaging allows dynamic measurements of cellular content and distribution of the targeted ion, giving a means of mapping the concentration of an analyte in a sample. The available fluorescent probes for intracellular magnesium are mainly derived from those designed for calcium (mag-fura, mag-indo, mag-fluo, etc.),[11] but despite the chemical modifications to increase their selectivity toward Mg^{2+}, they retain cross-reactivity with Ca^{2+} and dependence on pH. In addition, these Mg^{2+}-specific fluorophores are characterized by a K_d in the millimolar range, which is appropriate to measure mainly the free fraction of cellular Mg^{2+} (only 5% of the total). In fact, cytosolic free Mg^{2+} concentrations are in the range of 10^{-4} M, while total cellular Mg^{2+} is up to 100-fold higher. Increasing evidence shows that fluctuations of free intracellular Mg^{2+} concentrations are modest compared to massive changes of total cellular Mg^{2+};[12] thus, modifications of Mg^{2+} availability to influence different biological functions are thought to be accomplished

by substantial modifications of the distribution of total Mg^{2+} among cellular subcompartments. In this scenario, a tool able to detect and/or discriminate between free and total Mg^{2+} and between Mg^{2+} content of cytosolic and intracellular subcompartments would be particularly useful. Recently, a new family of Mg-binding fluorescent probes named KMGs has been designed, and their application to the study of intracellular Mg^{2+} homeostasis seems promising.[13] The unavailability of more specific and selective commercial compounds for total magnesium currently represents a technical limitation in the study of the intracellular content and distribution of this cation. Compelling evidence, in fact, demonstrates that cellular magnesium homeostasis is quite unusual: in response to a variety of hormonal and non-hormonal stimuli, significant fluxes of Mg^{2+} cross the cell membrane in either direction, with consequent major changes in plasma Mg^{2+} levels.[14] These fluxes, however, result in limited variations of free Mg^{2+} intracellular concentration, even though large changes in total Mg content within tissues and organelles have been observed.[15] This suggests that modifications of magnesium availability that influence different biological functions may be accomplished by changes in the distribution (binding) of magnesium among cellular ligands and/or sub-compartments rather than by major modifications of the free fraction.[16] In this perspective, the possibility to develop chemosensors able to detect total magnesium *in vivo* and discriminate specific intracellular ligands and/or compartments is particularly appealing. The synthesis and photophysical studies have recently been reported of a new class of fluorescent sensors for Mg^{2+} ion based on diaza-18-crown-6 appended with two 8-hydroxyquinoline groups (DCHQ) bearing different substituents.[17, 18]

8-Hydroxyquinoline (8-HQ), that is the second major Mg^{2+} chelating agent after EDTA,[19] is mostly non-fluorescent in aqueous or organic solutions and undergoes a fluorescence enhancement upon cation binding, which results in an intense yellow–green luminescence signal. Furthermore, the fluorescence of the complexed species depends on the environment and becomes higher as lipophilicity increases.[20,21] Even though the selectivity of 8-HQ for specific cations is poor, it can be improved by appropriate substitution. To this aim, by conjugation of a diaza-18-crown-6 with two 8-HQ derivatives (DCHQ, *Figure 3.1*) we obtained two UV-excitable fluorescent molecules (DCHQ1 and DCHQ2) that show an affinity for magnesium cations higher than any commercially available probe.[22,23] Indeed, the dissociation constants of all their magnesium complexes ($K_d(Mg^{2+})$) are in the micromolar range, that is the same order of magnitude as (and hence able to compete with) ATP, which is the major intracellular Mg^{2+} ligand.[22] Furthermore, fluorescence of these DCHQ-based compounds is not influenced by the presence of other divalent cations (including Ca^{2+}) in physiological conditions.[18,22]
In particular, DCHQ1 is well tolerated by the cells and it is capable to quantitatively assess total intracellular magnesium by a simple spectrofluorimetric assay.[23] Typically the synthetic approach to DCHQ1 is a classic thermal Mannich reaction of 1,10-diaza-18-crown-6 ether with a slight excess of paraformaldehyde and 8-HQ.[17] However, this method yields complex crude mixtures from which the pure product can be recovered only in low amounts after a sluggish purification. We have recently demonstrated that the synthesis of DCHQ1 can be greatly improved by microwave heating, with a reduction of the reaction time, an increase of the yield and the minimization of side reactions. This ultimately results in much easier purifications and higher quality products.[24] The new protocol allowed the straightforward synthesis of a panel of DCHQ analogues that carry task-specific substituents in position 2, 4 or 5 of the quinoline ring system.[24] New compounds were designed with the goal of improving fluorescence response upon cation binding, uptake and intracellular localization preserving the unique feature of selectively binding total intracellular magnesium.

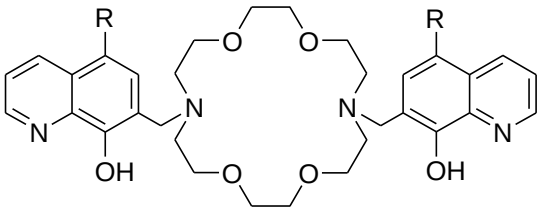

DCHQ1: R = H
DCHQ2: R = Cl
DCHQ3: R = $CH_2OCH_2C(CH_3)_2COOCH_3$
DCHQ4: R = $CH_2O(CH_2)_7CH_3$
DCHQ5: R = Ph
DCHQ6: R = CH_2OCH_2Ph

Figure 3.1: structure of the DCHQ-based chemosensors.

For example, a limitation of DCHQ1 is that it can be excited only in the UV region and it shows an incomplete intracellular retention. Thanks to the new synthetic approach recently developed, a number of DCHQ derivatives bearing a variety of functional groups has been synthesized. In particular, in the present study we demonstrate that even small variations within the basic structure significantly influence the behaviour of the DCHQ derivatives by either:

- enhancing pre-existing features of the reference probe DCHQ1 (i.e. increased fluorescence upon Mg^{2+} binding or cellular retention);
- introducing new characteristics (i.e. specific intracellular localization or red shift of the absorption spectrum).

Among the panel of the new synthesized DCHQ derivatives,[24] we chose four dyes that looked promising in terms of enhancement of one or more of the aforementioned characteristics of DCHQ1 (*Figure 3.1*). Two terminal AM (acetoxymethyl ester) groups have been inserted in the 5 position of the 8-HQ side arms to obtain DCHQ3 (*Figure 3.1*) to enhance cellular uptake and/or a more efficient trapping. The insertion of AM groups in dyes represents, indeed, a common strategy in the preparation of commercial probes since these groups can be recognized and hydrolyzed by intracellular esterases.[25] A probe (DCHQ4, *Figure 3.1*) bearing long alkyl chains on the 8-hydroxyquinoline side arms was synthesized to confer increased lipophilicity and, consequently, higher affinity for membranes. Finally, two aromatic groups on the 8-HQ side arms of DCHQ5 and DCHQ6 (*Figure 3.1*), contributing to the overall charge delocalization, were inserted in order to try to red-shift the absorption and emission spectra with respect to the mother probe DCHQ1.

3.1.2 Results and discussion

3.1.2.1 Photophysical properties

The absorption and fluorescence spectra of the DCHQ derivatives are mainly due to the presence in their structure of 8-HQ side arms, whose photophysical properties have been extensively studied.[26] The absorption spectra (*Figure 3.2*) of DCHQ1–6 in MeOH–H_2O (1 : 1) buffered at pH 7.4 with MOPS (3-morpholinopropane-1-sulfonic acid), show an intense band at around 240–250 nm (ε = 70000–83000 $M^{-1}cm^{-1}$) and a smaller and broader band at around 310–330 nm (ε = 5200–9000 $M^{-1}cm^{-1}$). The former can be attributed to a π–π* transition, while the latter presents a main charge transfer character with charge

density moving from the hydroxyl oxygen atom to the quinoline.[22,27] The substitution of the hydrogen in the 5 position of the quinoline structure of DCHQ1 caused a slight red-shift of both bands in all the cases examined, and affected the molar absorption coefficients. These effects were significant for DCHQ5, probably since conjugation of the phenyl ring with the quinoline nucleus contributes to a higher charge delocalization (*Figure 3.2*). All the compounds showed a weak emission band at around 465–510 nm with a fluorescence quantum yield in the range $6 \cdot 10^{-5} – 1 \cdot 10^{-4}$ (see *Table 3.1*).

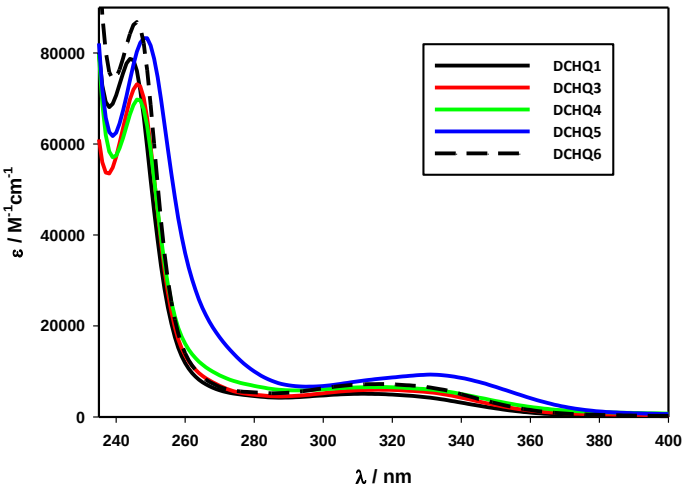

Figure 3.2: Absorption spectra of probes DCHQ1-6 (25 μM) in MeOH–H_2O (1 : 1) buffered at pH 7.4 with MOPS (3-morpholinopropane-1-sulfonic acid) at room temperature.

According to literature,[26] low values of fluorescence quantum yields for similar substituted 8-HQ have been ascribed to two main mechanisms, intramolecular photoinduced proton transfer (PPT) between the hydroxyl group and the nitrogen atom, and photoinduced electron transfer (PET) between the nitrogen atom of the macrocycle and the 8-HQ derivative. In addition, in protic media, intermolecular PPT processes involving solvent molecules can also occur, further decreasing the fluorescence quantum yield of this kind of fluorophores. A systematic study of the new compounds was then performed in order to explore their affinity and photochemical behaviour in presence of Mg^{2+} and of possible competitors (i.e. Zn^{2+}, Cd^{2+}, Hg^{2+}, Cu^{2+}, Ni^{2+}, Na^{+}, K^{+}, Ca^{2+}, Fe^{2+}, Fe^{3+}). Interestingly, all the DCHQ derivatives presented the same trends in terms of complexation ability: no changes either in absorption or in emission spectra were observed for the addition of Na^{+}, K^{+}, Ca^{2+}, Fe^{2+} and Fe^{3+}, indicating that these species do not form any complex with the DCHQ ligands at the studied concentrations. On the contrary, Hg^{2+}, Cu^{2+} and Ni^{2+} were efficiently bound to the molecules but formed non-luminescent complexes. Among all the considered metal ions, only Mg^{2+}, Zn^{2+} and Cd^{2+} induced a significant enhancement of the fluorescence of the system (*Table 3.1*).

The addition of increasing amounts of Mg^{2+} caused changes in the absorption spectra of all the DCHQ derivatives, in particular the decrease of the bands centered at 240–250 nm and at 310–330 nm and the appearance of new bands around 260–265 and 370–390 nm (see, for example, the absorption spectrum of DCHQ5, *Figure 3.3(a)*). These new bands are characteristic of 8-HQ derivatives when the complexation process is accompanied by the deprotonation of the hydroxyl group in position 8.[26e,f] In this respect, it should be noted that the complexation with Mg^{2+} does not cause the complete deprotonation of the 8-hydroxyquinoline, while this process is complete in the case of Zn^{2+} and Cd^{2+}. On the other hand Mg^{2+} binding causes a dramatic enhancement of the emission spectra for all the studied species, up to 21 times the fluorescence intensity of the free ligand (see *Figure 3.3(b))* for DCHQ5). This can be explained by the fact that both PPT and PET are inhibited by complexation.[26e,f] Titrations with Zn^{2+} and Cd^{2+} induced even

higher fluorescence relative intensity changes, up to a further enhancement factor of 3 compared to the values obtained for Mg^{2+}, showing similar binding constants (*Table 3.1*).

Table 3.1: photophysical properties of DCHQ1–6 and their complexes in CH_3OH–MOPS.

Compound	***LogK$_a$***	***Absorption***	***Fluorescence***	
		λ_{max} / nm (ε / $M^{-1}cm^{-1}$)	λ_{max} / nm	Φ
DCHQ1	-	244 (79000), 311 (5200)	505	$6.4\cdot10^{-5}$
DCHQ1·Mg^{2+}	5.02 ± 0.08[(a)],10.2 ± 0.2[(b)]	244 (65000), 318 (4600)[(a)]	506	$2.3\cdot10^{-2}$
DCHQ1·Zn^{2+}	5.85 ± 0.06[(a)]	261 (58000), 370 (4200)	519	$2.0\cdot10^{-2}$
DCHQ1·Cd^{2+}	9.39 ± 0.05[(b)]	263 (138000), 375 (11500)	519	$3.2\cdot10^{-2}$
DCHQ3	-	246 (77000), 316 (6300)	510	$1.0\cdot10^{-4}$
DCHQ3·Mg^{2+}	10.1 ± 0.1[(b)]	246 (129000), 330 (10500)	513	$7.7\cdot10^{-3}$
DCHQ3·Zn^{2+}	6.12 ± 0.07[(a)]	263 (59000), 376 (5500)	528	$1.8\cdot10^{-2}$
DCHQ3·Cd^{2+}	9.53 ± 0.05[(b)]	264 (140000), 379 (15000)	524	$2.4\cdot10^{-2}$
DCHQ4	-	247 (70000), 315 (6700)	463	$5.7\cdot10^{-5}$
DCHQ4·Mg^{2+}	11.2 ± 0.4[(b)]	246 (132000), 319 (12000)	513	$6.7\cdot10^{-3}$
DCHQ4·Zn^{2+}	6.5 ± 0.2[(a)]	263 (52000), 374 (6000)	525	$1.4\cdot10^{-2}$
DCHQ4·Cd^{2+}	9.30 ± 0.06[(b)]	264 (126000), 378 (16500)	525	$1.6\cdot10^{-2}$
DCHQ5	-	249 (81000), 330 (9000)	512	$1.0\cdot10^{-4}$
DCHQ5·Mg^{2+}	5.08 ± 0.06[(a)]	249 (66000), 338 (8500)	517	$2.4\cdot10^{-2}$
DCHQ5·Zn^{2+}	6.6 ± 0.2[(a)]	263 (69000), 386 (7600)	551	$1.4\cdot10^{-2}$
DCHQ5·Cd^{2+}	9.4 ± 0.2[(b)]	265 (177000), 388 (23500)	544	$2.1\cdot10^{-2}$
DCHQ6	-	246 (83000), 317 (6900)	504	$1.1\cdot10^{-4}$
DCHQ6·Mg^{2+}	4.8 ± 0.4[(a)], 9.9 ± 0.1[(b)]	245 (92000), 312 (8500)[(a)]	514	$9.8\cdot10^{-3}$
DCHQ6·Zn^{2+}	5.80 ± 0.09[(a)]	263 (66000), 376 (6200)	528	$1.5\cdot10^{-2}$
DCHQ6·Cd^{2+}	8.91 ± 0.06[(b)]	264 (202000), 379 (22000)	533	$1.2\cdot10^{-2}$

[a] Value obtained for 1:1 metal-to-ligand stoichiometry. [b] Value obtained for a 1:2 metal-to-ligand stoichiometry

However, these ions are not expected to cause substantial interference in total intracellular Mg determination, since:

1) the intracellular Zn^{2+} concentration is around 100 times lower than that of Mg^{2+} and, moreover, most of Zn^{2+} is bound to zinc fingers with particularly high association constants;[28]
2) cadmium is not present in non-poisoned cells.

The fluorescence quantum yields of the complexes of the new DCHQ derivatives with Mg^{2+} are similar or lower than that measured for DCHQ1 (0.023), ranging from 0.024 to 0.007 in hydroorganic solvent (*Table 3.1*). It is worth to notice, however, that the fluorescence of these hydroxyquinoline-based compounds depends on the environment and becomes higher increasing its lipophilicity.[26,27] As an example, the fluorescence quantum yield of compound DCHQ5 increases from 0.024 to 0.029 on going from MeOH–H_2O (1:1) solutions to micellar systems. Results obtained in MeOH–H_2O (1:1) solution buffered at pH 7.4 with MOPS are thus not representative of the highly complex cellular environment, in which instead the

aromatic compounds DCHQ5 and DCHQ6 showed the highest fluorescence in flow cytometry, fluorescence spectroscopy and confocal microscopy (*see 3.1.2.2-4*).

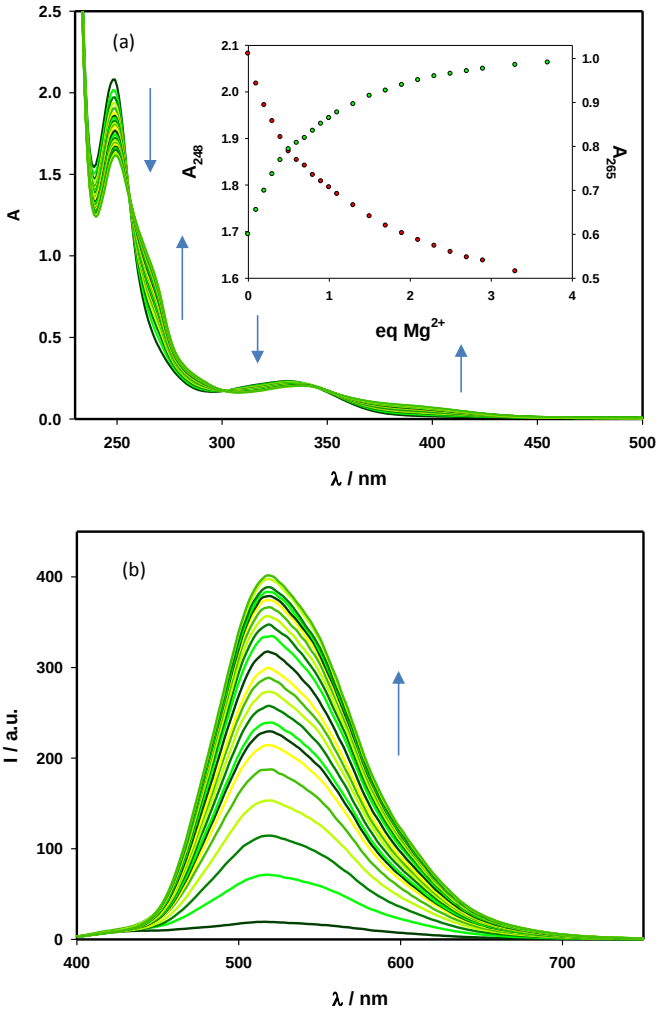

Figure 3.3: absorption (a) and emission (b) spectra of DCHQ5 (25 µM) in MeOH:H_2O (1:1) buffered at pH 7.4 with MOPS at room temperature upon addition of increasing amounts of Mg^{2+} ions (from 0 to 4 equivalents).

3.1.2.2 Intracellular and extracellular distribution

To analyze the fluorescence characteristics of the new probes in biological samples, we exploited fluorimetric methods to evaluate the repartition of each probe between intra- and extracelluar compartments. HL60 cells, loaded with different concentrations of each DCHQ derivative and counterstained with propidium iodide (PI), were analyzed by flow cytometry to discriminate live cells from damaged ones and selectively analyze the intracellular fluorescence of the chemosensors. Each compound has been tested for cell staining at several concentrations (5–25 µM) in order to identify the concentration range allowing the best compromise between high signal/noise ratio and low cytotoxicity. *Figure 3.4* reports, for each chemosensor, one cytogram representative of the most suitable staining conditions for HL60 cells: PI-positive cells (quadrant A) are distinct from cells with high DCHQ fluorescence (quadrant D), which confirms that all the DCHQ derivatives selectively stain live cells. After about 30 min from loading, DCHQ3, with the AM groups, seems to be well tolerated by the cells at a loading concentration of 10 µM, which resulted in a good fluorescence signal (*Figure 3.4*, panel 1). DCHQ4 is poorly soluble due to its long

aliphatic side chains, therefore a loading concentration of 5 µM was used. In these conditions, DCHQ4 was less fluorescent but still detectable (*Figure 3.4*, panel 2). The aromatic compounds DCHQ5 and DCHQ6 (*Figure 3.4*, panels 3 and 4 respectively) were highly cytotoxic at a loading concentration of 10 µM or higher. However these probes showed a strong fluorescence enhancement with respect to the other DCHQ derivatives: thus a good fluorescence signal was obtained at a loading concentration of 5 µM, at which a very low cytotoxicity was measured. Interestingly, for the phenyl-based probe DCHQ5 the fluorescence signal could be satisfactorily excited by UV as well as visible (488 nm) wavelengths. To verify the sensitivity of DCHQ5 in detecting changes in total cell Mg contents upon UV or visible excitation, we compared the fluorescence distribution of control and DMSO-treated HL60 cells. It is well known that upon differentiation (1.3% DMSO) this cell line undergoes a sizeable decrease of total intracellular Mg (around 50% decrease after 3 days of treatment).[29]

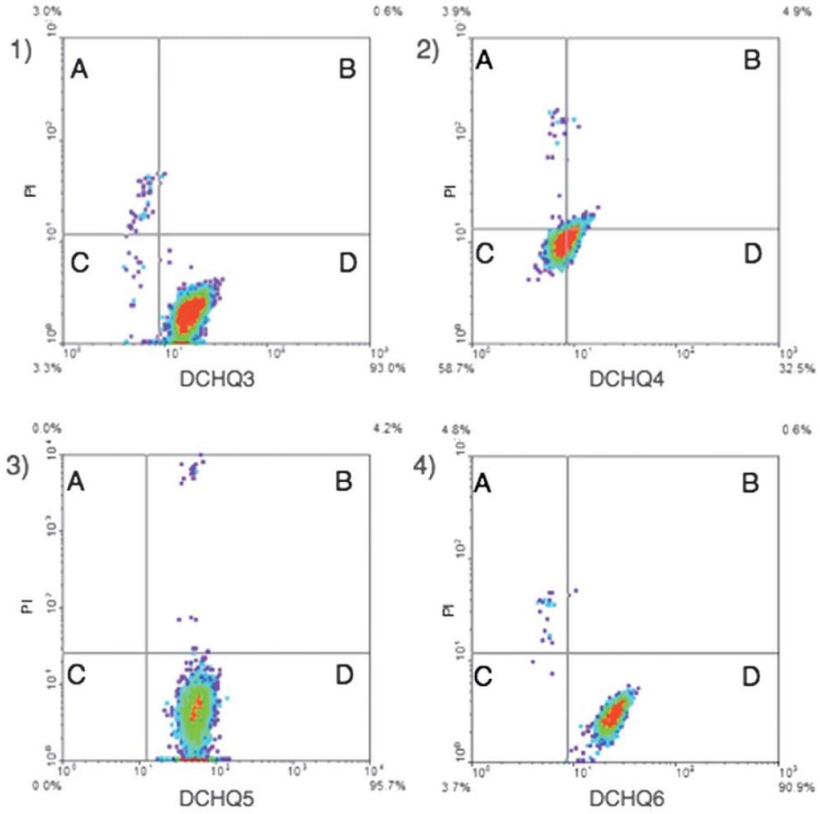

Figure 3.4: cytograms of HL60 cells ($5 \cdot 10^5$ cells mL^{-1}) loaded with each DCHQ derivative at the most suitable concentration (DCHQ3: 10 µM, panel 1; DCHQ4: 5 µM, panel 2; DCHQ5: 5 µM, panel 3; DCHQ6: 5 µM, panel 4) and PI 10 µM analyzed after 30 min of incubation in the dark at room temperature. Quadrant A: PI-positive/damaged cells with low DCHQ fluorescence; Quadrant D: PI-negative/viable cells with high DCHQ fluorescence. The percentage of cell population is indicated in each quadrant. Results from a typical experiment.

We assessed the differentiation process by a flow cytometric assay of cellular DNA content, which revealed that upon DMSO treatment 80% of HL60 cells were in the G0/G1 phase compared to the 45% of control cells. *Figure 3.5* reports the fluorescence distributions of DCHQ5 in control and differentiated HL60 cells: DMSO-induced growth arrest led to a decrease in fluorescence detected both by UV (panel A) and visible (panel B) excitation, which is consistent with the expected decrease in total cellular Mg content upon differentiation. Moreover, UV and visible excitation provided essentially the same output in terms of fluorescence mean channels (*Figure 3.5*). Since almost any confocal microscope and the large majority of cytofluorimeters are equipped with a 488 nm laser, our results suggest that DCHQ5 can provide a ready to

use, sensitive and versatile tool for qualitative evaluation of total cell Mg content, competitive with the previously proposed DCHQ1.[22]

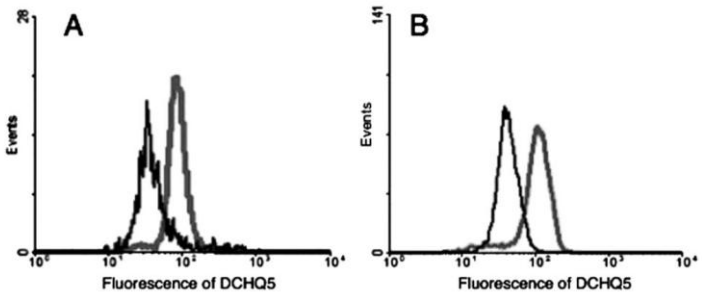

	Fluorescence Mean Channel	
	Ctrl	DMSO-treated
UV excitation	84	45
visible excitation	93	43

Figure 3.5: fluorescence distributions of control (grey, right distribution) and DMSO-differentiated (black, left distribution) HL60 cells (10^6 cells mL^{-1}) loaded with DCHQ5 (5 μM). Panel A: fluorescence distributions acquired with UV excitation; panel B: fluorescence distributions acquired with visible excitation (488 nm). Results from a typical experiment.

3.1.2.3 Intracellular uptake

We used fluorescence spectroscopy to further investigate cell loading and the distribution of the probes between cells and medium. The amount of each DCHQ derivative inside the cells was calculated by difference, measuring the total fluorescence intensity of each probe in the cell suspension (F_{cells}) and then the residual fluorescence in the supernatants after centrifugation ($F_{supernatant}$), as shown in *Figure 3.6*.
The probe distribution between cells and medium was studied for each DCHQ derivative at its optimal loading concentration derived from the cytofluorimetric measurements previously discussed (*Figure 3.4*). For DCHQ1 we found that about 75% of the probe was present within the cells (*Figure 3.6*). Our previous observation that the probe redistributed almost equally between cells and medium can be ascribed to impurities accompanying DCHQ1 when synthesized with the classical method.[22] Only 60% of the hydrophobic derivative DCHQ4 was retained inside the cells, while all the other probes showed an improved retention with respect to the parent dye DCHQ1. This result, combined with the cytofluorimetric observation that cells loaded with DCHQ4 show a shift towards the PI-positive quadrant (*Figure 3.4*, panel 2), led us to hypothesize that DCHQ4 could induce membrane permeabilization, which limits its use for long time-course measurements. With the insertion of the AM groups a significantly improved uptake was achieved for DCHQ3, since over 85% of the probe was retained in the cell suspension. As previously reported, the fluorescence response of the aromatic dyes (DCHQ5 and DCHQ6) in aqueous solution and DPBS was low. Therefore, to obtain a good fluorescence response in the cell suspension and in the supernatant, we assessed total fluorescence intensities by adding directly in a cuvette an equal amount of MeOH–H_2O (1:1) buffered at pH 7.4 with MOPS. Following this procedure we were able to calculate that about 80% of DCHQ6 and over 95% of DCHQ5 was retained in the cell suspension after washing (*Figure 3.6*). Taken together, these data suggest that, the insertion of an AM group is not necessary to enhance cellular retention of the DCHQ compounds, since the introduction of aromatic substituents on the core structure of DCHQ1 is sufficient. Typically the AM-probes, and thus also DCHQ3, exist inside the cells in two different species (hydrolyzed and non-hydrolyzed). This represents an obvious disadvantage for a correct assessment of total intracellular magnesium.

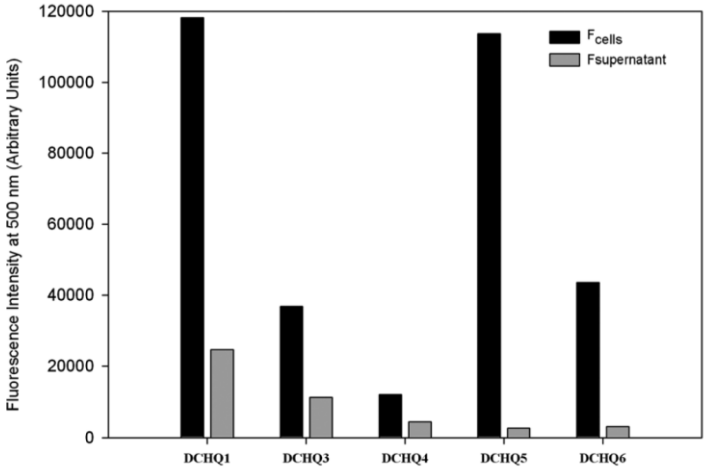

Figure 3.6: fluorescence intensities at 500 nm (λ_{exc} = 360 nm) of intact HL60 cells (10^6 cells mL^{-1}) loaded with each DCHQ derivative (DCHQ1 25 µM; DCHQ3 10 µM; DCHQ4 5 µM; DCHQ5 5 µM; DCHQ6 5 µM). F_{cells} (black bars) represents the total fluorescence of the probe in the cell suspension, registered upon addition of $MgSO_4$ 8 mM. $F_{supernatant}$ (grey bars) represents the total fluorescence of the probe that is not retained after washing, obtained upon addition of $MgSO_4$ 8 mM to the supernatants. Data collected in DPBS for DCHQ1, DCHQ3 and DCHQ4; data collected in DPBS plus an equal amount of MeOH–H_2O buffered at pH 7.4 with MOPS for DCHQ5 and DCHQ6. Results from a typical experiment.

3.1.2.4 Mapping intracellular distribution of Mg by two-photon confocal imaging

We tested the newly synthesized compounds by two-photon imaging to exploit their advantageous photochemical properties in the study of intracellular total Mg distribution. Excitation of the probes in the UV region was achieved by quasi-simultaneous absorption of two photons at a longer wavelength (750 nm). Compared to conventional confocal microscopy, two-photon excitation allows higher depth resolution and lower photodamage and photobleaching, thus extending the possible window for measurements.[30] Even though the parent probe DCHQ1 was not specifically designed for two-photon microscopy, it is the first published example of two-photon excitable Mg^{2+} probe:[22] a good staining of live cells was achieved in spite of the non-optimal photophysical properties of the compound. Recently, other promising two photon specific Mg^{2+} probes have been synthesized and efficiently used to stain brain tissues: these compounds, however, can only detect free Mg^{2+} ions and do not provide information about the distribution of its bound species.[31] *Figure 3.7* compares the fluorescence intensity and distribution of cells loaded with each of the DCHQ derivatives in DPBS without Mg^{2+}. In all the samples, and according to what has been previously published for DCHQ1,[22] fluorescence appeared to be diffused over the cytosol, with a higher signal in correspondence to the perinuclear region, where most of intracellular organelles and particularly mitochondria, are located. This is in agreement with the hypothesis that intracellular magnesium stores exist inside the cells.[22,32] Cells loaded with the AM-derivative DCHQ3 (*Figure 3.7*, panel B) were much less fluorescent than those stained with DCHQ1 (*Figure 3.7*, panel A): this compelled us to increase the gain of the photomultipliers during image acquisition and that caused a higher noise. This behaviour partly depends on the fact that DCHQ3 is less fluorescent than DCHQ4–6, but more cytotoxic than the parent dye DCHQ1 and its optimal loading concentration for staining living cells has to be lower than that of DCHQ1 (i.e. 10 µM instead of 25 µM), as a consequence of the cytofluorimetric assays previously discussed.

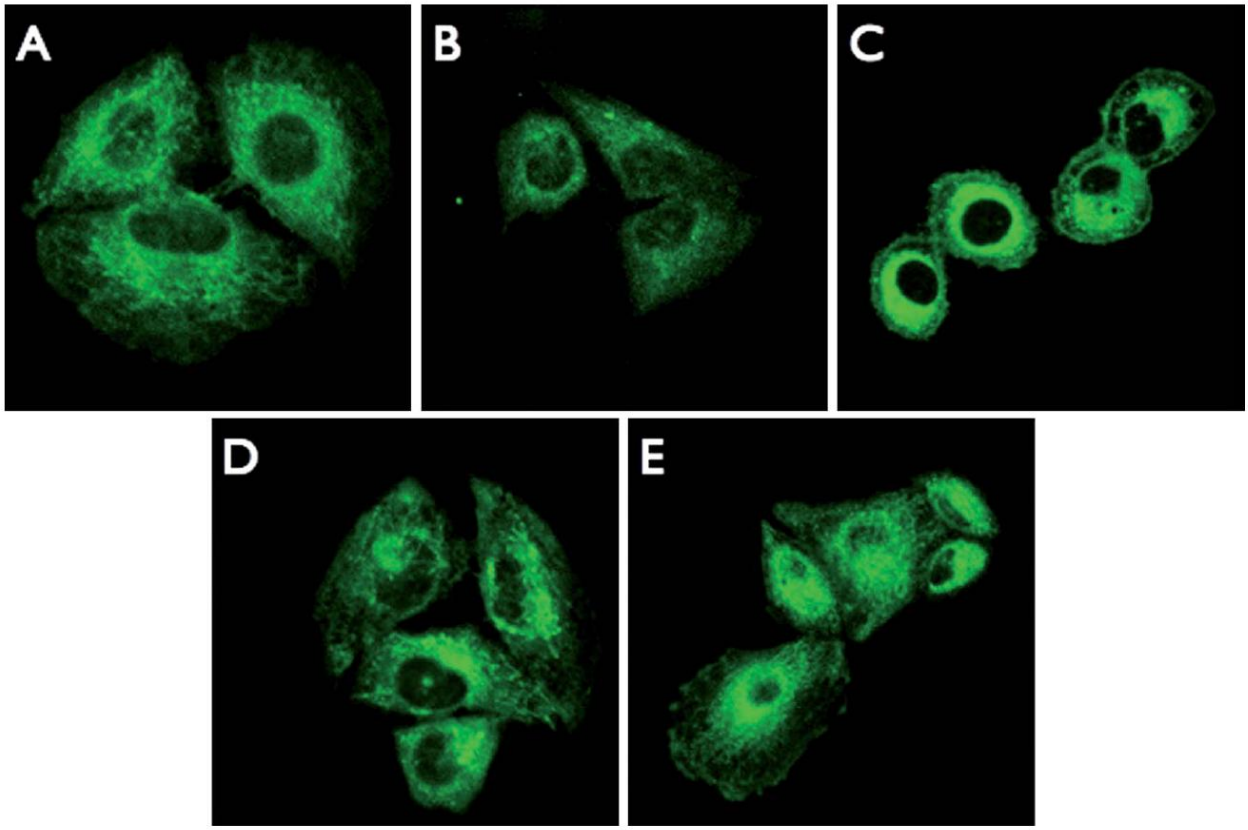

Figure 3.7: two-photon fluorescence microscopy images (λ_{exc} = 750 nm, as detailed in the Experimental section) of ROS rat osteosarcoma cells stained with DCHQ1 (25 µM, panel A), DCHQ3 (10 µM, panel B), DCHQ4 (5 µM, panel C), DCHQ5 (10 µM, panel D) and DCHQ6 (5 µM, panel E).

Figure 3.7 panel C displays the fluorescence intensity of cells loaded with DCHQ4 at a loading concentration of 5 µM in DPBS without Mg^{2+}: this dye was specifically synthesized with two long hydrophobic side chains to improve the staining of the cellular membranes. As expected, both the plasma and the intracellular membranes were more defined compared to DCHQ1 as well as the AM-derivative DCHQ3. Moreover, almost no fluorescence was found in the cytoplasm or inside the nucleus, revealing the preference of the probe for the lipophilic environment. For this reason, despite its poor cell retention, DCHQ4 appears a good tool for the static detection of membrane Mg^{2+} content, that is a goal of great importance.[33] However, for studying Mg^{2+} fluxes from plasma membrane binding sites in response to appropriate stimuli, a new highly retained DCHQ derivative needs to be designed. Finally, cells loaded with 5 µM of the aromatic dyes DCHQ5 and DCHQ6 (*Figure 3.7*, panels D and E respectively) were significantly more brilliant than cells loaded with the other DCHQ derivatives: as expected, fluorescence was diffused over the cytosolic portion with a higher intensity in the perinuclear region. Cells loaded with either DCHQ5 or DCHQ6, but not DCHQ1, yielded good fluorescence signals also for the plasma membranes, and therefore more defined images were obtained. Thanks to their large fluorescence enhancement, DCHQ5 and DCHQ6 could also allow imaging of thick tissues. In particular, the phenyl-derivative DCHQ5 presents unique characteristics:

1) higher fluorescence than any other DCHQ derivative;
2) fluorescence signal stable up to 30 min;
3) high retention within loaded cells;
4) excitation possible both in the UV and visible wavelength regions;
5) good imaging of membranes by two-photon microscopy.

For all of these features, DCHQ5 appears to be a valuable candidate in integrating the information obtained from commercial probes for free Mg^{2+} to better understand the homeostasis of this important element.

3.1.3 Conclusion

The optimization of the synthesis of DCHQ compounds allowed a more flexible approach to generate a panel of substituted derivatives with improved fluorescence, uptake and selective localization to overcome some of the limitations in the application of DCHQ1. As expected, the AM-probe DCHQ3 showed a high intracellular retention, which was unexpectedly higher in the aromatic probes DCHQ5 and DCHQ6. These dyes also revealed the highest fluorescence enhancement after magnesium binding. The hydrophobic derivative DCHQ4 yielded a specific staining of the cell membranes, although its applicability is limited by its poor retention inside the cells. Our results show the potential of these new fluorescent compounds in providing a versatile approach to the study of total intracellular Mg distribution and homeostasis in whole cells. In particular, the aromatic probe DCHQ5 presents the most promising characteristics, such as a high fluorescence response to cation binding, membrane staining and the possibility to be excited both in the UV and visible spectrum. For these reasons, we believe that this magnesium probe can be successfully employed in a wide variety of fluorescence measurements, helping to shed light on the role of this important element. In general, our results are of great importance for the design of increasingly efficient probes, a task we are currently working at.

3.2 Analytical applications

DCHQ5, the phenyl derivative belonging to the family of DCHQs, was found to be suitable for the quantitative assessment of total intracellular Mg content. The results showed comparable results with respect to those obtained with atomic absorption spectroscopy (AAS).

3.2.1 Introduction

DCHQ1, the first member of this family, binds Mg^{2+} with much higher affinity than any other available probe (having a K_d = 44 μM) showing a strong fluorescence increase upon complexation. Remarkably, its fluorescence is not significantly affected either by other divalent cations, most importantly Ca^{2+}, or by pH changes within the physiological range.[18,22] DCHQ1 readily permeates cells, binds intracellular Mg^{2+}, and it has been employed to map intracellular ion distribution and movements in live cells by confocal imaging.[34,35] Furthermore, this probe has been shown to be a suitable analytical tool capable to quantitatively assess the total intracellular magnesium in different cell lines[23] providing comparable results to AAS. Besides the unquestionably analytical value of DCHQ1, some limitations of this probe have restricted its application. Indeed, its poor retention inside the cell prevents its application for monitoring Mg intracellular uptake to study the Mg-channel activity upon stimuli[23] or in mutant cells with impaired Mg-channel activity.[36] Particularly interesting features were observed for the derivative bearing a phenyl group as a substituent in position 5 of each hydroxyquinoline arm, named DCHQ5 (see *Figure 3.1*), that showed improved characteristics compared to DCHQ1 such as higher response to cation binding, membrane staining, a much higher intracellular retention and the possibility to be excited both in the UV and visible spectrum range.[37] However, due to its very low solubility in aqueous buffers such as phosphate buffered salines (DPBS buffers), the photophysical characterization of DCHQ5 was performed in methanol-

based buffers.[37] This indeed precludes the possibility to use a K_d for a quantitative analytical protocol for the intracellular Mg assessment like the one employed for DCHQ1.[22] On the other hand, in DPBS, even when incubated with cells, we found a very good staining. In fact, measurements by flow cytometry on leukemic cells, both differentiated and not, showed that the distribution of fluorescence intensity of DCHQ5 strongly correlates with the total magnesium content assessed by AAS.[37] Nevertheless, the possibility to quantitatively assess the intracellular total Mg by DCHQ5 still remained to be established. Thus we thoroughly investigated the analytical performance of DCHQ5 for the quantitative assessment of intracellular total Mg content. To accomplish this task, we chose to compare the results obtained with DCHQ5 with the parent probe DCHQ1 and flame AAS, one of the most common routinely used analytical techniques. Furthermore we tested different protocols in several cell lines both by flow cytometry and by steady state fluorescence spectroscopy assays.

3.2.2 Results and discussion

We reported that DCHQ5 shows an appreciable increase in fluorescence intensity in the presence of Mg ions in MeOH:MOPS.[37] However, the buffer of choice in mammalian cellular investigation is Dulbecco's Phosphate Buffered Saline (DPBS) which mimics the extracellular environment, as far as Na^+, K^+ and phosphate ionic species concentrations. Other simpler saline buffers are proposed in the literature for other magnesium dyes, such as the MOPS:KCl buffer.[35,38] For a complete characterization we have investigated the performance of our two probes in the three buffers mentioned above and we also acquired the absorption spectra of both dyes under all conditions. MeOH:MOPS was found to be the most suitable buffer to perform a comparison of the two probes, as it showed a solubility in the micromolar concentration range. We report in *Figure 3.8* the titration profiles of the chemosensors in the presence of increasing amounts of Mg^{2+} in MeOH:MOPS and also in DPBS for DCHQ1. Due to the different luminescence quantum yields of the Mg complexes formed with our two dyes, the comparison was performed using each probe at its optimal concentration (DCHQ1 25 µM and DCHQ5 10 µM) in order to optimize the signal to be measured.[37] *Figure 3.8* shows that DCHQ5 had a higher response (steeper slope) and higher fluorescence intensity for all the Mg concentrations than DCHQ1. It is worth noting that fluorescence intensities are reported normalized by the concentration of the respective probe. Therefore these results indicate that the better performance of DCHQ5 was obtained even when using a much lower amount than DCHQ1.

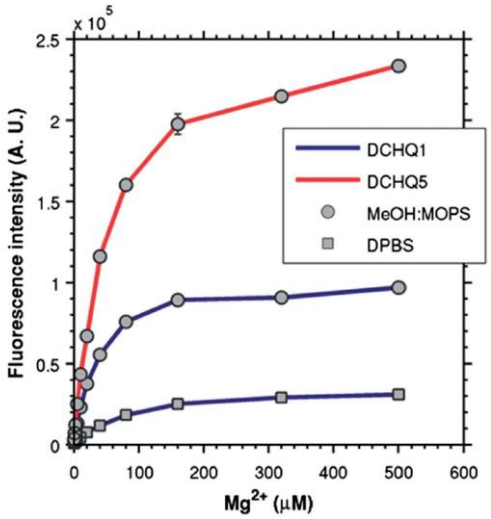

Figure 3.8: fluorescence intensity of DCHQ1 (blue) and DCHQ5 (red) at 500 and 510 nm respectively in MeOH : MOPS reported as a function of Mg concentration. Titration of DCHQ1 in DPBS is also reported for comparison. The

fluorescence intensities are normalized by dividing by the concentration of the respective probe (25 μM for DCHQ1 and 10 μM for DCHQ5).

We also evaluated the stability over time of the fluorescence of DCHQ1 and DCHQ5 at two different concentrations of magnesium, having a Mg:dye ratio of 1:2 and 100:1 in MeOH:MOPS and in DPBS. *Table 3.2* reports the percentage of fluorescence attenuation after 30 minutes of continuous exposure to the excitation light for the two chemosensors. The signal decrease in MeOH:MOPS is similar for the two dyes. Since the buffer employed in the standardized analytical protocol for the intracellular Mg assessment by DCHQ1 is DPBS, we also performed the stability test of DCHQ1 under these conditions. The results showed a marked decrease of fluorescence at the Mg:dye ratio of 1:2, used in the previously proposed intracellular Mg assay protocol. However, to perform assays in cells it is required to use a physiological buffer. The presence of MeOH obviously has a detrimental effect, due to the permeabilisation effect of this solvent on cell membranes. Therefore, we decided to design a new protocol to quantitatively assess intracellular total magnesium in sonicated cellular samples by using a simple spectrofluorimetric assay, based on a standard titration curve. DCHQ1 was dissolved in DPBS, which is also the buffer of the sonicated samples, while DCHQ5 in MeOH:MOPS with 10% of DPBS. It is worth underlining that the assay based on DCHQ5, due to its high fluorescence intensity, requires the use of a concentration of 15 μM, against the 25 μM of DCHQ1. The quantitative assessment of total magnesium in different cell types was performed by comparing the fluorescence intensities of sonicated cells suspended in DPBS to the fluorescence intensities registered for the relative standard curve. Results indicated that DCHQ5 can quantitatively assess intracellular total magnesium in cellular samples of the order of $30–50 \cdot 10^3$ cells per mL, while the minimum cells per mL size in which the DCHQ1 probe can be used is $100 \cdot 10^3$.

Table 3.2: percentage decrements of fluorescence intensity of the two chemosensors after 30 minutes of continuous exposure to the excitation light at 500 nm for DCHQ1 and at 510 nm for DCHQ5.

Mg:dye	1:2	100:1
DCHQ1 in MeOH:MOPS	19%	4%
DCHQ1 in PBS	44%	2%
DCHQ5 in MeOH:MOPS	15%	8%

We compared the data obtained, in a total of 24 cell samples, using DCHQ5 and DCHQ1, with the ones given by AAS, chosen, as previously motivated, as the reference technique for the quantification of total intracellular magnesium (*Figure 3.9*). Statistical analysis showed that the data could be well fitted with linear equations and we also found a good correlation between the datasets given by the two techniques for both probes, DCHQ5 presenting the closest values to the identity line. The 95% confidence interval values of linear regressions are somewhat smaller for DCHQ5 than DCHQ1 being 0.17 and 0.26 respectively for the slope and 4.27 and 7.09 for the intercept. We also performed a paired and unpaired t-test between the dye fluorimetric assays and AAS. Results show no statistical difference in the unpaired t-test for both dyes, while DCHQ5 showed a $p < 0.01$ in the paired t-test. Taken together, these data demonstrate that the values of Mg concentration assessed by both dyes overlap the AAS measurements. The regression line equation of DCHQ5 has coefficients closer to the identity line than those of DCHQ1. However, the paired t-test analysis showed that DCHQ5 displays a positive systematic deviation from AAS measurements, as can be also noted by the comparison of the correlation with the identity line (*Figure 3.9*, right panel).

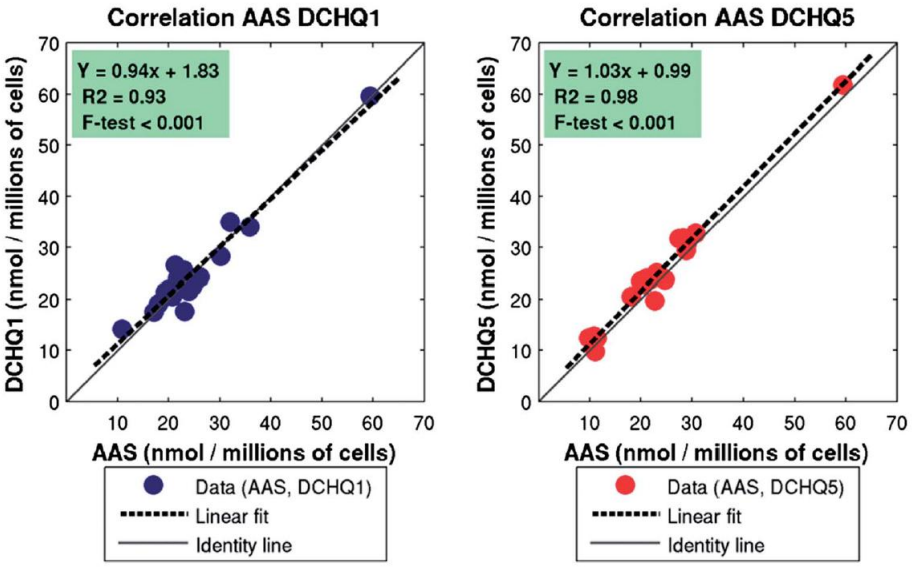

Figure 3.9: correlation between the total intracellular magnesium assessed by AAS and the value of fluorescence intensity obtained using DCHQ1 (left) or DCHQ5 (right). The identity line is plotted for comparison.

We then evaluated the Limit of Detection (LOD) for both chemosensors in the assay buffer (MeOH:MOPS + 10% of DPBS for DCHQ5 and DPBS for DCHQ1) and also in sonicated cellular samples (*Table 3.3*). The LOD of the two probes was similar for the cell population of $250 \cdot 10^3$ and $100 \cdot 10^3$. As already pointed above, DCHQ1 can be used in a sample size of at least $100 \cdot 10^3$ cells per mL, while DCHQ5 can quantify Mg in much smaller samples. Therefore, we could assess the LOD for DCHQ5 for cellular samples of even $50 \cdot 10^3$ cells per mL. It is interesting to note that the LOD of DCHQ5 for the lowest sample size, obtained with this simple fluorimetric procedure, is of the same order of the AAS one, a value of great analytical interest.

Table 3.3: limit of detection (LOD) of DCHQ1 and DCHQ5 reported in µM evaluated in the buffer solution and in the cell sample.

		Mg^{2+} LOD in µM sample size (cells per mL)		
Mg^{2+} LOD in µM in buffer solution		$50 \cdot 10^3$	$100 \cdot 10^3$	$250 \cdot 10^3$
DCHQ1	0.3	n.d	0.2	0.5
DCHQ5	0.2	0.2	0.2	0.5

Finally, we performed cytofluorimetric assays to evaluate the intracellular retention of DCHQ1 and DCHQ5 after washing, as well as their fluorescence stability over time. *Figure 3.10* reports the mean channel of DCHQ fluorescence of the viable population. The cytofluorimetric analyses show that the staining is quite stable up to 60 minutes for both probes with a maximum decrease of 20% for DCHQ5. The slight intracellular fluorescence decay of the probes over time is probably due to the suffering of cells suspended in a medium lacking of any energetic substrate leading to a decrease of intracellular magnesium. The DCHQ5 probe resulted to be much more efficiently retained within the cells than DCHQ1. It is worth noting that the DCHQ5 intracellular fluorescence change is almost negligible after the second washing. The overall fluorescence decrease of DCHQ5 is around 30% of the initial value. Conversely, DCHQ1 fluorescence decreases after the second washing, with a total decrement of 80% from the initial value. These results suggest that for DCHQ5 the first washing eliminates only the dyes loosely bound to the cellular surface, and

not the probe entrapped within the cell which, unlike DCHQ1, is not removed by the second washing. Finally, we would like to underline again that the amount of DCHQ5 required for the cytofluorimetric assays is one fifth than that for DCHQ1 (DCHQ5 5 µM and DCHQ1 25 µM). This indicates that DCHQ5 compared to DCHQ1 exhibits an analytical efficiency in cytofluorimetry even higher than that observed in fluorescence spectroscopy where the ratio of the dye concentration [DCHQ5]/[DCHQ1] was 1:2.5 (DCHQ5 10 µM and DCHQ1 25 µM).

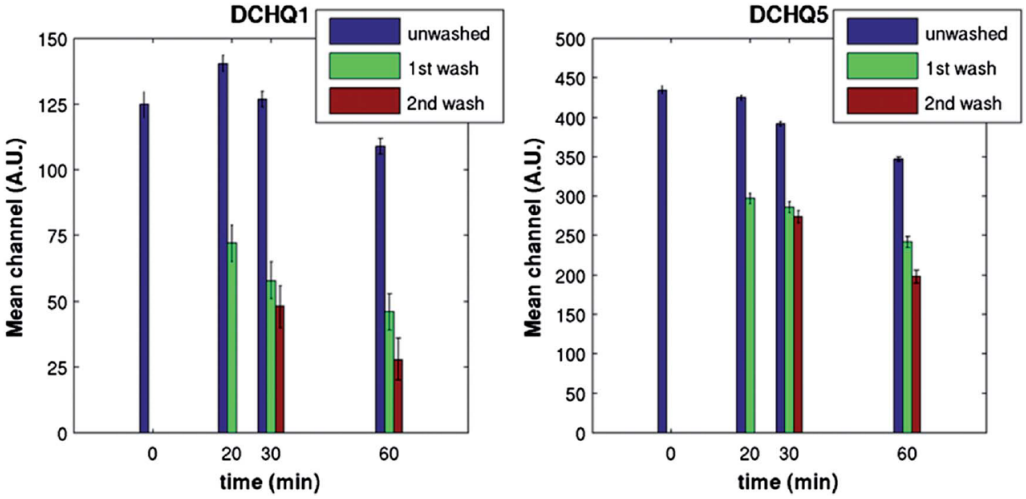

Figure 3.10: Mean channel of fluorescence distribution of cells stained with DCHQ1 (left) and DCHQ5 (right) and after washing, data were acquired over a time lapse of 60 minutes after staining. Experiments repeated three times. Data are expressed as mean ± SD.

3.2.3 Conclusion

This study showed the possibility to use the fluorescent chemosensor DCHQ5:

- to accurately quantify the intracellular total Mg with comparable performance than the reference species DCHQ1;
- to assess intracellular total Mg in much lower number of cells by loading a smaller amount of chemosensor in comparison with DCHQ1;
- in cytofluorimetric assays by loading a smaller amount of it, with the advantage of displaying a more stable intracellular staining after washing than DCHQ1.

All these features, combined with other remarkable characteristics such as the high fluorescence enhancement upon Mg^{2+} binding, the membrane staining and the possibility to be excited both in the UV and visible spectrum,[37] make DCHQ5 a valuable analytical tool for Mg assessment in biological samples.

3.3 Zinc sensing

3.3.1 Introduction

Zinc is a biologically essential element, being a structural constituent in numerous proteins, including growth factors, cytokines, receptors, enzymes and transcription factors belonging to cellular signalling pathways[39]. Zinc is the most abundant transition metal ion in the human body after iron, with a µM intracellular total concentration in eukaryotic cells. It has a great affinity to proteins, as approximately 10% of all proteins in the cells can bind to it and this makes the amount of free zinc, defined also as chelable or labile pool of zinc, very low (down to the picomolar concentration range[40]). Nevertheless, this free fraction plays a pivotal role in a number of cellular processes, such as in the neurotransmission activity (in synaptic vesicles[41] and, as second messenger[42], within the cells), in the regulation[43] of G protein-coupled receptors and in apoptosis, which is a fundamental process of many physiological and pathological functions. Despite its biological significance, much information on its activities is very recent and, even if the discovery of zinc transporters has expanded the understanding on zinc metabolism, still much remains to be elucidated. The reason of this apparent anomaly can be explained considering the physicochemical properties of zinc: it is a transition metal with a d^{10} electronic configuration, colourless, diamagnetic and, as a result, invisible to most spectroscopic methods. Therefore, zinc resulted to be elusive to most analytical approaches, which brought comparatively less insight into its biology than into that of, e.g. copper or iron [44]. Moreover, unlike iron, where 80% of its total concentration in humans is in the heme group, the corresponding fraction of zinc is spread among thousands of proteins. This dilution effect makes it even more difficult to establish the presence and the role of this ion in low-abundance proteins. This explains the present widespread interest of the scientific community in developing new species and methods to determine the concentration of Zn^{2+} in living cells[45], a crucial step for elucidating its biological roles. In particular, impressive research efforts are devoted to the design of fluorescent non-toxic zinc probes. The use of luminescent chemosensors, in fact, remains the election strategy to sense both *in vitro* and *in vivo* biologically relevant species[46,47], due to the relative simplicity and the very high sensitivity of these tools. These species, however, must meet many more requirements to provide an efficient detection, such as, to cite only the main ones, a high selectivity or specificity for the relevant target, a stable luminescent signal (high photochemical stability) not affected by environmental interferences and a high brightness[48]. Moreover, for an effective zinc sensing in cells, the probe must be non-toxic, sufficiently water soluble and the kinetics of the complexation–decomplexation event must be fast. Many different strategies have been proposed that take advantage of a variety of fluorophores[49] and receptor units[50] such as di-2-picolylamide, quinoline, bipyridine and polyamines, including many of their derivatives. In particular, 6-methoxy-8-p-toluenesulphonamidoquinoline[51] and Zinquin[52] are commercial species commonly used for zinc imaging in biological environments. Here, we propose three compounds, DCHQ7, DCHQ8 and DCHQ9 (*Figure 3.11*) obtained by conjugation of a diaza-18-crown-6 with a pair of different 8HQ derivatives. Interestingly, the results presented here show that an appropriate substitution can also increase the affinity for Zn ions, and, in particular, DCHQ9 revealed suitable characteristics to be considered for the application in biological zinc imaging.

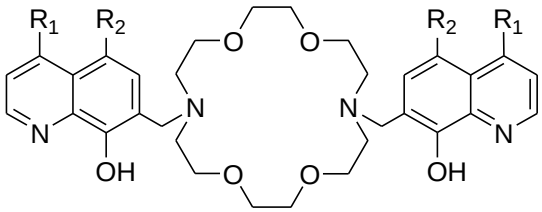

DCHQ7: R_1 = H, R_2 = CH_3
DCHQ8: R_1 = H, R_2 = CH_2OCH_3
DCHQ9: R_1 = OCH_3, R_2 = H

Figure 3.11: schematic representation of the molecular structure of chemosensors DCHQ7-9.

3.3.2 Results and discussion

3.3.2.1 Photophysical properties in aqueous solution

The absorption and emission spectra of the chemosensors DCHQ7-9 are, as expected, similar to those of the other DCHQs showed in *Paragraph 3.1*, so they are dominated by the contribution of the 8HQ derivatives present in their structure. The photophysical properties of this family of fluorogenic ligands, due to their wide use in analytical chemistry, have been intensively studied[26]. In particular, as shown in *Figure 3.12*, the absorption spectra of DCHQ7 and DCHQ8 in MeOH:H_2O (1:1) buffered at pH 7.4 with 3-morpholinopropane-1-sulphonic acid (MOPS) present an intense band at around 245–250 nm (ε = 53000–76000 $M^{-1}cm^{-1}$) and a broader less intense band in the 315–335 nm region (ε = 3500–7000 $M^{-1}cm^{-1}$). The former band can be attributed to a π–π* transition, while the latter band can be attributed to a charge transfer transition from the hydroxyl oxygen atom to the quinoline moiety[27]. Compound DCHQ9 shows a different behaviour because of the presence of the methoxy group in position 4, which causes an hypsochromic shift of both bands, so that the higher energy π–π* transition cannot be observed any longer in the transparent window of the solvent (λ < 230 nm).

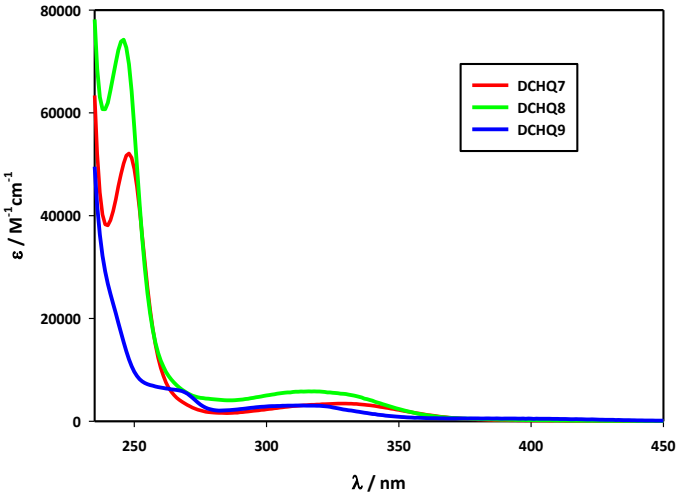

Figure 3.12: absorption spectra of DCHQ7 (red line), DCHQ8 (green line), DCHQ8 (blue line) in MeOH:H_2O (1:1) buffered at pH 7.4 with MOPS at room temperature.

Changing the substitution in position 5 induces modification in the spectra: the presence of a methyl group in DCHQ7 reduces the molar extinction coefficient with respect to DCHQ8. All the chemosensors show a weak emission band centred around 490–520 nm with a fluorescence quantum yield in the range of $1.3 \cdot 10^{-6}$–$7.1 \cdot 10^{-5}$, except for DCHQ9 (Φ = $3.3 \cdot 10^{-3}$) (see *Table 3.4*). According to literature[26], the low fluorescence quantum yield values of the substituted 8HQ can be ascribed to intramolecular photoinduced proton transfer (PPT) processes between the hydroxyl group and the nitrogen atom; in protic media,

intermolecular PPT processes involving solvent molecules lead to an even further decrease in fluorescence intensity[26a,b]. Moreover, in these kinds of structures, characterised by the presence of a tertiary amine close to the fluorogenic units, a photoinduced electron transfer (PET) between these two moieties generates an additional non-radiative pathway for the deactivation of the excited state. This family of compounds, however, is able to form complexes with metal cations with a selectivity and affinity that strongly depend on the substituents on the 8HQ moiety, and the complexation generally causes a fluorescence recovery blocking both PPT and PET processes[53].

Table 3.4: photophysical properties of DCHQ7-9 and their complexes in CH_3OH-MOPS.

			Fluorescence		
Compound	$\log K_a$[a]	Absorption λ_{max}/nm (ε/$M^{-1}cm^{-1}$)	λ_{max} (nm)	Φ[b]	τ_{ave}[c]/ns
DCHQ7	-	248 (53000)	518	$7.09\cdot10^{-5}$	-[d]
DCHQ7·Mg^{2+}	10.1 ± 0.3	249 (96000)	534	$6.51\cdot10^{-4}$	-[d]
DCHQ7·Zn^{2+}	10.0 ± 0.3	265 (99000)	546	$6.98\cdot10^{-3}$	1.9
DCHQ7·Cd^{2+}	9.63 ± 0.07	264 (95000)	548	$9.17\cdot10^{-3}$	2.4
DCHQ8	-	246 (73000)	510	$1.23\cdot10^{-6}$	-[d]
DCHQ8·Mg^{2+}	9.51 ± 0.06	261(89000)	514	$5.25\cdot10^{-2}$	7.8
DCHQ8·Zn^{2+}	9.6 ± 0.2	263 (169000)	544	$3.83\cdot10^{-3}$	3.1
DCHQ8·Cd^{2+}	9.2 ± 0.4	264 (179000)	542	$1.32\cdot10^{-2}$	3.8
DCHQ9	-	269 (9200)	490	$3.26\cdot10^{-3}$	-[d]
DCHQ9·Mg^{2+}	9.28 ± 0.04	252 (41000)	490	$1.74\cdot10^{-2}$	2.7
DCHQ9·Zn^{2+}	11.6 ± 0.2	253 (78000)	499	$9.10\cdot10^{-2}$	6.3
DCHQ9·Cd^{2+}	11.1 ± 0.2	253 (103000)	494	$1.04\cdot10^{-1}$	6.5

[a] For 1:2 metal:ligand complexes
[b] fluorescence quantum yield
[c] Average excited state lifetime
[d] Below instrumental resolution

For this reason, we proceed with a systematic study exploring the affinity of these chemosensors for a number of possible metal ions of biological importance, such as Zn^{2+}, Mg^{2+}, Cd^{2+}, Hg^{2+}, Cu^{2+}, Ni^{2+}, Na^{+}, K^{+}, Ca^{2+}, Fe^{2+} and Fe^{3+}. Very interestingly, the binding ability of compounds DCHQ7-9 presents many similarities. No changes, either in absorption or in emission spectra, were observed in the presence of an excess of Na^{+}, K^{+}, Ca^{2+}, Fe^{2+} and Fe^{3+}, indicating no or totally negligible affinity of the ligands for these ions. On the contrary, from the significant absorption spectral changes, it is clearly possible to observe that they are able to complex Hg^{2+}, Cu^{2+} and Ni^{2+} ions. In particular, this binding event leads to the decrease of the bands centred at 245–250 nm and at 315–335 nm and the appearance of new bands around 265 and 375–385 nm. This is a known and typical behaviour for 8HQ derivatives when they undergo a coupled deprotonation/complexation process. Nevertheless, the interaction with these cations did not lead to the formation of luminescent complexes. Similar changes in the absorption spectra have also been observed on addition of Zn^{2+}, Cd^{2+} and Mg^{2+} ions (see *Figure 3.13* for DCHQ9), but these three species induce a noticeable increase the emission intensity. The fluorescence enhancement is generally remarkably high, for example in the case of DCHQ9 upon addition of Zn^{2+} (see *Figure 3.14*) it is of 69 folds. As already mentioned, the complexation with these metal ions inhibits both PPT and PET processes, without

introducing other efficient non-radiative processes, such as heavy atom effects (typical of Hg^{2+}) or energy or electron transfer processes, as Cu^{2+} and Ni^{2+} typically can do[54].

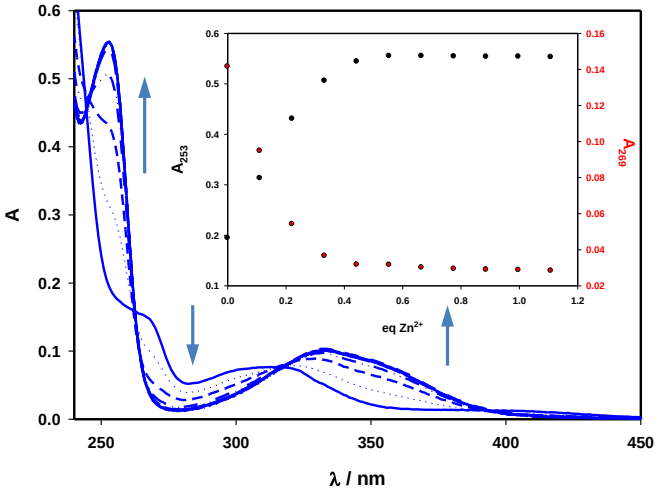

Figure 3.13: absorption spectra of DCHQ9 (25 µM) in CH_3OH:H_2O (1:1) buffered at pH 7.4 with MOPS at room temperature, upon addition of increasing amounts of Zn^{2+} ioni (from 0 to 1.1 equivalents). In the inset the absorbance at 253 nm (black circles) and at 268 nm (red circles) are reported.

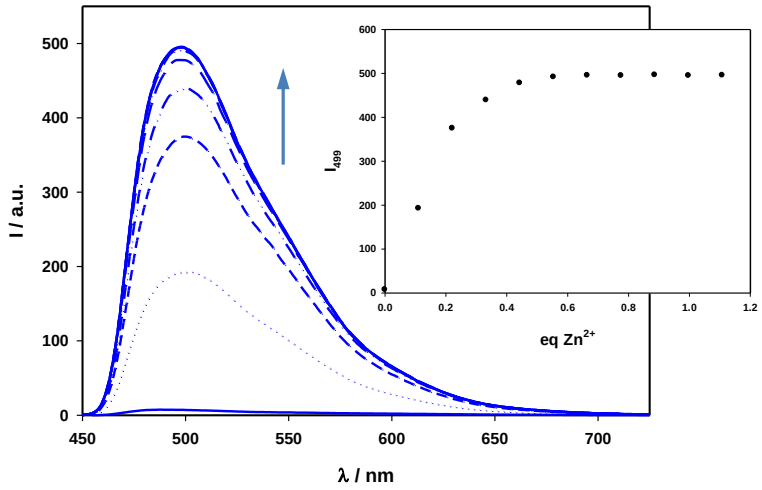

Figure 3.14: emission spectra of DCHQ9 (25 µM) in CH_3OH:H_2O (1:1) buffered at pH 7.4 with MOPS at room temperature, upon addition of increasing amounts of Zn^{2+} ions (from 0 to 1.1 equivalents). In the inset the emission intensity at 499 are reported.

It is also important to stress that Mg^{2+} ion represents the main interfering cation in intracellular zinc assessment due to its high concentration (about a 100-fold higher with respect to the Zn^{2+} ion). Therefore, as both chemosensors DCHQ7 and DCHQ8 have comparable association constant values for Mg^{2+}, Cd^{2+} and Zn^{2+} (*Table 3.4*), they could be seen as sensors for Mg^{2+} rather than for Zn^{2+} in physiological conditions. Conversely, DCHQ9 shows a clear specificity for Zn^{2+} with respect to Mg^{2+}, with an association constant higher of about two orders of magnitude, and a fluorescence quantum yield that, interestingly, follows the same trend (*Table 3.4*). The affinity of DCH9 for Cd^{2+}, instead, is very similar to the affinity shown for Zn^{2+}; however, cadmium ions should not be present at all in cells in physiological conditions, if not specifically poisoned by this precise pollutant. Taken together, these features indicate that DCHQ9 is a very promising candidate for sensing zinc ions in cells, and in particular the most promising among the new species herein studied.

3.3.2.2 Intracellular uptake

In this study, the chemosensors have demonstrated a good performance in zinc sensing in buffered mixed solution and we have, therefore, proceeded in testing their behaviour in cells. We have used promyelocytic leukaemic HL60 and osteosarcoma U2OS cells for two different reasons: the first is that HL60 can be rapidly differentiated by dimethylsulphoxide (DMSO) treatment, a procedure that is known to be able to drastically reduce intracellular zinc; the second is that U2OS cells, instead, can be a valuable model for microscopic investigations due to their large dimensions. The first parameter to check in biological environment is fluorescence, as an intense signal in solution not always corresponds to high luminescence intensity in more complex matrixes. Moreover, it is not possible, or at least easy, to correlate cytotoxicity with the molecular structure, and a direct experimental investigation is the only reliable approach to obtain precise data. Both these characteristics, together with cellular uptake, can be tested taking advantage of cytofluorimetric analysis. To this goal, we have used propidium iodide (PI)-counterstained HL60 cells.

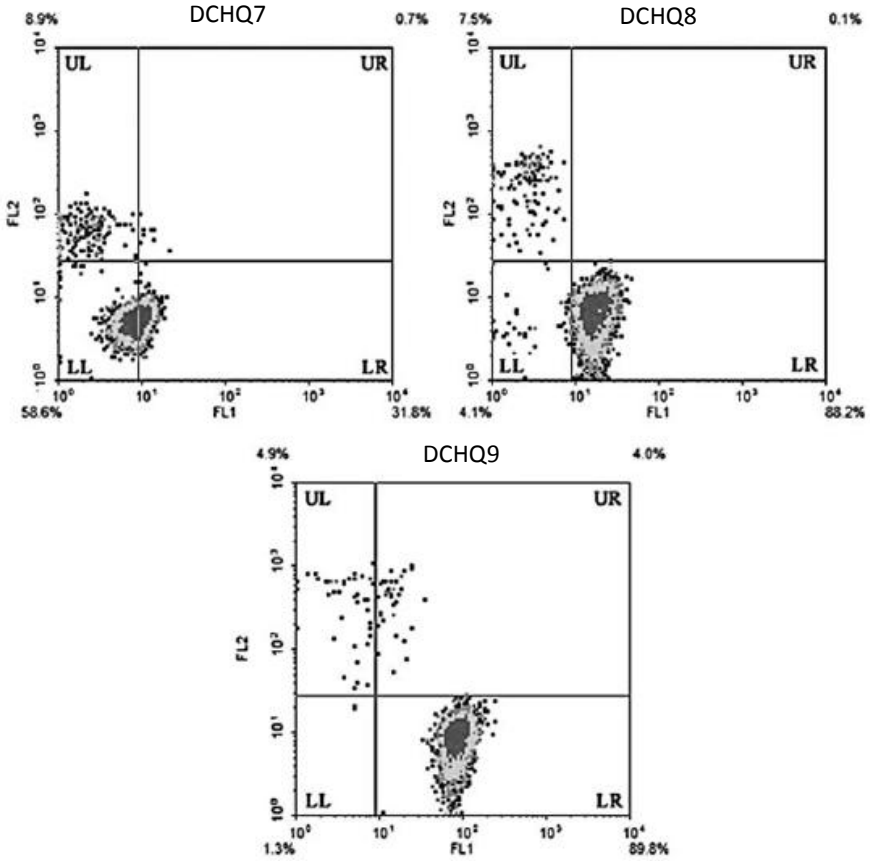

Figure 5. Cytograms of HL60 cells loaded with probes DCHQ7-9 and PI analysed after 15 min of incubation at room temperature. Quadrant LL: PI-negative/viable cells with low or any DCHQs fluorescence; quadrant LR: PI-negative/viable cells with high DCHQs fluorescence; quadrant UL: PI-positive/damaged cells with low DCHQs fluorescence; quadrant UR: PI-positive/damaged cells with high DCHQs fluorescence. The percentage of cell population is indicated at the external edge of each quadrant. HL60 cells $5 \cdot 10^5$ ml^{-1}; DCHQ7-9 20 µM; PI 10 µM. Data from a typical experiment, each was repeated three times with completely similar results.

This label, in fact, is able to enter only non-integer cell membranes, allowing to discriminate live from damaged cells. Four different samples were loaded with the same amount of the three probes (20 µM, for 15 min) following the same procedure, in order to analyse and compare their intracellular fluorescence. The cytograms are reported in *Figure 3.15* and clearly show that upon staining with DCHQ7, the majority of

the cells results in the Lower Left (LL) quadrant, which indicates a negative response for both PI and DCHQ signals. This can be explained with an overall negligible interaction of DCHQ7 with the cells. Different results were obtained with DCHQ8, which was able to penetrate the membrane of viable cells (high cell population of Lower Right (LR) quadrant), but is also characterised by a very low fluorescence intensity in this kind of environment, even at this relatively high concentration.

The best performance was obtained with DCHQ9 (*Figure 3.15*), which gave a high fluorescence intensity in live cells (quadrant LR), while dead cells (PI positive in the Upper Left (UL) and Upper Right (UR) quandrants) did not present any typical DCHQs fluorescence. This suggests that DCHQ9 is able to selectively and efficiently stain viable cells, and it does not induce significant damage in the cells (ca. 5% of the total are dead and this is very close to the physiological mortality in the experimental conditions). Taken together, these data indicate DCHQ9 as the most promising species among those studied and, consequently, our further investigations were focused on this probe. We have assessed in more detail the performances of DCHQ9, examining the dose dependence of fluorescence intensity and cell mortality. The results (*Figure 3.16*) clearly show that viable cells fluorescence intensity is strongly dependent on chemosensor concentration, while negligible cytotoxic effects could be revealed for all the tested doses, which are the typical ones used in cell imaging measurements. In order to qualitatively investigate the response of the chemosensor to zinc concentration variations, we have performed measurements with fluorescence microscopy and flow cytometry on cells with different zinc contents. As mentioned above, the promyelocytic HL60 can be induced to granulocytic differentiation quite easily by treatment with 1.3% DMSO for 5 days. We recently demonstrated[55] that this procedure decreases the total cellular zinc content of more than 50% cells (27 ± 3 ng/10^6 cells and 12 ± 1 ng/10^6 cells in normal HL60 cells and differentiated cells, respectively).

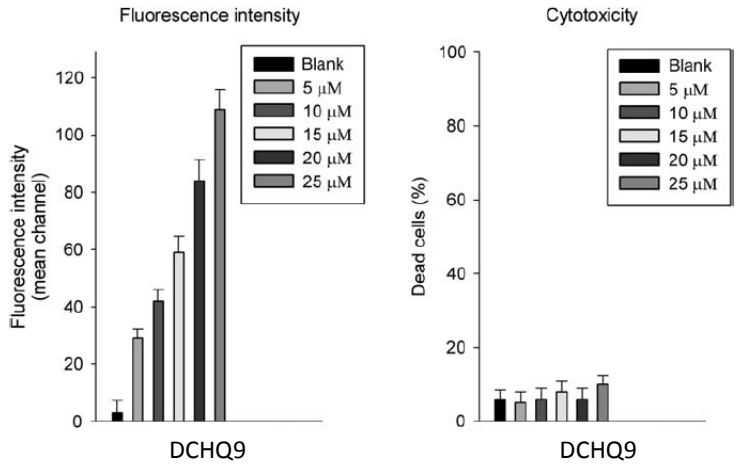

Figure 3.16: dose dependence of cellular fluorescence intensity, expressed as mean channel of the fluorescence distribution histogram of viable cells and cytotoxicity of DCHQ9. PI-stained (10 μM) HL60 cells ($5 \cdot 10^5$ ml^{-1}) were added with increasing amounts (legend) of DCHQ9.

We used DCHQ9 to stain two samples of control and differentiated HL60 cells. In the DMSO-treated cells, the fluorescence intensity of DCHQ9 decreased by a factor of about 2.5 (*Figure 3.17*), which is consistent with the decrease (2.3-fold) in zinc content that was measured by atomic absorption spectroscopy. Finally, to assess the specificity of probe DCHQ9 for zinc ions, we have stained both osteosarcoma-adherent U2OS cells and leukaemic HL60 cells before and after their treatment with N,N,N^1,N^1-tetrakis(2)[2-pyridylmethyl]-ethylenediamine (TPEN), which is a very well-known efficient zinc chelator.

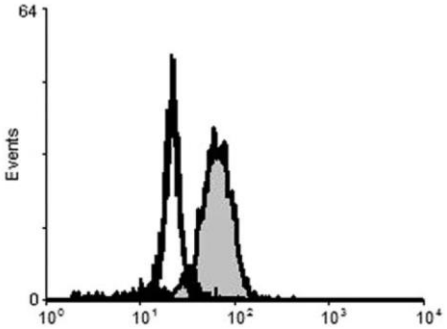

Figure 3.17: Fluorescence intensity distributions of HL60 cells stained with 20 µM of DCHQ9. Grey-filled distribution: control cells (mean channel 45); empty-distribution: DMSO-treated cells (mean channel 17). Data are from a typical experiment repeated three times with similar results.

It is evident from the microphotographs of U2OS, fixed cells reported in *Figure 3.18*, that control cells (*Figure 3.18(a)*) are noticeably brighter than TPEN-treated cells (*Figure 3.18(b)*). Similarly, the overlaid flow cytometry plots of control and TPEN-treated HL60 cells, stained with DCHQ9 [5 µM (*Figure 3.19(a)*) or 20 µM (*Figure 3.19(b)*)], evidence the drastic decrease of the fluorescence in the low zinc content samples.

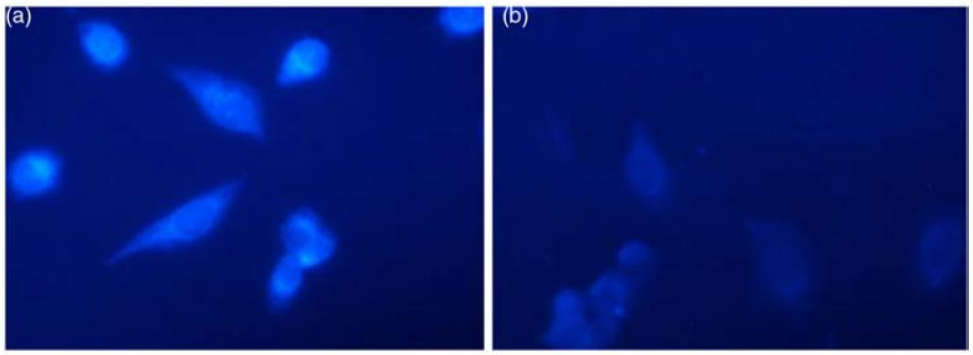

Figure 3.18: human osteosarcoma-adherent cells stained with DCHQ9 (15 µM) in absence (a) and in presence (b) of TPEN (100 µM).

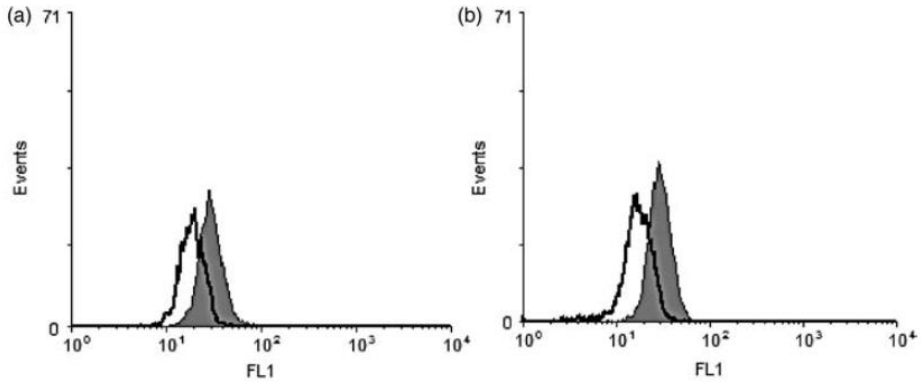

Figure 3.19: HL60 cells stained with DCHQ9 in absence (grey-filled distribution) and in presence (empty distribution) of TPEN (10 µM) for different concentration of DCHQ9: (a) 5 µM; (b) 20µM. Data are from a typical experiment repeated three times with similar results.

3.3.3 Conclusion

Among the different families of chemosensors for intracellular sensing of cationic species, the one based on DCHQ compounds is of particular interest. We have reported here, for the first time, on the sensing abilities, also in cell environments, of three of them. Interestingly, DCHQ9 shows properties making it a very promising candidate for effective Zn(II) ion detection, presenting a very low toxicity, Zn^{2+}/Mg^{2+} selectivity and a very large fluorescence enhancement upon complexation. Cytofluorimetric analyses of HL60-stained cells clearly indicate that DCHQ9 is able to permeate cell membranes without significantly affecting their mortality. All these aspects were confirmed by microscopy experiments performed on living cells, which also evidenced its ability to follow Zn(II) concentration variations. These results add new elements that can greatly support the design of increasingly efficient probes, a task that we are currently pursuing.

References and notes

The contents of this chapter are based on C. Marraccini, G. Farruggia, M. Lombardo, L. Prodi, M. Sgarzi, V. Trapani, C. Trombini, N. Zaccheroni, F.I. Wolf, S. Iotti, *Chem. Sci.*, **2012**, *3*, 727 – Reproduced by permission of The Royal Society of Chemistry, on A. Sargenti, G. Farruggia, E. Malucelli, C. Cappadone, L. Merolle, C. Marraccini, G. Andreani, L. Prodi, N. Zaccheroni, M. Sgarzi, C. Trombini, M. Lombardo, S. Iotti, *Analyst*, **2014**,*139*, 1201 – Reproduced by permission of The Royal Society of Chemistry, and on M. Sgarzi, M. Lombardo, C. Trombini, N. Zaccheroni, G. Farruggia, L. Merolle, A. Sargenti, S. Iotti, C. Marraccini, L. Prodi, *Supramol. Chem.*, **2013**, *25*, 7 – Reproduced with permission of Taylor and Francis Group.

[1] (a) F. I. Wolf, A. Cittadini, *Front. Biosci.*, **1999**, *4*, 607; (b) H. Rubin, *BioEssays*, **2005**, *27*, 311

[2] R. Eskes, B. Antonsson, A. Osen Sand, R. Montessuit, C. Richter, R. Sadoul, G. Mazzei, A. Nichols, J. C. Martinou, *J. Cell Biol.*, **1998**, *143*, 217

[3] *Magnesium and the Cell*, N. J. Birch, Ed, Academic Press, San Diego, CA, **1993**

[4] (a) F. Ramirez, J. F. Marecek, *Biochim. Biophys. Acta*, **1980**, *589*, 21; (b) S. A. Kuby, E. A. Noltman, *In The Enzymes*, 2nd ed.; P. D. Boyer, Ed., Academic Press, New York, **1959**, *Vol. 6*, 515-603; (c) K. R. H. Repke, *Ann. N.Y. Acad. Sci.*, **1982**, *402*, 272

[5] J. A. Wells, C. Knoeber, M. C. Sheldon, M. M. Werber, R. G. Yount, *J. Biol. Chem.*, **1980**, *255*, 11135

[6] (a) A. Romani, A. Scarpa, *Front. Biosci.*, **2000**, *5*, 720; (b) C. Schmitz, A.-L. Perraud, C. O. Johnson, K. Inabe, M. K. Smith, R. Penner, T. Kurosaki, A. Fleig, A. M. Scharenberg, *Cell*, **2003**, *114*, 91; (c) F. I. Wolf, *Sci. STKE*, **2004**, *233*, 23

[7] (a) J. S. Taylor, D. B. Vigneron, J. Murphy-Boesch, S. J. Nelson, H. B. Kessler, L. Coia, W. Curran, T. R. Brown, *Proc. Natl. Acad. Sci. U.S.A.*, **1991**, *88*, 6810; (b) H. R. Halvorson, A. M. Q. Vande Linde, J. A. Helpern, M. A. Welch, *NMR Biomed.* **1992**, *5*, 53; (c) P. B. Barker, E. J. Butterworth, M. D. Boska, J. Nelson, K. M. A. Welch, *Magn. Reson. Med.*, **1999**, *41*, 400; (d) S. Iotti, C. Frassineti, L. Alderighi, A. Sabatini, A. Vacca, B. Barbiroli, *NMR Biomed.*, **1996**, *9*, 24; (e) K. M. Ward, S. S. Rajan, M. Wysong, D. Radulovic, D. J. Clauw, *Magn. Reson. Med.*, **1996**, *36*, 475; (f) A. B. Irish, A. B.; C. H. Thompson, G. J. Kemp, D. J. Taylor, G. K. Radda, *Nephron*, **1997**, *76*, 20; (g) S. Iotti, C. Frassineti, L. Alderighi, A. Sabatini, A. Vacca, B. Barbiroli, *Magn. Reson. Imaging*, **2000**, *18*, 607; (h) S. Iotti, C. Frassineti, A. Sabatini, A. Vacca, B. Barbiroli, *Biochim. Biophys. Acta - Bioenerg.*, **2005**, *1708*, 164

[8] A. Romani, M. Maguire, *Biometals*, **2002**, *3*, 271

[9] S. Iotti, G. Gottardi, B. Barbiroli, In *Proceedings of the International Society for Magnetic Resonance in Medicine*, 6th Scientific Meeting, Sydney, Australia, **1998**, 1796

[10] (a) M. Bond, G. Vadasz, A. V. Somlyo, A. P. Somlyo, *J. Biol. Chem.*, **1987**, *262*, 15630; (b) A. Di Francesco, R. W. Desnoyer, V. Covacci, F. I. Wolf, A. Romani, A. Cittadini, M. Bond, *Arch. Biochem. Biophys.*, **1998**, *360*, 149

[11] *The Handbook - A Guide to Fluorescent Probes and Labeling Technologies*, 10th ed, Haugland, R. P., Ed., Molecular Probes, Eugene, OR, **2005**

[12] (a) M. Fatholahi, K. LaNoue, A. Romani, A. Scarpa, *Arch. Biochem. Biophys.*, **2000**, *374*, 395; (b) F. I. Wolf, V. Covacci, N. Bruzzese, A. Di Francesco, A. Sacchetti, D. Corda, A. Cittadini, *J. Cell. Biochem.*, **1998**, *71*, 441

[13] (a) H. Komatsu, N. Iwasawa, D. Citterio, Y. Suzuki, T. Kubota, K. Tokuno, Y. Kitamura, K. Oka, K. Suzuki, *J. Am. Chem. Soc.*, **2004**, *126*, 16353; (b) T. Kubota, Y. Shindo, K. Tokuno, H. Komatsu, H. Ogawa, S. Kudo, Y. Kitamura, K. Suzuki, K. Oka, *Biochim. Biophys. Acta*, **2005**, *1744*, 19; (c) H. Komatsu, T. Miki, D. Citterio, T. Kubota, Y. Shindo, Y. Kitamura, K. Oka, K. Suzuki, *J. Am. Chem. Soc.*, **2005**, *127*, 10798

[14] A. Romani, *Front. Biosci.*, **2007**, *12*, 308

[15] A. Romani, *Arch. Biochem. Biophys.*, **2007**, *458*, 90

[16] (a) V. Covacci, N. Bruzzese, A. Sgambato, A. Di Francesco, M. A. Russo, F. I. Wolf, A. Cittadini, *J. Cell. Biochem.*, **1998**, *70*, 313; (b) M. Fatholahi, K. LaNoue, A. Romani, A. Scarpa, *Arch. Biochem. Biophys.*, **2000**, *374*, 395

[17] A. V. Bordunov, J. S. Bradshaw, X. X. Zhang, N. K. Dalley, X. Kou, X., R. M. Izatt, *Inorg. Chem.*, **1996**, *35*, 7229

[18] L. Prodi, F. Bolletta, M. Montalti, N. Zaccheroni, P. B. Savage, J. S. Bradshaw, R. M. Izatt, *Tetrahedron Lett.*, **1998**, *39*, 5451

[19] K. Soroka, R. S. Vithanage, D. A. Phillips, B. Walker and P. K. Dasgupta, *Anal. Chem.*, **1987**, *59*, 629

[20] (a) A. Sanz-Medel, R. Fernandez de la Campa and J. I. Garcia-Alonso, *Analyst*, **1987**, *112*, 493; (b) L. Prodi, M. Montalti, J. S. Bradshaw, R. M. Izatt and P. B. Savage, *J. Inclusion Phenom. Macrocyclic Chem.*, **2001**, *41*, 123

[21] I. Devol and E. Bardez, *J. Colloid Interface Sci.*, **1998**, *200*, 241

[22] G. Farruggia, S. Iotti, L. Prodi, M. Montalti, N. Zaccheroni, P. B. Savage, V. Trapani, P. Sale, F. I. Wolf, *J. Am. Chem. Soc.*, **2006**, *128*, 344

[23] G. Farruggia, S. Iotti, L. Prodi, N. Zaccheroni, M. Montalti, P. B. Savage, G. Andreani, V. Trapani, F. I. Wolf, *J. Fluoresc.*, **2008**, *9*, 11

[24] G. Farruggia, S. Iotti, M. Lombardo, C. Marraccini, D. Petruzziello, L. Prodi, M. Sgarzi, C. Trombini and N. Zaccheroni, *J. Org. Chem.*, **2010**, *75*, 6275

[25] R. Y. Tsien, *Nature*, **1980**, *290*, 527

[26] (a) E. Bardez, I. Devol, B. Larrey, B. Valeur, *J. Phys. Chem. B*, **1997**, *101*, 7786; (b) M. Goldman, E. L. Wehry, *Anal. Chem.*, **1970**, *42*, 1178; (c) L. Prodi, C. Bargossi, M. Montalti, N. Zaccheroni, N. Su, J. S. Bradshaw, R. M. Izatt, P. B. Savage, *J. Am. Chem. Soc.*, **2000**, *122*, 6769; (d) L. Prodi, M. Montalti, N. Zaccheroni, J. S. Bradshaw, R. M. Izatt, P. B. Savage, *Tetrahedron Lett.*, **2001**, *42*, 2941; (e) A. Casnati, F. Sansone, A. Sartori, L. Prodi, M. Montalti, N. Zaccheroni, F. Ugozzoli, R. Ungaro, *Eur. J. Org. Chem.*, **2003**, 1475; (f) R. T. Bronson, M. Montalti, L. Prodi, N. Zaccheroni, R. D. Lamb, N. K. Dalley, R. M. Izatt, J. S. Bradshaw, P. B. Savage, *Tetrahedron*, **2004**, *60*, 11139

[27] (a) R. Ballardini, G. Varani, M. T. Indelli, F. Scandola, *Inorg. Chem.*, **1986**, *25*, 3858; (b) R. E. Ballard, J. W. Edwards, *J. Chem. Soc.*, **1964**, 4868

[28] O. Sénèque, J. Latour, *J. Am. Chem. Soc.*, **2010**, *132*, 17760

[29] F. I. Wolf, V. Covacci, N. Bruzzese, A. Di Francesco, A. Sacchetti, D. Corda, A. Cittadini, *J. Cell. Biochem.*, **1998**, *71*, 441

[30] (a) W. R. Zipfel, R. M. Williams, W. W. Webb, *Nat. Biotechnol.*,**2003**, *21*, 1369; (b) F. Helmchen, W. Denk, *Nat. Methods*, **2005**, *2*, 932; (c) R. M. Williams, W. R. Zipfel, W. W. Webb, *Curr. Opin. Chem. Biol.*, **2001**, *5*, 603

[31] (a) V. Trapani, G. Farruggia, C. Marraccini, S. Iotti, A. Cittadini, F. I. Wolf, *Analyst*, **2010**, *135*, 1855; (b) Y. Suzuki, H. Komatsu, T. Ikeda, N. Saito, S. Araki, D. Citterio, D. Hisamoto, Y. Kitamura, T. Kubota, J. Nakagawa, K. Oka, K. Suzuki, *Anal. Chem.*, **2002**, *74*, 1423; (c) H. Komatsu, N. Iwasawa, D. Citterio, Y. Suzuki, T. Kubota, K. Tokuno, Y. Kitamura, K. Oka, K. Suzuki, *J. Am. Chem. Soc.*, **2004**, *126*, 16353; (d) T. Kubota, K. Tokuno, J. Nakagawa, Y. Kitamura, H. Ogawa, Y. Suzuki, K. Suzuki, K. Oka, *Biochem. Biophys. Res. Commun.*, **2003**, *303*, 332; (e) E. J. Park, M. Brasuel, C. Behrend, M. A. Philbert, R. Kopelman, *Anal. Chem.*, **2003**, *75*, 3784; (f) Y. Shindo, A. Fujimoto, K. Hotta, K. Suzuki and K. Oka, *J. Neurosci. Res.*, **2010**, *88*, 3125; (g) H. M. Kim, C. Jung, B. R. Kim, S. Y. Jung, J. H. Hong, Y. G. Ko, K. J. Lee, B. R. Cho, *Angew. Chem. Int. Ed.*, **2007**, *46*, 3460; (h) H. M. Kim, P. R. Yang, M. S. Seo, J. S. Yi, J. H. Hong, S. J. Jeon, Y. G. Ko, K. J. Lee, B. R. Cho, *J. Org. Chem.*, **2007**, *72*, 2088

[32] (a) M. Fatholahi, K. LaNoue, A. Romani, A. Scarpa, *Arch. Biochem. Biophys.*, **2000**, *374*, 395; (b) T. Kubota, Y. Shindo, K. Tokuno, H. Komatsu, H. Ogawa, S. Kudo, Y. Kitamura, K. Suzuki, K. Oka, *Biochim. Biophys. Acta*, *Mol. Cell Res.*, **2005**, *1744*, 19

[33] H. Rubin, *BioEssays*, **2005**, *27*, 311

[34] F. Bonomini, S. Tengattini, A. Fabiano, R. Bianchi, R. Rezzani, *Histol. Histopathol.*, **2008**, *23*, 381

[35] H. M. Kim, C. Jung, B. R. Kim, S. Y. Jung, J. H. Hong, Y. G. Ko, K. J. Lee, B. R. Cho, *Angew. Chem. Int. Ed.*, **2007**, *46*, 3460

[36] F. Y. Li, B. Chaigne-Delalande, C. Kanellopoulou, J. C. Davis, H. F. Matthews, D. C. Douek, J. I. Cohen, G. Uzel, H. C. Su, M. Lenardo, *J. Nat.*, **2011**, *475*, 471

[37] C. Marraccini, G. Farruggia, M. Lombardo, L. Prodi, M. Sgarzi, V. Trapani, C. Trombini, F. I. Wolf, N. Zaccheroni, S. Iotti, *Chem. Sci.*, **2012**, *3*, 727

[38] H. M. Kim, P. R. Yang, M. S. Seo, J. S. Yi, J. H. Hong, S. J. Jeon, Y. G. Ko, K. J. Lee, B. R. Cho, *J. Org. Chem.*, **2007**, *72*, 2088

[39] T. Fukada, S. Yamasaki, K. Nishida, M. Murakami, T. J. Hirano, *Biol. Inorg. Chem.*, **2011**, *16*, 1123

[40] C. Andreini, L. Banci, I. Bertini, A. J. Rosato, *Proteome Res.*, **2006**, *5*, 196

[41] A. Takeda, H. Tamano, S. Imano, N. Oku, *Neuroscience*, **2010**, *168*, 715

[42] S. Yamasaki, K. Sakata-Sogawa, A. Hasegawa, T. Suzuki, K. Kabu, E. Sato, T. Kurosaki, S. Yamashita, M. Tokunaga, K. Nishida, T. Hirano, *J. Cell Biol.*, **2007**, *177*, 637

[43] G. Swaminath, T. W. Lee, B. Kobilka, *J. Biol. Chem.*, **2003**, *278*, 352

[44] W. Maret, *BioMetals*, **2001**, *14*, 187

[45] (a) Z. Huang, S. J. Lippard, In *Methods in Enzymology*, Conn, P.M., Ed., Academic Press, New York, **2012**, vol. 505, 445. (b) S. J. Lippard, *Curr. Opin. Chem. Biol.*, **2010**, *14*, 225. (c) H. M. Kim, M. S. Seo, M. J. An, J. H. Hong, Y. S. Tian, J. H. Choi, O. Kwon, K. J. Lee, B. R. Cho, *Angew. Chem. Int. Ed.*, **2008**, *47*, 5167. (d) E. M. Nolan, S. J. Lippard, *Acc. Chem. Res.*, **2009**, *42*, 193. (e) C. J. Chang, J. Jaworski, E. M. Nolan, M. Sheng, S. J. Lippard, *Proc. Natl Acad. Sci. USA*, **2004**, *101*, 1129

[46] (a) D. A. Pearce, N. Jotterand, I. S. Carrico, B. Imperiali, *J. Am. Chem. Soc.*, **2001**, *123*, 5160. (b) R. Parkesh, T. C. Lee, T. Gunnlaugsson, *Org. Biomol. Chem.*, **2007**, *5*, 310. (c) C. Bazzicalupi, A. Bencini, S. Puccioni, B. Valtancoli, P. Gratteri, A. Garau, V. Lippolis, *Chem. Commun.*, **2012**, *48*, 139. (d) P. Jiang, Z. Guo, *Coord. Chem. Rev.*, **2004**, *248*, 205. (e) C. Lodeiro, J. L. Capelo, J. C. Mejuto, E. Oliveira, H. M. Santos, B. Pedras, C. Nuñez, *Chem. Soc. Rev.*, **2010**, *39*, 2948

[47] (a) R.A.Bissel, A. P. de Silva, H. Q. N. Gunaratne, P. L. M. Lynch, G. E. M. Maguire, K. R. A. S. Sandanayake, *Chem. Soc. Rev.*, **1992**, *21*, 187. (b) A. P. de Silva, D. B. Fox, A. J. M. Huxley, T. S. Moody, *Coord. Chem. Rev.*, **2000**, *205*, 41. (c) A. P. de Silva, T. S. Moody, G. D. Wright, *Analyst*, **2009**, *134*, 2385. (d) J. F. Callan, A. P. de Silva, D. C. Magri, *Tetrahedron*, **2005**, *61*, 8551

[48] (a) L. Prodi, *New J. Chem.*, **2005**, *29*, 20. (b) S. Bonacchi, D. Genovese, R. Juris, M. Montalti, L. Prodi, E. Rampazzo, M. Sgarzi, N. Zaccheroni, *Top. Curr. Chem.*, **2011**, *300*, 93

[49] (a) E. Kimura, T. Koike, *Chem. Soc. Rev.*, **1998**, *27*, 179. (b) Z. Wang, M. A. Palacios, P. J. Anzenbacher, *Anal. Chem.*, **2008**, *80*, 7451

[50] Z. Xu, J. Yoon, D. R. Spring, *Chem. Soc. Rev.*, **2010**, *39*, 1996, and references therein

[51] (a) S. Bonacchi, E. Rampazzo, M. Montalti, L. Prodi, N. Zaccheroni, F. Mancin, P. Teolato, *Langmuir*, **2008**, *24*, 8387. (b) J. W. Meeusen, H. Tomasiewicz, A. Nowakowski, D. H. Petering, *Inorg. Chem.*, **2011**, *50*, 7563

[52] P. D. Zalewski, I. J. Forbes, W. H. Betts, *Biochem. J.*, **1993**, *296*, 403

[53] G. Xue, G., J. S. Bradshaw, N. K. Dalley, P. B. Savage, K. E. Krakoviak, R. M. Izatt, L. Prodi, M. Montalti, N. Zaccheroni, *Tetrahedron*, 2001, 57, 7623–7628

[54] F. Bolletta, I. Costa, L. Fabbrizzi, M. Licchelli, M. Montalti, P. Pallavicini, L. Prodi, N. Zaccheroni, *Dalton Trans.*, **1999**, 1381

[55] C. Bazzicalupi, A. Bencini, S. Biagini, E. Faggi, G. Farruggia, G. Andreani, P. Gratteri, L. Prodi, A. Spepi, B. Valtancoli, *Dalton Trans.*, **2010**, *39*, 7080

E corre l'uomo confuso verso
ciò che neanche lui capisce,
chi ha programmato la sua vita
non sa chi sia e dove; ma che
importa, se solo questo lo fa
già dubitare del suo equilibrio
e aperta è già la strada oscuramente
verso una nuova realtà

Mondo nuovo

Francesco Guccini

Chapter 4: Nanoparticle-based systems for metal ions sensing

The design of fluorescent chemosensors for biologically relevant chemical species has important impacts in many applications, and for this reason it has been the subject of active research in many laboratories worldwide. The achievements in this wide research topic have promoted enormous steps forwards, for example, in the field of cell biology, thanks to the comprehension of the role of different chemical species in many biological processes. Recently, researchers have been moving from molecular chemosensors based on two communicating units, a receptor and a dye, toward more complex and sophisticated structures, and have tried to push further the limits of sensitivity and selectivity. Many different solutions have been proposed but, among them, sensing systems based on nanoparticles are certainly one of the most interesting and promising.[1, 2] In particular, the use of dye-doped silica nanoparticles can offer intriguing advantages,[1–5] such as high sensitivity enhancement through the occurrence of amplification processes,[1, 6] the possibility of an internal reference signal, which avoids further calibrations,[2–5, 7] and good water solubility. An additional interesting feature is the possibility to monitor chemical species, *in vivo*, since silica is a biocompatible material.
In this context two nanoparticle-based system are presented for the dectection in water of Cu^{+} and Hg^{2+}, which have respectively biological and environmental importance.

4.1 Cu^{+} sensing

4.1.1 Introduction

Metallostasis alteration, namely, zinc and copper homeostatic levels, has already been observed both in biological fluids and tissues of patients affected by breast, prostate, lung and gastrointestinal tumours,[8, 9] and in some neurodegenerative disorders, like Parkinson's disease (PD) and Alzheimers disease (AD).[10] In particular, copper has been implicated in Amyloid β peptide (Aβ) aggregation and neurotoxicity, and it is generally accepted that in AD brain tissue there is an excess of Cu in the extracellular space and in amyloid plaques.[11,12] On the other hand, a decrease of intracellular copper in AD, as compared to healthy control brain tissue, has also been reported.[12] All these findings highlight the need for new efficient chemosensors for copper ions.[13] In this context, we have recently developed a new one pot approach for the synthesis of core-shell dye-doped silica nanoparticles based on the preparation of micelles of Pluronic® F127 in water.[1b,14] The final material is a versatile multicompartment system characterized by high water solubility, stability, and brightness. Most interestingly, we have very recently demonstrated the possibility of also hosting water-insoluble dyes in the outer shell, which are able to give rise to very efficient energy transfer processes with the molecules hosted in the core.[15] Thanks to the unique structure and properties of these nanoparticles, their application in sensing can be envisaged to involve a new type of transduction mechanism based on the addition of a hydrophobic chemosensor to a water solution of the nanoparticles (*Figure 4.1*).
It must be underlined, that the requirement related to the hydrophobicity of the chemosensor is not a limitation; rather, the use of dye-doped silica nanoparticles makes possible the use of a large series of systems that are usually precluded due to their insolubility in water-based environments. The fundamental requirement in this case is that, upon complexation with the analyte, an efficient energy transfer should occur between the dyes hosted in the core and in the shell. In order to test, as a first step, the proof-of-principle for this new strategy, we decided to use **1** (*Figure 4.1*), a very selective and promising chemosensor for Cu^{+}.[13a]

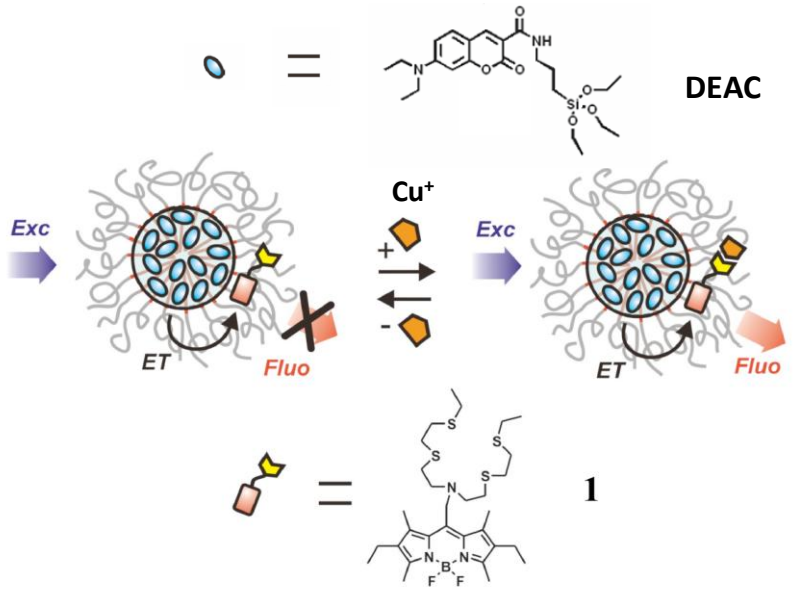

Figure 4.1: schematic representation of the proposed transduction mechanism.

4.1.2 Results and discussion

Given the spectral properties of the BODIPY dye in the structure of the chemosensor, we decided to synthesize a family of nanoparticles containing an average of seventeen molecules of 7-(diethylamino)coumarin-3-carboxamide, which is a good energy donor for **1**, covalently linked to the silica core (synthesis details are reported in the *Appendix*). The nanoparticles present a very high absorption coefficient (755 000 $M^{-1}cm^{-1}$) and a very high fluorescence quantum yield (0.36). The addition of an increasing amount of **1** (up to 1 equivalent) to the nanoparticle solution ($1.25 \cdot 10^{-7}$ M), buffered at pH 7.2, led to a dramatic decrease of the luminescence intensity of the coumarin dye, with a concomitant linear increase of the fluorescence of the BODIPY moiety (*Figure 4.2*). The same results were observed in the pH range 5.0–8.0. Moreover, the addition of bovine serum albumin did not have any influence on these titrations. As expected, the fluorescence anisotropy of **1** measured in the absence of nanoparticles is negligible. On the contrary, in the presence of nanoparticles, it becomes as high as 0.25 upon direct excitation of the BODIPY unit (λ_{exc}= 500 nm): this clearly confirms that **1** is located in the outer shell of the nanoparticles, where it experiences a reduced rotational freedom and forms the system **1**@NPs. The measurement of anisotropy can thus be used as an efficient tool to observe whether **1** is inserted in the nanoparticle structure. A negligible value for the fluorescence anisotropy is instead obtained for the same system in the same spectral region (550–700 nm) upon excitation of the coumarin dye (λ_{exc} =400 nm). The complete depolarization can be explained, in this case, by the occurrence of an energy transfer process from the coumarin dyes to the BODIPY unit. The efficiency of this process (80%) could be evaluated from the quenching of the coumarin donor, both through analysis of the spectra reported in *Figure 4.2* and of the decrease of the donor excited state lifetime. The properties of this system did not change for months, and prove its stability under these conditions.

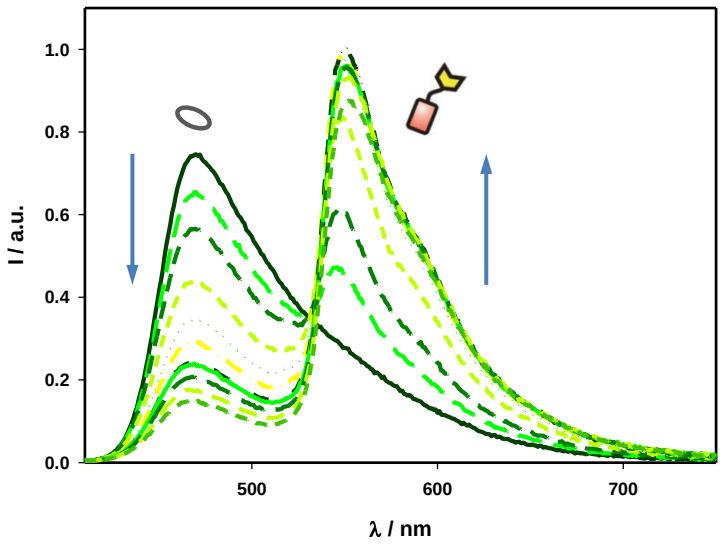

Figure 4.2: Fluorescence (λ_{exc} = 400 nm) spectra of nanoparticle aqueous solution ($1.25 \cdot 10^{-7}$ M) upon addition of increasing amounts of **1**.

To test the performance of this architecture as a chemosensor, we first added glutathione (1 mM), which has a very low apparent dissociation constant ($9.1 \cdot 10^{-12}$ M) towards Cu^+, in order to mimic cell conditions,[16] without observing any change in the fluorescence intensity. The subsequent addition of Cu^+ ions led to an increase of the absorbance in the 500–600 nm region (*Figure 4.3*), as already described[13a] for free **1**. As far as the fluorescence spectrum is concerned, upon excitation at 400 nm, where the light is predominantly absorbed by the coumarin moieties, the complexation process leads to a further decrease of the fluorescence intensity of the coumarin and to an increase of that of the BODIPY unit.

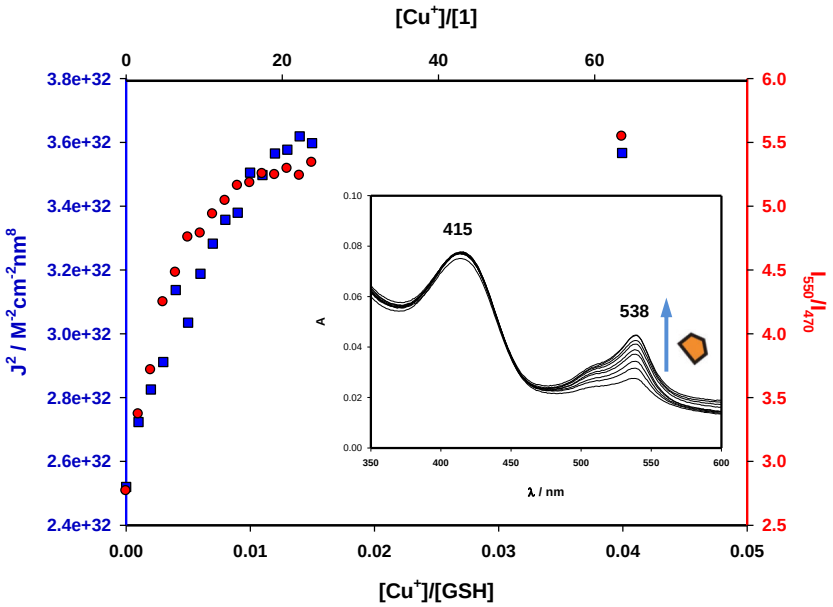

Figure 4.3: ratio of the fluorescence intensities measured at 550 and 470 nm (λ_{exc} = 400 nm, red circles) of an equimolar ($1.25 \cdot 10^{-7}$ M) aqueous solution of nanoparticles and chemosensor **1** upon addition of an increasing amount of Cu^+ in the presence of glutathione (1 mM) and the square of the overlap integral, J^2, calculated according to Förster equation (blue squares). Inset: absorption spectra recorded under the same conditions.

This can be seen in *Figure 4.3*, in which the ratio I_{550}/I_{470} is plotted between the intensities measured at 550 nm (emission of BODIPY) and 470 nm (emission of the coumarin dye) upon excitation at 400 nm versus the equivalents of added metal ion, indicating that this system has a ratiometric nature. The possibility for the metal ion to be directly involved in the quenching of the fluorescence of the coumarin moieties can be ruled out by the observation that the fluorescence of the coumarin in the nanoparticle is not affected by the addition of Cu^+ in the absence of **1**. Rather, this result can be explained by an increase in the efficiency of the energy transfer process: the observed increase of the absorbance of the donor in fact induces an increase of the overlap integral (J) according to the Förster equation. This conclusion is further supported by the similarity of the patterns shown by the I_{550}/I_{470} ratio (*Figure 4.3*, red circles) and J^2 (*Figure 4.3*, blue triangles), which relies on the fact that both the decrease of the coumarin band and the increase of the BODIPY band depend on J. We would like to stress that in **1**@NP the complexation of a single ion is able to strongly modify the photophysical properties of several dyes (all the coumarin units inside the silica nucleus) at the same time; this induces, among other effects, a very large signal change, which, as in previous cases,[1,6] can be seen as signal amplification. Interestingly, the dissociation constant between **1**@NP and Cu^+ was estimated to be $2.2\cdot10^{-13}$ M; this indicates that **1**@NP is able to complex ions with a 16-fold higher affinity than the one shown by free **1** ($K_d=3.6\cdot10^{-12}$ M),[13a] because of the different environment around **1**. Interestingly, also the selectivity observed for the free chemosensor was maintained in **1**@NPs; no changes in the absorption and emission spectra were in fact observed upon addition of Cu^{2+}, Zn^{2+}, Cd^{2+} even in a 1000-fold excess, both in the presence or absence of glutathione. All these results, therefore, show that the assembly **1**@NP, can compete even with some cytoplasmic copper chaperones and small Cu^+ ligands in binding copper in a marked selective manner.[17] Live cell fluorescence imaging was performed in order to assess whether: 1) the newly developed **1**@NP system is cell permeable, as the free sensor **1**, and 2) the sensing capability towards intracellular Cu^+ species, in terms of BODIPY-related emission enhancement ($\lambda_{em} \approx 570$ nm), is changed with respect to the well-established sensor system **1**.[13a] *Figure 4.4* shows the fluorescence response of neuroblastoma SHSY5Y cell line, for the different sensor and control treatments, both without exogenous copper addition and with $CuCl_2$ (100 μM) supplemented medium. It is evident that while the cells exposed to the free sensor **1** as well as those incubated with the equimolar **1**@NP solution exhibit a localized intracellular emission at 570 nm (by excitation at 543 nm), this is not the case for either the cells incubated with NPs or the control samples. These findings point to the fact that **1** in its complexed form with the nanoparticles maintains high selectivity and binds the intracellular Cu^+. In fact, due to the absence of emission for the cells treated with the nanoparticles alone, one can rule out the possibility that other intracellular components could cause the observed fluorescence response.

Interestingly, the quantitative analysis of fluorescence micrographs, in the explored Cu^{2+} concentration range (0–50 μM), evidence that the **1**@NP system is more efficient—up to about 35% of emission enhancement—than the free sensor **1** (while for 100 μM $CuCl_2$ supplemented cells the two probe systems are substantially equivalent). This is an obvious advantage of the nanoparticle-complexed sensor with respect to the "standard" copper sensor **1**, because under physiological conditions the concentration of copper, *in vivo*, is typically in the order of tens of μM, and higher levels can be toxic and/or related to a pathological condition for several cell lines.[18] The observed behaviour of the copper sensor complexed with the nanoparticles can be explained in terms of the higher binding affinity to intracellular copper of the **1**@NP system compared to the free sensor **1**, and takes into account a concentration saturation effect. The apparent Cu^+ dissociation constant of **1**@NP is about one order of magnitude lower than that reported for the free **1**. For this reason our system exhibits a higher efficiency in cells upon sensor uptake, without any addition of exogenous copper. A simplified simulation model of species distribution for Cu^+-binding ligands

in the intracellular environment was carried out by taking into account the recently determined dissociation constants for several copper chaperones and low-mass ligands.[16]

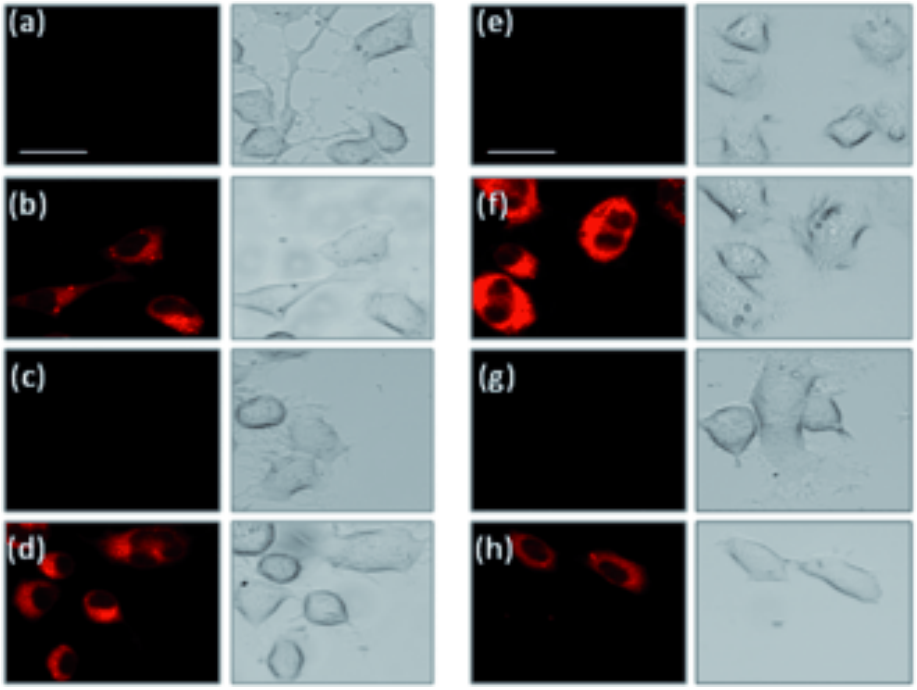

Figure 4.4: confocal microscopy emission (λ_{ex}=543 nm; λ_{em}=572 nm) and corresponding bright-field images for the SHSY5Y cell line: a)–d) cultured in DMEM medium for 24 h, and e)–h) supplemented with $CuCl_2$ (100 µM) for 5 h, incubated at 37 °C. The probe treatments (5 min incubation at 25 °C, then rinsed with PBS) are as follows: a), e) control PBS; b), f) Cu^+ sensor **1** (5 µM); c), g) nanoparticles (5 µM); d), h) **1**@NP complex (5 µM; 1:1 molar ratio); scale bar: 30 µm.

The results show that while copper sensor **1** (5 µM) has always the lowest binding affinity to Cu^+ at the examined conditions, the **1**@NP system might compete for Cu^+ binding with some of the intracellular copper chaperones and/or intracellular ligands at lower binding affinity.[16] This effect is even superior when the **1**@NP concentration is increased, and could be related to the observed enhancement of intracellular fluorescence without exogenous copper addition compared to the free **1** sensor. Accordingly, for the Cu^{2+} supplemented cells, the **1**@NP-incubated samples likely suffer from a saturation effect. This interpretation is supported by preliminary measurements performed at higher probe concentrations (10 µM), the results for which show a relative increase of emission enhancement for the **1**@NP-treated cells upon exogenous copper addition. Further measurements by systematically varying the concentration of the **1**@NP system as well as the relative molar ratio between the sensor **1** and the nanoparticles will elucidate this point.

4.1.3 Conclusion

The strategy for signal amplification that we have described here, for the first time, appears very effective and presents many advantages, such as: 1) a significant signal increase due to the much higher absorption of the nanoparticle compared to that of the single chemosensor, 2) less noise, because of the larger separation between excitation and emission wavelengths, 3) the possibility to apply ratiometric measurements, which avoids external calibration procedures, and, finally, 4) a high versatility that makes it

possible to massively enlarge the library of the possible chemosensors to be exploited. In addition, the advantage of the greater affinity shown by the **1**@NP system endows it with an enhanced detection capability for intracellular Cu^{+} either in the absence or at low concentrations of exogenous metal ion. Moreover, it can suggest its application in proteostasis processes, an additional possibility that will be further examined. For all these reasons, we strongly believe that this concept is very general and can be widely extended in many possible applications to obtain a large increase of the sensitivity in the fundamental field of chemical sensing.

4.2 Hg^{2+} sensing

4.2.1 Introduction

Mercury is a particularly toxic element of great environmental and health concern due to its widespread presence in the lithosphere and in water, mainly caused by its expanded use in industry and agriculture.[19] It accumulates in the food chain and reaches the human body mainly through food ingestion (in particular seafood), thus causing dangerous conditions of intoxication and determining a variety of serious metabolic, cognitive, and motor disorders, and sensory long-term diseases.[20–23] Famous collective human intoxications in some fisher villages are notorious, the disaster of Minamata Bay in Japan in the 1950s being probably the most dramatic case.[24] Health concerns about prolonged exposure to mercury and the need of understanding its toxicology are stimulating the development of new efficient, sensitive, and selective analytical tools for real-time monitoring aqueous Hg^{2+} in biological, environmental, and industrial milieus. Several screening methods including atomic absorption/emission spectroscopy[25] and inductively coupled plasma mass spectrometry[26] provide very low detection limits but present some drawbacks in terms of actual applicability: they require expensive/sophisticated instrumentations, laborious sample preparation, and they cannot be easily applied in on-line or in-field analysis. These flaws can be mended by sensor technology, which offers simplicity, reliability, and rapidity. In particular, optical methods and devices based on fluorescent molecular sensors offer many advantages in terms of versatility, sensitivity, response time, and cost, and they represent valid alternative approaches for simple and rapid environmental and biological monitoring of mercury and other toxic heavy-metal ions.[27–31] The most important challenge when fluorescence based devices for mercury(II) sensing have to be realized is the development of the "sensitive part", that is, a fluorescent chemosensor to detect Hg^{2+} possibly in water and selectively over competing metal ions such as the "silent ions" Zn^{2+}, Cd^{2+}, and Pb^{2+}. These metal ions, in fact, feature chemical properties similar to that of Hg^{2+} due to the common d^{10} closed-shell electronic configuration, which determines the absence of an intrinsic spectroscopic or magnetic signal. This part is responsible for the affinity and selectivity of the whole device, and, in many cases, also for the transduction process, determining, as a consequence, the sensitivity of the system. Several types of sensing molecules with fluorescent switching properties have been developed and examined to signal Hg^{2+} binding.[27-34] However, examples of easy to handle fluorescence devices for in-field Hg^{2+} detection and screening in environmental and industrial samples are much fewer.[35] In fact, the development of these systems generally requires the overcoming of many practical/technical problems inherent in the immobilization of the fluorescent molecular sensor on/in appropriate supports. The resulting receptor platforms then need to be coupled to a transducer part, which at least retains, and possibly improves, the selectivity and sensitivity of the molecular dye for the analyte in the desired media. Despite the fact that optical devices based on Hg^{2+}-responsive fluorescence molecules offer promising approach for simple and rapid tracking of Hg^{2+} in real matrices, their development is still a challenging task. We here focus our attention on some coumarin-based fluorescent chemosensors for Hg^{2+} featuring thia-aza macrocycles as receptor units. The sensing performances of these new species have been tested for Hg^{2+} detection within cells *in vitro* and in water solutions by using silica core–shell nanoparticles as vehicles. Furthermore, polyvinyl chloride (PVC) membranes containing the new fluorescent chemosensors have been combined with familiar computer screen photo-assisted technique (CSPT) devices to afford a new optical sensor for selective detection of mercury(II) ions in natural water samples. We consider CSPT, first introduced by Filippini et al.,[36] particularly interesting and it has, in fact, recently found lots of attention in optical sensing applications. This is due to its simplicity, low cost, and general availability because it uses common devices (LCD monitors

and web cameras) that allow avoiding costly spectroscopic equipment, to reduce the need of dedicated qualified trained personnel, and to take advantage of polychromatic illumination.

4.2.2 Results and discussion

4.2.2.1 Synthesis and photophysical properties of the ligands

The most common synthetic approach to the synthesis of fluorescent chemosensors is to covalently link, through an appropriate spacer, a fluorogenic fragment (signalling unit) to a guest-binding site (receptor unit). The recognition of the target species by the receptor unit (the result of a selective host–guest interaction between them) elicits an optical signal expressed as an enhancement or quenching of the fluorophore emission. The choice of both the signalling and the receptor unit can be critical to both the sensitivity and the selectivity of the sensor, especially if a direct interaction between the fluorophore and the target species is possible.[1,37–47] Different fluorophores (anthracene, 8-hydroxyquinoline, dansylamide, phenanthroline, and coumarin) are commonly used as signalling site, whereas macrocyclic receptors continue to represent the first choice as guest-binding sites for metal cations. This is due to the extensive possibilities, which they can offer for the modulation of the topology and the nature of the binding domain, thus providing an easy route to achieve strong and possibly selective interactions with the substrate of interest. Many of the reported luminescent chemosensors feature polyoxa, polyaza, and azaoxa macrocycles as receptor units,[37–47] whereas relatively few examples are reported of fluorescent probes for metal cations presenting S-donor macrocycles as the binding site.[40–57] Interestingly, although many fluorescent chemosensors for Hg^{2+} ions are known in the literature, which feature coumarin-based fluorogenic fragments (coumarins possess many advantage as signalling unit including a high fluorescence quantum yield, a large Stokes shift, excellent light stability, and low toxicity),[58] to the best of our knowledge none of them presents macrocyclic receptor units containing S-donor atoms, which in principle should guarantee a higher selective interaction with "soft" metal ions such us the thiophilic Hg^{2+} ion. Therefore, starting from the known macrocyclic ligands 1-aza-4,7,10-trithiacyclododecane ([12]aneNS$_3$), 1,7-diaza-4,10-dithiacyclododecane ([12]aneN$_2$S$_2$), and 2,8-dithia-5-aza-2,6-pyridinophane ([12]anePyNS$_2$), which we had already successfully used as receptor units in the construction of conjugated fluorescent chemosensors for heavy-metal ions,[59–61] we synthesized compounds **L1**–**L3** (*Figure 4.5*).

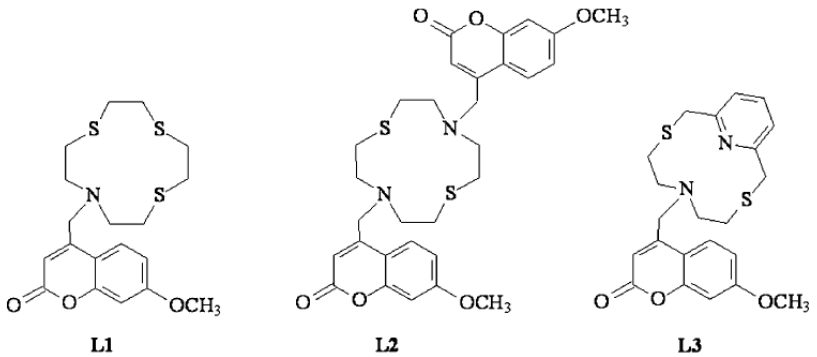

Figure 4.5: structures of the chemosensors **L1**-**L3**.

They consist of the aforementioned macrocyclic moieties, acting as ionophores, connected through a methylene linker at the 4-position of the 7-methoxy coumarin unit(s) acting as the fluorescent signalling unit of the system. Ligands **L1**–**L3** were easily prepared in reasonable yields by reacting the free macrocyclic

moieties with an excess of 4-bromomethyl-7-methoxycoumarin in dry CH_2Cl_2 in the presence of K_2CO_3. With the aim to use these ligands as sensing components in chemical sensors for mercury(II) ion detection in environmental and biomedical applications, we have investigated their photophysical properties in different solvents of increasing polarity, from CH_3CN to water. A screening of the optical properties of this kind of ligands under different conditions is fundamental due to the great influence of the environment on the emission properties of coumarin, a feature that can affect the whole sensing performance of these chemosensors. CH_3CN is a good solvent for these species, and in this milieu the absorption spectra of **L1**–**L3** present the typical large non-structured band of coumarins centred at around λ = 320 nm (ε = 12500 (**L1**), 10100 (**L2**), 12100 $M^{-1}cm^{-1}$ (**L3**)) as attended for 4,7-substituted derivatives.[58,62,63] This band can be assigned to transitions usually described as involving the highest occupied molecular orbital (HOMO) mainly centred on the aromatic fused ring and the lowest unoccupied molecular orbital (LUMO) mainly localized on the heterocycle ring of the coumarin system.[64] It has to be noted that in the case of ligand **L3** a band with maximum at λ = 279 nm (ε = 9500 $M^{-1}cm^{-1}$) is also present that can be attributed to the presence of the pyridine moiety in the macrocyclic unit. Ligands **L1**–**L3** exhibit in CH_3CN an emission band at around λ = 405 nm with quite low fluorescence quantum yields (Φ = $3.4\cdot10^{-3}$ (**L1**), $2.2\cdot10^{-3}$ (**L2**), $3.3\cdot10^{-3}$ (**L3**)) when excited at λ = 320 nm, which can be attributed to a photoinduced electron transfer (PET) process between the lone pair on the tertiary nitrogen atom(s) of the macrocyclic moieties and the coumarin fragments. The study of the optical response of ligands **L1**–**L3** in the presence of Ca^{2+}, Cd^{2+}, Co^{2+}, Cu^{2+}, Hg^{2+}, K^{+}, Mg^{2+}, Mn^{2+}, Ni^{2+}, Pb^{2+}, Zn^{2+}, Al^{3+}, Ga^{3+}, In^{3+}, Tl^{+}, and Fe^{3+} ions revealed significant and similar changes in the absorption spectra in the presence of Fe^{3+} and Al^{3+} ions. In particular, the band maximum shifts from λ = 320 nm to slightly higher wavelengths (λ = 330 nm) with the addition of in increasing amounts of these analytes. A similar behaviour with smaller red shift of the absorption band at λ = 320 nm was observed also for Cu^{2+} (**L1**–**L3**), Hg^{2+} (**L1** and **L2**), Pb^{2+} (**L1** and **L2**), and Zn^{2+} ions (**L3**) under these conditions. Interestingly, a significant chelation enhancement of the fluorescence emission (CHEF effect) was observed for all the three ligands only upon addition of Fe^{3+} and Al^{3+} ions up to a 1:1 metal-to-ligand molar ratio (*Figure 4.6*). Hg^{2+} ions, instead, induced only very minor changes in the emission band of the ligands. To gradually increase the polarity of the solvent we introduced water and we investigated the optical properties of the chemosensors in CH_3CN:H_2O 4:1 (v/v) buffered with MOPS (MOPS=3-(N-morpholino)propane-sulfonic acid) at pH 7.0. This buffered mixed solvent allows to control protonation and to maintain a reasonable solubility of the ligands.

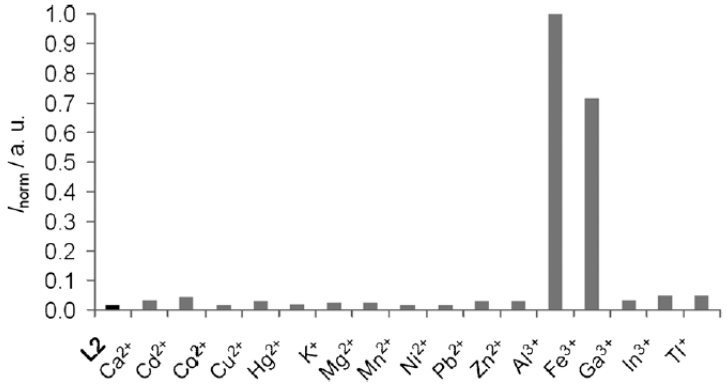

Figure 4.6: normalized relative fluorescence emission intensity of **L2** responding to one equivalent of all metal ions considered ([**L2**] = $3.6\cdot10^{-5}$ M, CH_3CN, 25 °C, λ_{exc} = 320 nm, λ_{em} = 405 nm).

The absorption spectra of ligands **L1**–**L3** exhibit the expected main band at around λ = 320 nm and a shoulder at about λ = 290 nm, in the case of ligand **L3** the band centered at λ = 275 nm due to the pyridine moiety was also observed. The optical response of ligands **L1**–**L3** to the presence of all the above-mentioned metal ions under these experimental conditions revealed a very different selectivity in the optical response of the three ligands in comparison with pure CH_3CN. Significant and similar changes in the UV/Vis spectra of all three coumarin derivatives were observed only upon addition of Hg^{2+} ions. In particular, the band at around λ = 320 nm (π-π* in nature) shifted to slightly higher wavelengths (λ = 330 nm), whereas a new band appeared at about λ = 250 nm (*Figure 4.7(a)* for ligand **L1**). No significant changes were instead observed in the UV/Vis spectra of the three ligands upon addition of the other metal ions studied including Fe^{3+} and Al^{3+}.

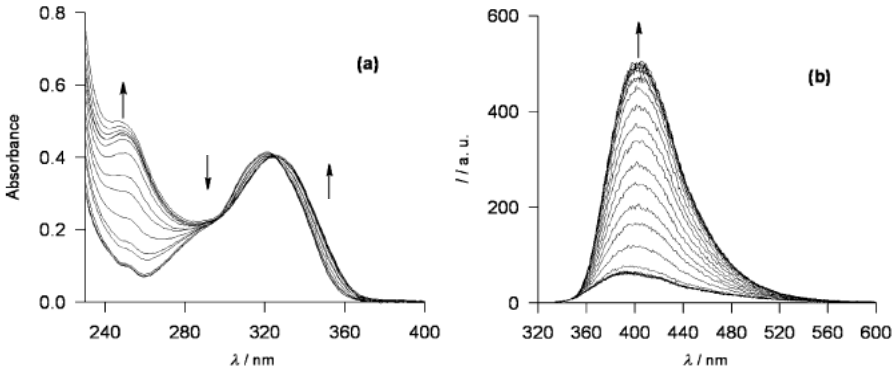

Figure 4.7: (a) changes in the absorption spectrum and (b) in the emission spectrum of **L1** ([**L1**] = $3.5 \cdot 10^{-5}$ M, $CH_3CN:H_2O$ 4:1 v/v, pH 7.0, 25 °C, λ_{exc} = 319 nm).

Also in $CH_3CN:H_2O$ 4:1 v/v solvent mixture, ligands **L1**–**L3** exhibit an emission band at about λ = 405 nm when excited at λ = 319 nm with a quite low fluorescence quantum yield (Φ = $1.7 \cdot 10^{-3}$ (**L1**), $1.0 \cdot 10^{-3}$ (**L2**), $5.0 \cdot 10^{-3}$ (**L3**)) due to the above-mentioned photoinduced electron transfer (PET) process. Interestingly, a significant CHEF effect with a very small red shift in the emission maxima was observed for all three ligands only upon addition of Hg^{2+} ions (Φ = $9.9 \cdot 10^{-2}$ (**L1**), $2.3 \cdot 10^{-2}$ (**L2**), $1.9 \cdot 10^{-2}$ (**L3**) under these experimental conditions (*Figure 4.7(b)* for **L1**. Fluorescence intensity versus molar ratio plots suggested the formation of both 1:2 and 1:1 metal-to-ligand complexes with the latter being responsible for the observed fluorescence intensity enhancement (*Figure 4.8* for **L1**).

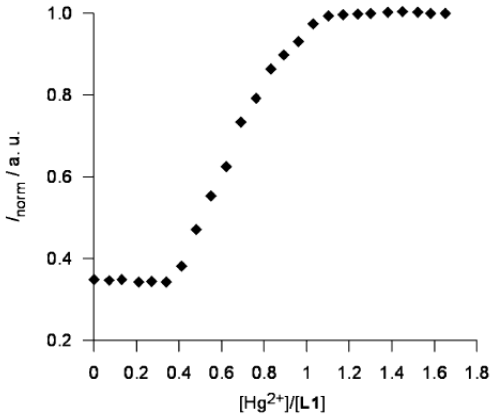

Figure 4.8: Normalized fluorescence intensity versus added equivalent of Hg^{2+} for **L1** ([**L1**] = $3.5 \cdot 10^{-5}$ M, $CH_3CN:H_2O$ 4:1 v/v, pH 7.0, 25 °C, λ_{exc} = 319 nm, λ_{em} = 405 nm).

Figure 4.9(a) clearly shows the high selective optical response of **L1** for Hg^{2+} ions; the fluorescence emission enhancement due to the presence of this ion, in fact, is much higher compared with that observed for the other metal ions considered, and this is the case also for ligands **L2** and **L3**. This result is further supported by ion competitive studies performed in CH_3CN:H_2O (4:1 v/v, 25 °C, pH 7.0) in the presence of one equivalent of Hg^{2+} ions and an tenfold excess of other ions, including d^{10} transition and post-transition heavy-metal ones such as Cd^{2+} and Pb^{2+} (see *Figure 4.9(b)* for **L1**).

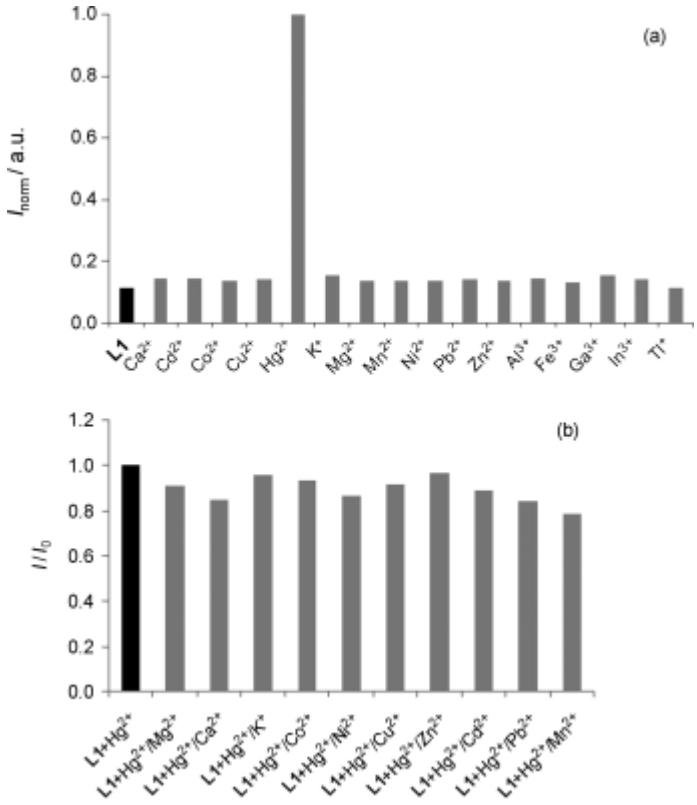

Figure 4.9: (a) normalized relative fluorescence emission intensity of **L1** responding to one equivalent of all metal ions considered ([**L1**]=3.6×10^{-5} M, CH_3CN:H_2O 4:1 v/v, pH 7, 25 °C); (b) ion competition study for **L1** in the presence of one equivalent of Hg^{2+} ions and ten equivalents of the other metal ions.

In order to investigate the reversibility of the complexation process we also performed spectrophotometric and spectrofluorimetric back-titration experiments with another very efficient ligand for mercury ions consisting of a diazacrown ether with two quinoline moieties at the periphery, in particular N,N'-bis-[(8-hydroxy-5-nitro-7-quinolinyl)methyl]-1,10-diaza[18]crown-6 ether (**R1**).[65] The addition of increasing amounts of this species to a solution of **L1** and Hg^{2+} ions in 1:1 molar ratio causes a gradual decrease in the emission band at λ = 406 nm to reach the typical spectra of the uncomplexed **L1** in the presence of an almost equimolar amount of the competitor ligand. The binding of **R1** with the mercury ions is also evidenced by the changes in the absorption spectra that present an increasing band at λ = 435 nm, characteristic of the complexed **R1**, and no band at λ = 460 nm where the free **R1** absorbs. It has also to be mentioned that we have performed these measurements both in acetonitrile and in the mixed solvent (CH_3CN:H_2O, 4:1 v/v), thereby obtaining completely analogous results proving the reversibility of the process in the different environments. As a final step we have investigated the complexation ability of these chemosensors in pure water. All the photophysical features of the free chemosensors resulted

extremely similar both in shape and energies to the ones obtained in the other two investigated solvent media.

Unfortunately the solubility of **L1–L3** in water is very poor, in the range of 10^{-6} M, preventing their use in practical sensing applications. Moreover, none of the considered metal ions (including Hg^{2+}, Fe^{3+}, and Al^{3+}) caused any variation either in the absorption or in the emission spectra of the ligands in this milieu at these concentrations. In the attempt to overcome these solubility problems, we have decided to use silica core–polyethylene glycol (PEG) shell nanoparticles as vehicles and incubators for favouring the binding events in water. This nanoparticles possess a total average hydrodynamic diameter of approximately 25 nm and a core diameter of 10 nm.[1,66] The structure of this material let us envisage the possibility to exploit the soft organic branches constituting the shell to allocate poorly water-soluble molecules that could more favourably interact with PEG. This can be an efficient way to transport them and also to allow their interaction with species present in the core[15a] and/or in the external water environment.[6c,67] We have, therefore, prepared 1 mL of a $3.5 \cdot 10^{-5}$ M solution of these nanoparticles in water, added 2 mg of **L2**, and stirred the mixture for 24 h. An analogous solution was obtained in the same way but in the absence of nanoparticles and used for comparison. After filtration both samples were photophysically characterized and, assuming as a reasonable approximation that the molar extinction coefficient measured in the mixed solvent could be used also for the molecules included in the PEG shell or in water, the absorption spectra revealed a higher amount of **L2** (around six times higher) in the presence of nanoparticles with respect to pure water. The comparison of three solutions containing different amounts of nanoparticles and stirred for the same time with the same quantity of **L2** shows that the active species has a direct and positive interaction with the nanoparticles because the dissolved amount of the chemosensor increases linearly with the concentration of the nanoparticles. It has to be noted, however, that the presence of a dynamic equilibrium between free and particle-interacting ligand **L2** cannot be ruled out and it is indeed quite likely. As far as the emission spectra are concerned they present a higher initial intensity than the ones observed in CH_3CN and in the mixed solvent CH_3CN:H_2O 4:1 (v/v), which can be explained with the different environment experienced by the chemosensors. Analogous experiments were done also with **L1** and **L3** yielding very similar results and even higher amounts of loaded species: eleven times higher for **L1** and thirteen times higher for **L3** in the presence of nanoparticles with respect to pure water. Moreover, even by using water buffered at pH = 10, we did not observe any significant difference in the dissolved amounts both in the presence and the absence of nanoparticles. The optical response of **L1–L3** under these conditions resulted extremely similar to that obtained in CH_3CN:H_2O 4:1 (v/v) buffered with MOPS, in fact Ca^{2+}, Cd^{2+}, Co^{2+}, Cu^{2+}, K^{+}, Mg^{2+}, Mn^{2+}, Ni^{2+}, Pb^{2+}, Zn^{2+}, and Al^{3+} ions did not cause any change either in the absorption or in the emission spectra of all the ligands. Significant variations were instead obtained in the presence of Hg^{2+} ions. The emission bands are centered at λ = 406 nm and mercury(II) complexation causes a CHEF effect: an enhancement of the intensity of a factor 1.5, 2.3, and 2.3 for **L1–L3**, respectively (*Figure 4.10* for **L3**).

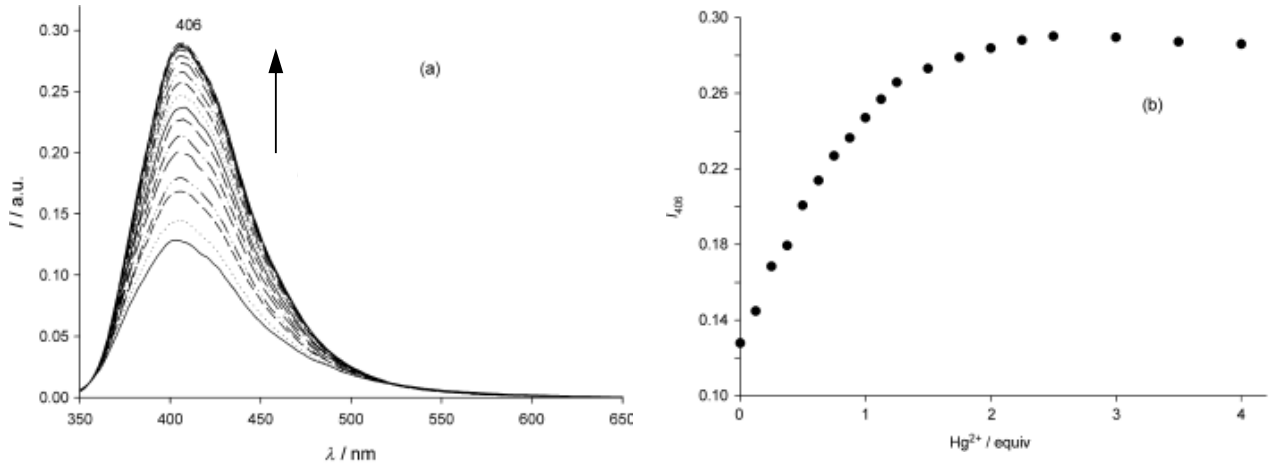

Figure 4.10: (a) emission spectra of **L3**@NPs (NP=nanoparticle) in H_2O ([**L3**]=1.0×10^{-5} M, [NPs]=1.0×10^{-5} M, 25 °C) in the presence of increasing amounts of Hg^{2+} ions; (b) emission intensity at λ = 406 nm versus the added equivalents of Hg^{2+}.

By plotting the intensity values of the maximum versus the amount of the added metal ion with a global analysis program (SPECFIT/32)[68] we could calculate association constant values of 1.3·10^5 (**L1**), 6.6·10^4 (**L2**), and 7.1·10^5 M^{-1} (**L3**), with a 1:1 complex stoichiometry under these conditions, for all the species. It has to be mentioned that all the ligands, under these conditions, interact weakly also with Fe^{3+} ions with changes in the absorption spectra dominated by the own band of the metal ion around λ = 300 nm, and a corresponding slight but constant increase in the emission intensity. An estimation of the association constant values was obtained from the emission intensity plot with the same global analysis program and they resulted in all cases lower than 100 M^{-1}. This metal ion, therefore, can be considered a very minor interfering species for Hg^{2+} ions. Finally, we investigated the response of these compounds to prolonged irradiation times (100 min) at λ = 313 nm with a medium pressure Hg lamp (125W, 1.2·10^{-9} E·cm^{-2}·s^{-1}) because photostability is always an issue in luminescent sensing and optical devices preparation, in particular when involving coumarin derivatives.[64] Major and increasing changes could be observed for all the ligands both in the absorption and the emission spectra in water in the presence of NPs and in CH_3CN, that is a red shift of the absorption band and a significant increase of the emission intensity. Moreover, the irradiation of the ligands in acidic CH_3CN causes the same responses, whereas the systems are stable in basic CH_3CN. Importantly, **L1**–**L3** are stable for short irradiation periods and all results discussed above have been obtained for ligand solutions irradiated for a period shorter than few seconds.

4.2.2.2 Solid-state studies

Despite numerous attempts to isolate the solid-state crystalline complexes of **L1**–**L3** with Hg^{2+} ions, only for [Hg(L1$_{-H}$)]NO_3 we could obtain crystals of diffraction quality by reacting **L1** and mercury(II) nitrate (1:1 molar ratio) in CH_3CN followed by a slow evaporation of the solvent. In this complex each [Hg(L1$_{-H}$)]$^+$ cation is arranged around a center of symmetry and forms a dimeric pair with a symmetry related counterpart through long Hg···O contacts of 3.006(6) Å involving the carbonyl oxygen donor atoms from the fluorogenic fragments (*Figure 4.11*).

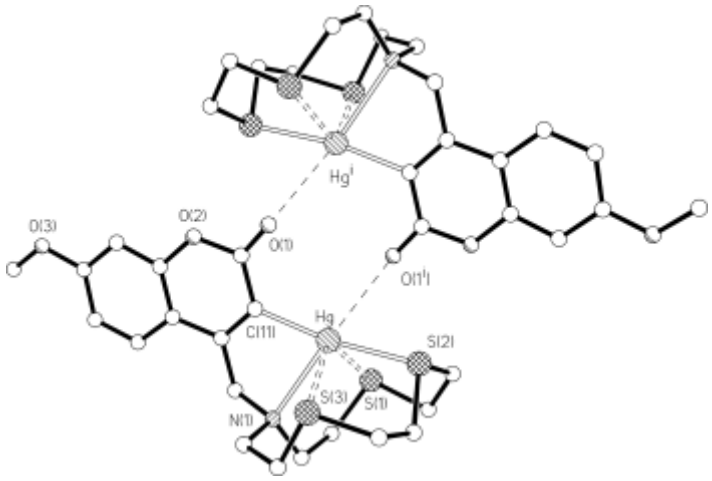

Figure 4.11: view of a dimeric unit in [Hg(**L1**$_{-H}$)]NO_3 with the adopted numbering scheme. Hydrogen atoms and counterions are omitted for clarity. Selected bond lengths [Å] and angles [°]: Hg-C(11) 2.092(10), Hg-S(2) 2.455(2), Hg-N(1) 2.610(8), Hg-S(1) 2.959(2), Hg-S(3) 3.018(3), Hg-O(1^i) 3.006(6); C(11)-Hg-S(2) 169.1(3), C(11)-Hg-N(1) 75.0(3), S(2)-Hg-N(1) 114.93(19), C(11)-Hg-S(1) 108.3(3), S(2)-Hg-S1 80.25(8), N(1)-Hg-S(1) 70.60(18), C(11)-Hg-S(3) 103.8(3), S(2)-Hg-S(3) 75.97(8), N(1)-Hg-S(3) 73.82(18), S(1)-Hg-S(3) 122.76(7), O(1^i)-Hg-C(11) 98.4(3), O(1^i)-Hg-N(1) 139.5(2), O(1^i)-Hg-S(2) 77.1(1), O(1^i)-Hg-S(1) 74.1(2).

Within each complex unit, the metal center is coordinated by the four donor atoms from the macrocyclic moiety of the ligand and by the deprotonated carbon atom in the 2-position of the coumarin fragment (C(11) in *Figure 4.11*), to afford an organometallic species. The bonds to the donor atoms are evenly distributed about the overall CNS_3O six-coordination sphere but some are significantly longer than others. In particular, the donor atoms N(1) and S(2) from the macrocyclic unit together with the carbon atom from the coumarin moiety are more strongly coordinated to the metal center with respect to the other two S-donor atoms and the carbonyl oxygen atom from the symmetry-related complex cation. To the best of our knowledge, this is the first case structurally characterized of a Hg^{2+} complex featuring a C-Hg bond from a coumarin derivative and a rare example of an organometallic compound involving a coumarin fragment.[69] The formation of an organometallic complex species in the solid state, prompted us to understand whether a similar species was responsible for the CHEF effect observed in solution on adding Hg^{2+} ions to **L1**. The ^1H NMR spectra of a CH_3CN:H_2O 4:1 (v/v) solution of Hg^{2+} ions and **L1** in 1:1 molar ratio shows, interestingly, no deprotonation of the coumarin moiety indicating that the [Hg (**L1**$_{-H}$)]$^+$ cation forms only upon crystallization. This is also in agreement with the reversibility of the complexation process verified in solution (*see 4.2.2.1*). The highest shift to lower field was observed for the signal of the methylene group connecting the coumarin moiety and the macrocyclic fragment of **L1**.

4.2.2.3 Intracellular fluorescence measurements

The interesting results obtained in solution have encouraged us to evaluate the ability of **L1–L3** as fluorescent probes to sense Hg^{2+} ions within cells by using confocal fluorescence microscopy. We used Cos-7 cells *in vitro*, and it was necessary to fix them due to the scarce solubility of **L1–L3** in water. The fixation technique with cold methanol:acetone 1:1 was chosen because it has been reported to preserve intracellular metals distribution.[70] The use of pure DMSO and CH_3CN for the preparation of **L1–L3** and $Hg(ClO_4)_2$ solutions respectively, did not affect the morphology of the cells. Images of Cos-7 cells in a control experiment without incubation with **L1–L3** and Hg^{2+} ions show no background fluorescence and no autofluorescence within the cellular environment. Analogously, cells incubated with 10 mL of **L1–L3** up to 5

min at 25 °C in the dark show no background fluorescence and no fluorescence in the cells and in the intracellular environment (*Figure 4.12(a)* for **L3**). Only cells treated first with $Hg(ClO_4)_2$ and then with **L3** (molar ratio $[Hg^{2+}]/[\mathbf{L3}]$ = 0.6) show enhanced cytosolic fluorescence emission (*Figure 4.12(b)*) demonstrating that **L3** can respond specifically to changes in intracellular Hg^{2+} ion levels.

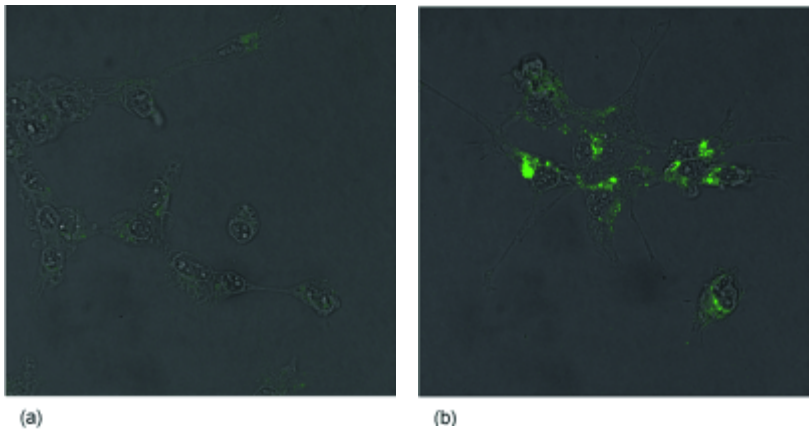

Figure 4.12: (a) confocal visualization of a Cos-7 cell culture pre-incubated with **L3** and (b) pre-incubated with Hg^{2+} ions and successively treated with ligand **L3**.

4.2.2.4 Development of solvent polymeric membrane optodes based on ligands L1–L3 for selective Hg^{2+} detection

Encouraged by the selectivity data obtained in solution, we investigated the possibility to go a step forward developing solvent polymeric membrane optodes based on the chemosensors **L1–L3**, and combining them with the familiar computer screen photo-assisted technique to afford new optical sensor devices for selective detection of mercury(II) in real samples. According to the CSPT,[36] the optical sensor (or sensor array) is placed in a transparent cuvette and exposed to various amounts of the target analyte while head-on illuminated by the polychromatic light sequence of 50 colors generated by a LCD monitor by blending the three primary red, green, and blue colors. The signal is registered by a frontally placed web camera, and two regions of interests (ROI) are selected from the obtained video stream, one for the sensing layer and the other for the background areas. The RGB (red/green/blue) intensity values of the pixel enclosed in the two ROI are averaged, and a fingerprint is then calculated subtracting the RGB sequence of the background ROI, a necessary procedure to take into account the non-homogeneity of computer-screen-illuminated camera images. The RGB fingerprint is an overall presentation of a polymeric film optic CSPT response, where the film optical signal intensity, in the presence of different analyte concentrations, is plotted versus the illuminating sequence. The output of a CSPT measurement is a matrix composed of the optode emission intensities for each excitation wavelength and for different analyte concentration. Chemometric methods of analysis are then applied for CSPT data treatment.[71] We prepared a series of PVC-based solvent polymeric membranes in order to test the suitability of the three chemosensors for the development of this kind of sensor devices. They were prepared according to literature by incorporation of the lipophilic **L1–L3** in a plasticized PVC membrane containing TpClPBK (potassium tetrakis-(4-chlorophenyl)borate) as a lipophilic anionic additive, to provide the optode membranes with the necessary ion-exchange properties.[27] In fact **L1–L3** operate as neutral carriers binding the charged Hg^{2+} analyte ions and, therefore, the incorporation of anionic lipophilic sites is required in order to induce the flux of the analyte ions into the membrane and to tune the ion-exchange properties. The compositions of the prepared membranes are listed in the *Table 4.1*.

Table 4.1: compositions of the studied PVC-based solvent polymeric membranes.

N	Ligand	Ligand molality[a]	Plasticizer[c]	TpClPBK [wt %]	L/TpClPB$^-$ molality ratio
Mb 1	**L1**	0.07	oNPOE	1	1:0.3
Mb 2	**L1**	0.07	DOS	1	1:0.3
Mb 3	**L1**	0.07	DOS	–	–
Mb 4	**L2**[b]	0.02	oNPOE	1	1:1
Mb 5	**L2**[b]	0.02	DOS	1	1:1
Mb 6	**L2**[b]	0.02	DOS	–	–
Mb 7	**L3**	0.07	oNPOE	1	1:0.3
Mb 8	**L3**	0.07	DOS	1	1:0.3
Mb 9	**L3**	0.07	DOS	–	–
Mb 10.1	**L3**	0.07	DOS	1.8	1:0.5
Mb 10.2	**L3**	0.07	DOS	5.3	1:1.5
Mb 10.3	**L3**	0.07	DOS	8.2	1:2.3
Mb 11.1	**L3**	0.07	oNPOE	1.8	1:0.5
Mb 11.2	**L3**	0.07	oNPOE	5.3	1:1.5
Mb 11.3	**L3**	0.07	oNPOE	8.2	1:2.3
Mb 12	**L3**	0.07	oNPOE	2.6[d]	1:0.5

[a] Moles of ligand for weight of membrane in [kg]. [b] The amount of ligand **L2** was 1 wt % due to its low solubility in the membrane phase. [c] Bis(2-ethylhexyl) sebacate (DOS), *o*-nitrophenyl octyl ether (oNPOE). [d] $T(CF_3)_2PBK$ (potassium tetra(bis)-3,5-trifluoromethylphenylborate) was used as cation exchanger.

We have already developed another highly sensitive Hg^{2+}-selective optode functioning in a wide analyte concentration range, incorporating 3 wt% of a fluorescent probe in a PVC-based solvent polymeric membrane.[27b] Taking advantage of those results, we have prepared membranes containing 3 wt% of **L1** or **L3**, whereas the membranes based on **L2** (Mb 4–Mb 6, *Table 4.1*) contain only 1 wt% of the ligand due to its low solubility in this phase. Considering our experimental conditions and the initial formation of 1:2 metal-to-ligand complexes (*see 4.2.2.1*), we decided to initially use 1 wt% of TpClPBK salt (Mb 1–Mb 9, *Table 1*).
The influence of the pH value of the background solution on the optical response towards Hg^{2+} ions of the prepared PVC-based membranes was first evaluated. The fluorescence intensity was measured on the UBS (Universal Buffer Solution) background at an initial pH of 2.7 in the presence of a $2.7 \cdot 10^{-6}$ M solution of Hg^{2+} ions, and then adding increasing amounts of a 1 M NaOH solution to reach the final pH = 10.3. We found that the fluorescence response of the membranes based on **L1**–**L3** is almost pH independent in the range pH 4.8–8.0, and for this reason we have performed our further tests in buffered solutions at pH 5.5 with 0.01 M 2-(N-morpholino)ethanesulfonic acid (MES). The sensitivity of the optode membranes, however, can also be varied by the rational design of the polymeric membrane composition, and in particular, the choice of the plasticizer is very important, because it improves the permeability, reduces the brittleness, and tunes the fluorescence emission intensity.[27] The membranes Mb 8 and Mb 9 based on **L3** and plasticized with DOS, exhibited the highest fluorescence intensity enhancement in the presence of Hg^{2+} ions, indicating an optimal Hg^{2+} binding ability of **L3** under these conditions (*Figure 4.13*). Moreover, the addition of $TpClPB^-$ significantly improved the optical response of **L3**-based membranes, as it can be noted by comparing Mb 8 (L3/DOS/TpClPBK) and Mb 9 (L3/DOS).

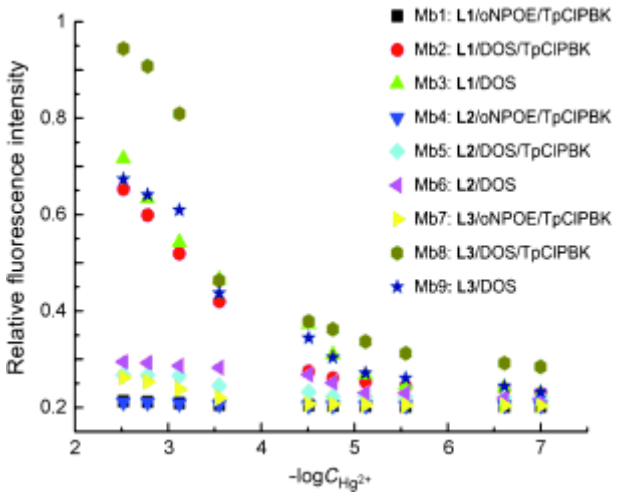

Figure 4.13: fluorescence response of membranes based on **L1–L3** in 0.01 M MES background solutions buffered at pH 5.5 upon addition of increasing amounts of Hg^{2+} ions.

We also investigated the highly polar plasticizer oNPOE that promotes the dissociation of membrane-active components, thereby improving the ionic transport. It had already been shown, however, that it can also present a drawback, like other organic nitro compounds it can act as a luminescence quencher for several fluorophores.[72] In fact, as it can be seen from *Figure 4.13*, the oNPOE-plasticized membranes Mb 1, Mb 4, and Mb 7 containing **L1**, **L2**, and **L3**, respectively, present a very low fluorescence emission in comparison with membranes plasticized with DOS. After analyzing all the fluorescence responses of membranes Mb 1–Mb 9 based on **L1–L3** reported in *Figure 4.13*, we decided to focus our attention in the optimization of the systems based on membranes containing **L3**, which appeared to be the most promising for both fluorescence and CSPT measurements. Interestingly, on passing on to CSPT measurements, the oNPOE-plasticized membrane Mb 7 resulted more effective in the Hg^{2+} content evaluation and demonstrated higher optical intensity changes in comparison with the DOS-plasticized membrane Mb 8. This is probably due to the higher polarity of the plasticizer oNPOE in comparison with DOS (ε(oNPOE) = 24 and ε(DOS) = 4.6), which permits faster Hg^{2+} ion exchange processes among the sample and the membrane phase. We report in *Figure 4.14* the averaged CSPT optical intensity response (obtained as mean value of the RGB signals) of the oNPOE-plasticized membrane Mb 7 based on **L3** to the presence of Hg^{2+} ions and other possible interfering cations (Na^{+}, Zn^{2+}, Cu^{2+}, Ni^{2+}, Cd^{2+}, and Pb^{2+}) in different concentrations. The selectivity revealed by membrane Mb 7 containing **L3** towards Hg^{2+} ions over the other tested cations clearly demonstrates that ligand **L3** is suitable also to be used for the development of effective solvent polymeric optode membranes. To this goal, as mentioned above, the incorporation of anionic lipophilic $TpClPB^{-}$ sites is required for membranes based on neutral carriers such as **L1–L3**. It has to be considered that for our probes the formation of a 1:2 metal-to-ligand complex is prevalent in CH_3CN:H_2O 4:1 (v/v) solution at low Hg^{2+} concentration, whereas the 1:1 complexes is the observed form at high Hg^{2+} concentrations. Therefore, in the membrane phase, a molar content of lipophilic anions of 30–50% with respect to the carrier is sufficient to stabilize the ion-exchange process when the mercury concentration is low, but an excess of the anions is necessary at high mercury concentrations to guarantee the membrane ion-exchange efficacy.

The attended equilibria in the two different mercury(II) regimes, low and high concentrations of Hg^{2+}, are given in Equations (1) and (2), respectively.

$$2L_{org} + Hg^{2+}_{aq} + 2TpClB^-_{org} + 2K^+_{org} \leftrightharpoons L_2Hg^{2+}_{org} + 2TpClB^-_{org} + 2K^+_{org} \quad (1)$$

$$L_2Hg^{2+}_{org} + Hg^{2+}_{aq} + 4TpClB^-_{org} + 4K^+_{org} \leftrightharpoons 2LHg^{2+}_{org} + 4TpClB^-_{org} + 4K^+_{aq} \quad (2)$$

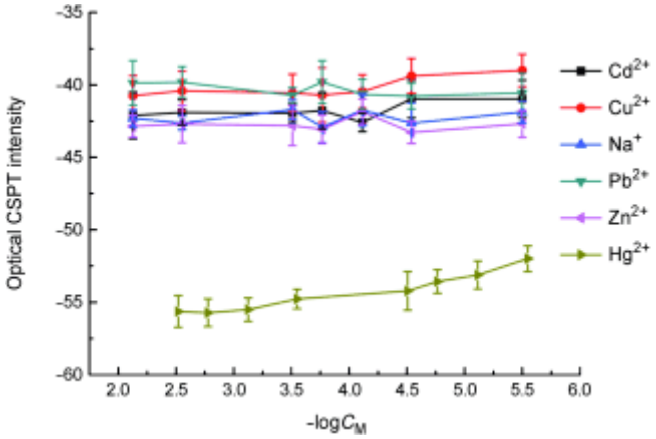

Figure 4.14: averaged CSPT response of membrane Mb 7 (**L3**/oNPOE/TpClPBK) to different amounts of Hg^{2+} ions and other possible interfering cations in 0.01 M MES background solution buffered at pH 5.5.

In order to evaluate the optimal ratio between the ligand and the cation exchanger in the Hg^{2+}-selective optode membrane, we compared the properties of seven new membranes based on 3 wt% of **L3**, and doped with different amounts of TpClPBK (except Mb 12 doped with $T(CF_3)_2PBK$, see *Table 1*). We also tested the possible influence of the different plasticizers and, therefore, we prepared Mb 10.1–Mb 10.3 with DOS, and Mb 11.1–Mb 11.3 and Mb 12 with oNPOE. Once again, the DOS-plasticized membranes were found to be more effective for fluorimetric detection of Hg^{2+} ions that in the polymeric solvent optode membrane **L3** functions as a neutral carrier and prevalently forms a 1:1 complex with the target Hg^{2+} ion. However, CSPT detection of Hg^{2+} ions indicated that, among all tested membranes based on **L3** and containing a different ligand/cation exchanger molar ratio, the oNPOE-plasticized membrane Mb 11.2, doped with 5.3 wt% of TpClPBK showed the highest response to the presence of the target cation (see *Figure 4.15(b)*). The negative gradient of CSPT optical intensity in *Figure 4.15(b)* indicates an enhancement of the film emission upon Hg^{2+} exposure.

The polarity of plasticizer oNPOE favours the dissociation of TpClPBK, and, hence, a lower amount of the cation exchanger (5.3 vs. 8.2 wt%, respectively) is needed in the oNPOE-plasticized membranes to achieve the same analytical performances of the DOS-plasticized ones, thus confirming the 1:1 complexation stoichiometry already observed for the membranes prepared with DOS. The substitution of TpClPK with the more hydrophobic cation exchanger $T(CF_3)_2PBK$ in Mb 12 did not lead to an improvement of the membrane properties as expected, but on the contrary, resulted in a quenched fluorescence intensity of the membrane. The photophysical characterization in solution of **L1–L3** evidenced a certain photosensitivity of these systems under prolonged irradiation at λ = 313 nm. Because this could influence the selectivity, the lifetime, and the reproducibility of developed optodes, we have studied the influence of a prolonged direct light exposure of membranes based on **L3** on their fluorescence and CSPT responses to the presence of Hg^{2+} ions. To this purpose we freshly prepared membranes Mb 10.2 and Mb 11.2 (plasticized with DOS and

oNPOE, respectively) and the films obtained were in part stored in darkness and tested one day after, and in part kept under direct daylight for a period of time ranging from one to three months.

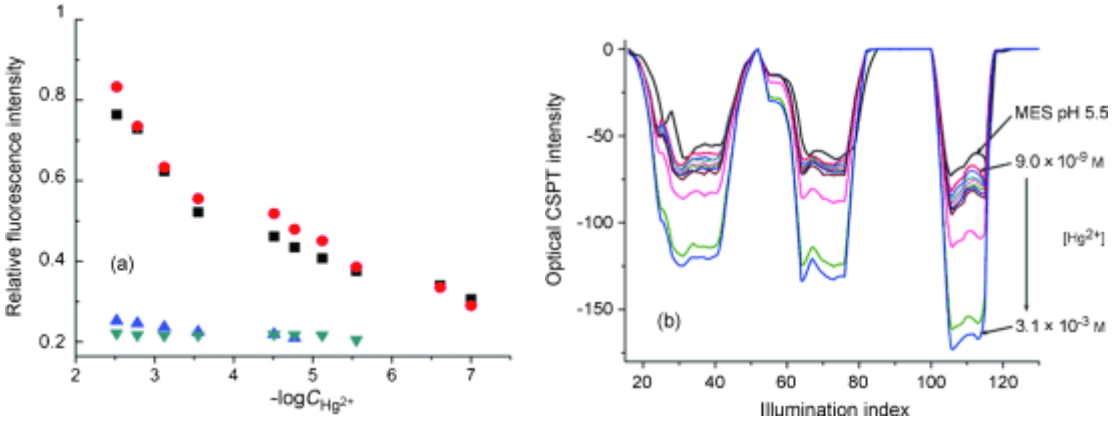

Figure 4.15: (a) fluorescence response towards Hg^{2+} ion of membranes based on **L3** containing different amount of lipophilic anionic sites (black squares=Mb 10.2, **L3**/DOS/TpClPBK 5.3 wt %; red circles=Mb 10.3, **L3**/DOS/TpClPBK 8.2 wt %; blue triangles=Mb 11.1, **L3**/oNPOE/TpClPBK 1.8 wt %; green triangles=Mb 11.2, **L3**/oNPOE/TpClPBK 5.3 wt %); (b) CSPT response of Mb 11.2 (**L3**/oNPOE/TpClPBK 5.3 wt %) towards the following concentrations of Hg^{2+} ions: 9.0×10^{-9}, 9.8×10^{-8}, 2.4×10^{-7}, 2.8×10^{-6}, 7.7×10^{-6}, 1.7×10^{-5}, 3.1×10^{-5}, 2.8×10^{-4}, 7.5×10^{-4}, 1.7×10^{-3}, 3.1×10^{-3} M. Measurements were performed in 0.01 M MES background solution buffered at pH 5.5.

The freshly prepared DOS-plasticized membrane Mb 10.2 presented two fluorescence emission peaks at λ = 380 and 414 nm, respectively, with similar slopes of luminescence intensity versus p[Hg] in the range 3.5–7.0 p[Hg] units (*Figure 4.16*).

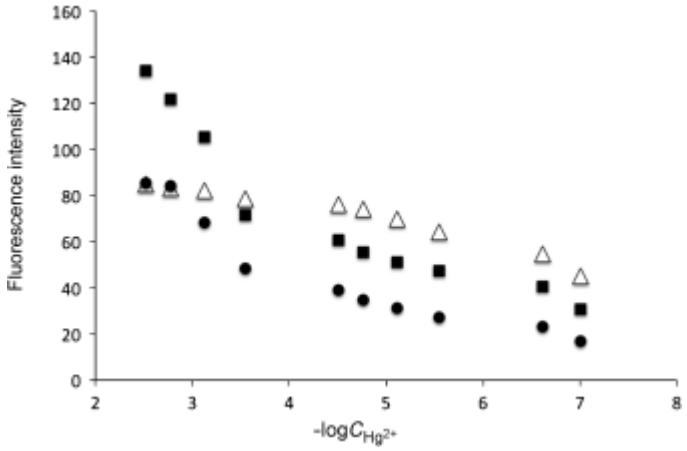

Figure 4.16: comparison of the fluorescence response of freshly prepared (▪: λ=414, •: λ=380 nm) and one month daylight-illuminated films (△) made on membrane Mb 10.2 (**L3**/DOS/TpClPBK 5.3 wt %) towards different Hg^{2+} amounts.

In the case of one month daylight-illuminated membranes the peak at λ = 380 nm disappeared, and an overall increase of the fluorescent signal intensity was registered.[73] A similar result was obtained for the CSPT response of membrane Mb 10.2 (see *Figures 4.17 (a)* and *(b)*), whereas the optical activity of membrane Mb 11.2 did not degrade with time and daylight illumination exposure (*Figures 4.17 (c)* and *(d)*). On the contrary, the calibration curve of membrane Mb 11.2 becomes linear in an even wider p[Hg] range with a higher slope (*Figure 4.17 (d)*). These results indicate that membrane Mb 11.2 is the most effective membrane for the CSPT detection of mercury(II) ions, but they also confirm the importance of the correct

handling and storage of these systems. The freshly prepared DOS-plasticized membrane Mb 10.2, for example, should be stored in the dark in order to avoid the fluorescence intensity baseline correction procedure. The practical applicability of the proposed optical sensors based on **L3** for selective mercury ions detection was checked in the natural superficial and potable water samples taken in the Rome area and the results obtained are gathered in *Table 4.2*.

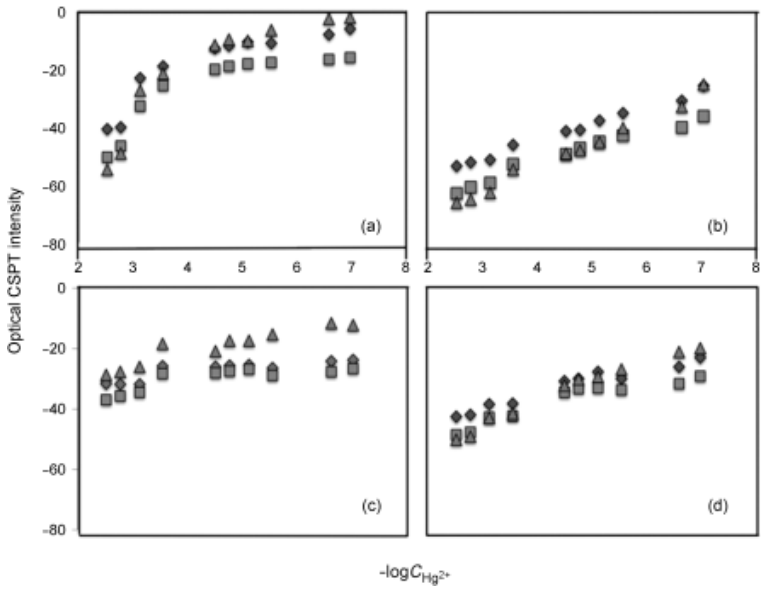

Figure 4.17: comparison of the CSPT optical response of freshly prepared (a and c) and one month period daylight-illuminated films (b and d) based on membrane Mb 10.2 (**L3**/DOS/TpClPBK 5.3 wt %) (on the top) and membrane Mb 11.2 (**L3**/oNPOE/TpClPBK 5.3 wt %) (on the bottom) towards Hg^{2+} ions (♦=red channel, ▪=green channel, ▲=blue channel).

Table 4.2: determination of Hg^{2+} contents in natural water samples by using the proposed optodes based on **L3**

	[Hg^{2+}] in natural water samples [μg L^{-1}]		**[Hg^{2+}] found after addition of 1000 μg L^{-1} of Hg^{2+} [μg L^{-1}]**			
	fluorescence sensor[a]	**DMA[b]**	**fluorescence sensor[a]**		**CSPT sensor array[c]**	
			[Hg^{2+}] [μg L^{-1}]	**R.S.D. [%][d]**	**[Hg^{2+}] [μg L^{-1}]**	**R.S.D. [%][d]**
lake	0.036	<0.1	936	5.83	1136	13.6
river	0.071	<0.1	1018	2.32	1088	8.80
tap	0.035	<0.1	896	9.81	1046	4.60

[a] Average value from three fluorescence determinations with freshly prepared membrane Mb 10.2 stored in the dark. [b] Atomic absorption spectroscopy by using the Milestone DMA-80 direct mercury analyzer. [c] Array composed of triplicated spots of freshly prepared membranes Mb 10.2 and Mb 11.2 stored in the dark. [d] R.S.D. is the relative standard deviation evaluated for three replicated measurements.

The Hg^{2+} amount was determined in natural water samples both by means of fluorescence and CSPT and the results were compared with the data obtained by atomic absorbance spectroscopy coupled with mercury amalgam formation in a direct mercury analyzer (DMA-80). From the data shown in *Table 4.2*, we can conclude that the mercury contents determined in natural water samples by means of the proposed fluorescence sensor lies well below the maximal permissible concentrations of 0.001 and 0.002 mgL^{-1} recommended respectively by WHO (World Health Organization) and EPA (United States Environmental Protection Agency),[74, 75] and even under the limit of detection of the standard DMA method. To compare

the performances of membrane Mb 10.2 based on **L3** by using classical fluorescence technique and the CSPT approach we tested the same natural water samples spiked with 1 mgL^{-1} of [Hg^{2+}]. The measurements were performed in triplicates for every sample. The standard calibration curve method[27b] was applied for the fluorimetric optodes, whereas the partial least squares (PLS) regression technique was used to obtain a correlation between the CSPT responses and the mercury ion content in calibration solutions of known concentrations. The CSPT optical sensor array was composed of triplicated freshly prepared and stored in the dark membranes Mb 10.2 and Mb 11.2, in total six sensing spots deposited on the same glass slide. The optical intensity at red, green, and blue light channels of every sensing spot was measured in the presence of increasing Hg^{2+} concentrations. The final data set was composed of two membranes x three replicates x three RGB mean signals x ten Hg^{2+} concentrations (180 points in total) and was used for the partial least squares regression model construction. The standard calibration curve method was applied for the fluorimetric optodes, whereas the PLS regression technique was used to obtain the correlation between the CSPT responses and the mercury(II) ion content in calibration solutions of known concentrations. Due to the limited number of the analyzed samples the validation was performed by using a leave-one-out cross-validation procedure. The correlation coefficient of the CSPT optical intensity measured versus the known amount of mercury(II) in the calibration solutions was R^2_{cal} = 0.996, root mean square error of calibration (RMSEC)=0.02 mM; on validation step R^2_{val} = 0.994 and root mean square error of validation (RMSEV) = 0.186 mM. In terms of the RMSEC and RMSEV values, the arrays based on membranes Mb 10.2 and Mb 11.2 resulted to be the most effective for mercury(II) detection in comparison with only DOS- (RMSEC = 0.218 and RMSEV = 0.285 mM) or only oNPOE plasticized membranes (RMSEC = 0.178 and RMSEV = 0.269 mM). It is worth mentioning that the CSPT multisensor array application permitted to obtain a linear response towards mercury(II) ion in the concentration range from $9.0 \cdot 10^{-9}$ to $3.1 \cdot 10^{-3}$ M with a low detection limit of $9.1 \cdot 10^{-9}$ M and a high detection limit of $1.7 \cdot 10^{-3}$ M.[76] Considering the above reported maximal permissible concentrations of mercury in potable water, the device, even though very simple and cheap, can be applied for the analysis of real samples. Even the drift observed in the optical features of pristine and aged membranes can be easily solved for the analysis in the real field, by application of a calibration protocol before measurements.

4.2.3 Conclusion

We have shown the photochemical characterization of new coumarin-based fluorescent molecular probes in different media. We have also successfully used these chemosensors for imaging Hg^{2+} ions in cells *in vitro* and for the development of optical sensors for the same heavy metal in natural water, taking advantage from the computer screen photo-assisted (CSPT) measuring method. Despite the great scientific effort devoted to the field in the last decades, there is still a great need of easy to handle and disposable fluorescent devices for *in situ* monitoring of target analytes in real matrices, especially toxic metal ions. Their development is a challenging task both for the preparation of the sensing material and for its coupling with an appropriate transducer part without loss of selectivity and sensitivity in the desired media. This study demonstrates the great versatility and efficacy of coumarin derivatives in the field of supramolecular chemistry due to their photophysical properties that also allow preparing sensitive materials when interacting with silica core–PEG shell nanoparticles or supported in PVC-based polymeric membranes. It has to be mentioned that the known photodegradation of these type of compounds in solution is surely an issue and research is in due course to design and obtain more stable systems maintaining, or even improving, their sensing features. Nevertheless, it has to be remarked that this drawback is not a constrain in the preparation of the sensing devices, as demonstrated by the reported data. The obtained results, in fact, show that by using membranes prepared with **L3** we could fluorimetrically determine the mercury(II)

content in natural water samples in concentrations that lay well below the maximal presence recommended respectively by WHO and EPA, and even under the limit of detection of the standard DMA method. Moreover, devices obtained with the same membranes and the very convenient CSPT can be also applied to efficiently measure the mercury(II) ion content in real samples presenting a linear response in a concentration range compatible with the current regulation.

References and notes

The contents of this chapter are based on E. Rampazzo, S. Bonacchi, D. Genovese, R. Juris, M. Sgarzi, M. Montalti, L. Prodi, N. Zaccheroni, G. Tomaselli, S. Gentile, C. Satriano, E. Rizzarelli, *Chem. Eur. J.*, **2011**, *17*, 13429 - Reproduced by permission of WILEY-VCH Verlag GmbH & Co. and on C. Bazzicalupi, C. Caltagirone, Z. Cao, Q. Chen, C. Di Natale, A. Garau, V. Lippolis, L. Lvova, H. Liu, I. Lundström, M. C. Mostallino, M. Nieddu, R. Paolesse, L. Prodi, M. Sgarzi, N. Zaccheroni, *Chem. Eur. J.*, **2013**, *19*, 14639 - Reproduced by permission of WILEY-VCH Verlag GmbH & Co.

[1] a) L. Prodi, *New J. Chem.*, **2005**, *29*, 20; b) S. Bonacchi, D. Genovese, R. Juris, M. Montalti, L. Prodi, E. Rampazzo, N. Zaccheroni, *Angew. Chem.* **2011**, *123*, 4142, *Angew. Chem. Int. Ed.* **2011**, *50*, 4056; c) S. Bonacchi, D. Genovese, R. Juris, M. Montalti, L. Prodi, E. Rampazzo, M. Sgarzi, N. Zaccheroni, *Top. Curr. Chem.*, **2011**, *300*, 93

[2] T. Doussineau, A. Schulz, A. Lapresta-Fernandez, A. Moro, S. Körsten, S. Trupp, G. J. Mohr, *Chem. Eur. J.*, **2010**, *16*, 10290

[3] L. Wang, K. M. Wang, S. Santra, X. J. Zhao, L. R. Hilliard, J. E. Smith, J. R. Wu, W. H. Tan, *Anal. Chem.*, **2006**, *78*, 646

[4] A. Burns, H. Ow, U. Wiesner, *Chem. Soc. Rev.*, **2006**, *35*, 1028

[5] K. T. Yong, I. Roy, M. T. Swihart, P. N. Prasad, *J. Mater. Chem.*, **2009**, *19*, 4655

[6] a) M. Montalti, L. Prodi, N. Zaccheroni, *J. Mater. Chem.*, **2005**, *15*, 2810; b) S. Bonacchi, E. Rampazzo, M. Montalti, L. Prodi, N. Zaccheroni, F. Mancin, P. Teolato, *Langmuir*, **2008**, *24*, 8387; c) E. Oliveira, D. Genovese, R. Juris, N. Zaccheroni, J. L. Capelo, M. M. M. Raposo, S. P. G. Costa, L. Prodi, C. Lodeiro, *Inorg. Chem.*, **2011**, *50*, 8834

[7] P. Teolato, E. Rampazzo, M. Arduini, F. Mancin, P. Tecilla, U. Tonellato, *Chem. Eur. J.*, **2007**, *13*, 2238

[8] a) R. B. Franklin, L. C. Costello, *Arch. Biochem. Biophys.*, **2007**, *463*, 211; b) A. Gonzalez, M. Peters, J. W. Lampe, E. White, *Nutr. Cancer*, **2009**, *61*, 206

[9] a) Q. Pasha, S. A. Malik, J. Iqbal, N. Shaheen, M. H. Shah, *Biol. Trace Elem. Res.*, **2008**, *125*, 30; b) M. Yaman, *Curr. Med. Chem.*, **2006**, *13*, 2513

[10] a) A. I. Bush, *Curr. Opin. Chem. Biol.*, **2000**, *4*, 184; b) K. J. Barnham, A. I. Bush, *Curr. Opin. Chem. Biol.*, **2008**, *12*, 222

[11] P. J. Crouch, K. J. Barnham, A. I. Bush, A. R. White, *Drug News Perspect.*, **2006**, *19*, 469

[12] G. Filiz, K. A. Price, A. Caragounis, T. Du, P. J. Crouch, A. R. White, *Eur. Biophys. J.*, **2008**, *37*, 315

[13] a) L. Zeng, E.W. Miller, A. Pralle, E. Y. Isacoff, C. J. Chang, *J. Am. Chem. Soc.*, **2006**, *128*, 10; b) D. W. Domaille, L. Zeng, C. J. Chang, *J. Am. Chem. Soc.*, **2010**, *132*, 1194; c) A. F. Chaudhry, M. Verma, M. T. Morgan, M. M. Henary, N. Siegel, J. M. Hales, J. W. Perry, C. J. Fahrni, *J. Am. Chem. Soc.*, **2010**, *132*, 737; d) A. F. Chaudhry, S. Mandal, K. I. Hardcastle, C. J. Fahrni, *Chem. Sci.*, **2011**, *2*, 1016

[14] S. Zanarini, E. Rampazzo, S. Bonacchi, R. Juris, M. Marcaccio, M. Montalti, F. Paolucci, L. Prodi, *J. Am. Chem. Soc.*, **2009**, *131*, 14208

[15] a) E. Rampazzo, S. Bonacchi, R. Juris, M. Montalti, D. Genovese, N. Zaccheroni, L. Prodi, D. C. Rambaldi, A. Zattoni, P. Reschiglian, *J. Phys. Chem. B*, **2010**, *114*, 14605; b) D. Genovese, M. Montalti, L. Prodi, E. Rampazzo, N. Zaccheroni, K. Altenhöner, F. May, J. Mattay, *Chem. Commun.*, **2011**, *47*, 10975

[16] L. Banci, I. Bertini, S. Ciofi-Baffoni, T. Kozyreva, K. Zovo, P. Palumaa, *Nature*, **2010**, *465*, 645

[17] L. A. Finney, T. V. O'Halloran, *Science*, **2003**, 300, 931

[18] a) L. Tapia, M. Gonzalez-Agüero, M. F. Cisternas, M. Suazo, V. Cambiazo, R. Uauy, M. González, *Biochem. J.*, **2004**, *378*, 617; b) H.W. Chan, T. Liu, G. Verdile, G. Bishop, R. J. Haasl, M. A. Smith, G. Perry, R. N. Martins, C. S. Atwood, *Int. J. Clin. Exp. Med.*, **2008**, *1*, 76

[19] P. Vernet, *Heavy Metals in The Environment*, Elsevier, New York, **1991**

[20] A. Siegel, H. Siegel, R. K.O Siegel, *Metal Ions in Life Sciences. Neurodegenerative Diseases and Metal Ions*, Vol. 1, Wiley, New York, **2006**

[21] G. F. Nordberg, B. A. Fowler, M. Nordberg, L. Friberg, *Handbook on the Toxicology of Metals*, 3rd ed., Elsevier, New York, **2007**

[22] W. F. Fitzgerald, C. H. Lamborg, C. R. Hammerschmidt, *Chem. Rev.*, **2007**, *107*, 641

[23] L. Charlet, Y. Chapron, P. Faller, R. Kirsch, A. T. Stone, P. C. Bayeye, *Coord. Chem. Rev.*, **2012**, *256*, 2147

[24] (a) T. Tsubaki, K. Irukayama, *Minamata disease*, Kodansha Ltd, Tokyo, 1977; (b) N. J. Langford, R. E. Ferne, *J. Hum. Hypertens.*, **1999**, *13*, 651

[25] a) C. Burrini, A. Cagnini, *Talanta*, **1997**, *44*, 1219; b) A. Shafawi, L. Eddon, M. Foulkes, P. Stockwell, W. Corns, *Analyst*, **1999**, *124*, 185; c) Y. Yamini, N. Alizadeh, M. Shamsipur, *Anal. Chim. Acta*, **1997**, *355*, 69; d) Z. Liu, Z. Zhu, H. Zheng, S. Hu, *Anal. Chem.*, **2012**, *84*, 10170

[26] a) M. J. Powell, E. S. K. Quan, D. W. Boomer, D. R. Wiederin, *Anal. Chem.*, **1992**, *64*, 2253; b) I. Gelaude, R. Dams, F. Vanhaecke, L. Moens, *Anal. Chem.*, **2002**, *74*, 3833; c) Y. Gao, Z. Shi, Z. Long, P. Wu, C. Zheng, X. Hou, *Microchem. J.*, **2012**, *103*, 1

[27] a) A. Segura-Carretero, J. M. Costa-Fernndez, R. Pereiro, A. Sanz-Medel, *Talanta*, **1999**, *49*, 907; b) M. Shamsipur, M. Hosseini, K. Alizadeh, N. Alizadeh, A. Yari, C. Caltagirone, V. Lippolis, *Anal. Chim. Acta*, **2005**, *533*, 17; c) W. H. Chan, R. H. Yang, K. M. Wang, *Anal. Chim. Acta*, **2001**, *444*, 261

[28] H. N. Kim, W. X. Ren, J. S. Kim, J. Yoon, *Chem. Soc. Rev.*, **2012**, *41*, 3210

[29] E. M. Nolan, S. J. Lippard, *Chem. Rev.*, **2008**, *108*, 3443

[30] K. Kaur, R. Saini, A. Kumar, V. Luxami, N. Kaur, P. Singh, S. Kumar, *Coord. Chem. Rev.*, **2012**, *256*, 1992

[31] E. S. Childress, C. A. Roberts, D. Y. Sherwood, C. L. M. LeGuyard, E. S. Harbron, *Anal. Chem.*, **2012**, *84*, 1235

[32] H. Dai, Y. Yan, Y. Guo, L. Fan, Z. Che, H. Xu, *Chem. Eur. J.*, **2012**, *18*, 11188

[33] H. Lee, H.-S. Lee, J. H. Reibenspies, R. Hancock, *Inorg. Chem.*, **2012**, *51*, 10904

[34] J. Dessingou, K. Tabbasum, A. Mitra, V. K. Hinge, C. P. Rao, *J. Org. Chem.*, **2012**, *77*, 1406

[35] a) G. K. Darbha, A. Ray, P. C. Ray, *ACSNano*, **2007**, *1*, 208; b) Nuriman, B. Kuswandi, W. Verboom, *Sensors Actuators B*, **2011**, *157*, 438

[36] D. Filippini, S. Svensson, I. Lundström, *Chem. Commun.*, **2003**, 240

[37] A. P. de Silva, H. Q. N. Gunaratne, T. Gunnlaugsson, A. J. M. Huxley, C. P. McCoy, J. T. Rademacher, T. E. Rice, *Chem. Rev.*, **1997**, *97*, 1515

[38] Special issue on luminescent sensors: *Coord. Chem. Rev.*, **2000**, *205*, 1, guest editor L. Fabbrizzi

[39] Special issue on chemical sensors: *Chem. Rev.*, **2000**, *100*, 2477, guest editors A. B. Ellis, D. R. Walt

[40] K. Rurack, *Spectrochimica Acta, Part A*, **2001**, *57*, 2161

[41] L. Fabbrizzi, M. Licchelli, A. Taglietti, *Dalton Trans.*, **2003**, 3471

[42] T. W. Bell, N. M. Hext, *Chem. Soc. Rev.*, **2004**, *33*, 589

[43] Theme issue on fluorescent sensors: *J. Mater. Chem.*, **2005**, *15*, 2617, guest editors A. P. de Silva, P. Tecilla

[44] V. Amendola, L. Fabbrizzi, F. Foti, M. Licchelli, C. Mangano, P. Pallavicini, A. Poggi, D. Sacchi, A. Taglietti, *Coord. Chem. Rev.*, **2006**, *250*, 273

[45] L. Basabe-Desmonts, D. N. Reinhoudt, M. Crego-Calama, *Chem. Soc. Rev.*, **2007**, *36*, 993

[46] C. Lodeiro, F. Pina, *Coord. Chem. Rev.*, **2009**, *253*, 1353

[47] M. Formica, V. Fusi, L. Giorgi, M. Micheloni, *Coord. Chem. Rev.*, **2012**, *256*, 170

[48] R. T. Bronson, J. S. Bradshaw, P. B. Savage, S. Fuangswasdi, S. C. Lee, K. E. Krakowiak, R. M. Izatt, *J. Org. Chem.*, **2001**, *66*, 4752

[49] S. C. Lee, R. M. Izatt, X. X. Zhang, E. G. Nelson, J. D. Lamb, P. B. Savage, J. B. Bradshaw, *Inorg. Chim. Acta*, **2001**, *317*, 174

[50] a) G. De Santis, L. Fabbrizzi, M. Licchelli, C. Mangano, D. Sacchi, N. Sardone, *Inorg. Chim. Acta*, **1997**, *257*, 69; b) S. Yoon, E. W. Miller, Q. He, P. H. Do, C. J. Chang, *Angew. Chem.*, **2007**, *119*, 6778; *Angew. Chem. Int. Ed.*, **2007**, *46*, 6658

[51] a) A. J. Blake, A. Bencini, C. Caltagirone, G. De Filippo, L. S. Dolci, A. Garau, F. Isaia, V. Lippolis, P. Mariani, L. Prodi, M. Montalti, N. Zaccheroni, C. Wilson, *Dalton Trans.*, **2004**, 2771; b) M. C. Aragoni, M. Arca, A. Bencini, A. J. Blake, C. Caltagirone, G. De Filippo, F. A. Devillanova, A. Garau, T. Gelbrich, M. B. Hursthouse, F. Isaia, V. Lippolis, M. Mameli, P. Mariani, B. Valtancoli, C. Wilson, *Inorg. Chem.*, **2007**, *46*, 4548; c) A. Tamayo, B. Pedras, C. Lodeiro, L. Escriche, J. Casab, J. L. Capelo, B. Covelo, R. Kivekas, R. Sillanpää, *Inorg. Chem.*, **2007**, *46*, 7818

[52] a) D. Jiménez, R. Martínez-Máñez, F. Sancenón, J. Soto, *Tetrahedron Lett.*, **2004**, *45*, 1257; b) J. V. Ros-Lis, R. Martínez-Máñez, K. Rurack, F. Sancenón, J. Soto, M. Spieles, *Inorg. Chem.*, **2004**, *43*, 5183; c) A. B. Descalzo, R. Martínez-Máñez, R. Redeglia, K. Rurack, J. Soto, *J. Am. Chem. Soc.*, **2003**, *125*, 3418

[53] a) K. Rurack, C. Trieflinger, A. Koval'chuck, J. Daub, *Chem. Eur. J.*, **2007**, *13*, 8998; b) J. L. Bricks, A. Kovalchuck, C. Trieflinger, M. Nofz, M. Büschel, A. I. Tolmachev, J. Daub, K. Rurack, *J. Am. Chem. Soc.*, **2005**, *127*, 13522

[54] a) M.-J. Li, B. W.-K. Chu, N. Zhu, V. W.-W. Yam, *Inorg. Chem.*, **2007**, *46*, 720; b) M.-J. Li, C.-C. Ko, G.-P. Duan, N. Zhu, V.W.-W. Yam, *Organometallics*, **2007**, *26*, 6091

[55] a) M. Kadarkaraisamy, A. G. Sykes, *Polyhedron*, **2007**, *26*, 1323; b) M. Kadarkaraisamy, A. G. Sykes, *Inorg. Chem.*, **2006**, *45*, 779

[56] S. Yoon, A. E. Albers, A. P. Wong, C. J. Chang, *J. Am. Chem. Soc.*, **2005**, *127*, 16030

[57] a) M. Yuan, Y. Li, J. Li, C. Li, X. Liu, J. Lv, J. Xu, H. Liu, S. Wang, D. Zhu, *Org. Lett.*, **2007**, *9*, 2313; b) M.-L. Ho, K.-Y. Chen, G.-H. Lee, Y.-C. Chen, C.-C. Wang, J.-F. Lee, W.-C. Chung, P.-T. Cjou, *Inorg. Chem.*, **2009**, *48*, 10304

[58] Y. Song, Z. Chen, H. Li, *Curr. Org. Chem.*, **2012**, *16*, 2690

[59] M. Mameli, M. C. Aragoni, M. Arca, C. Caltagirone, F. Demartin,G. Farruggia, G. De Filippo, F. A. Devillanova, A. Garau, F. Isaia, V.Lippolis, S. Murgia, L. Prodi, A. Pintus, N. Zaccheroni, *Chem. Eur. J.*, **2010**, *16*, 919

[60] M. Mameli, V. Lippolis, C. Caltagirone, J. L. Capelo, O. N. Faza, C. Lodeiro, *Inorg. Chem.*, **2010**, *49*, 8276

[61] M. C. Aragoni, M. Arca, A. Bencini, A. J. Blake, C. Caltagirone, A. Decortes, F. Demartin, F. A. Devillanova, E. Faggi, L. S. Dolci, A. Garau, F. Isaia, V. Lippolis, L. Prodi, C. Wilson, B. Valtancoli, N. Zaccheroni, *Dalton Trans.*, **2005**, 2994

[62] a) K. Sen, P. Bagchi, *J. Org. Chem.*, **1959**, *24*, 316; b) M. Chatterjee, S. Chatterjee, M. B. Roy, S. Ghosh, P. Bandyopadhyay, P. K. Bharadwaj, *J. Lumin.*, **2002**, *99*, 175; c) C. P. Kulatilleke, S. A. De Silva, Y. Eliav, *Polyhedron*, **2006**, *25*, 2593

[63] W. Jivaramonaikul, P. Rashatasakhon, S. Wanichewecharungruang, *Photochem. Photobiol. Sci.*, **2010**, *9*, 1120

[64] H. Abbas, *Comput. Theor. Chem.*, **2012**, *992*, 55

[65] a) L. Prodi, C. Bargossi, M. Montalti, N. Zaccheroni, N. Su, J. S. Bradshaw, R. M. Izatt, P. B. Savage, *J. Am. Chem. Soc.*, **2000**, *122*, 6769; b) G. Farruggia, S. Iotti, M. Lombardo, C. Marracini, D. Petruzziello, L. Prodi, M. Sgarzi, C. Trombini, N. Zaccheroni, *J. Org. Chem.*, **2010**, *75*, 6275

[66] M. Montalti, E. Rampazzo, N. Zaccheroni, L. Prodi, *New J. Chem.*, **2013**, *37*, 28

[67] E. Rampazzo, S. Bonacchi, D. Genovese, R. Juris, M. Sgarzi, M. Montalti, L. Prodi, N. Zaccheroni, G. Tomaselli, S. Gentile, C. Satriano, E. Rizzarelli, *Chem. Eur. J.*, **2011**, *17*, 13429

[68] a) H. Gampp, M. Maeder, C. J. Mayer, A. D. Zuberbhler, *Talanta*, **1985**, *32*, 95; b) H. Gampp, M. Maeder, C. J. Mayer, A. D. Zuberbhler, *Talanta*, **1985**, *32*, 257; c) M. Maeder, A. D. Zuberbhler, *Anal. Chem.*, **1990**, *62*, 2220

[69] a) T. Yu, S. Yang, J. Meng, Y. Zhao, H. Zhang, D. Fan, X. Han, Z. Liu, *Inorg. Chem. Commun.*, **2011**, *14*, 159; b) Q. Lin, W. K. Leong, *Organometallics*, **2003**, *22*, 3639; c) M. C. DeRosa, D. J. Hodgson, G. D. Enright, B. Dawson, C. E. B. Evans, R. J. Crutchley, *J. Am. Chem. Soc.*, **2004**, *126*, 7619

[70] L. Yang, R. McRae, M. M. Henary, R. Patel, B. Lai, S. Vogt, C. J. Fahani, *Proc. Natl. Acad. Sci. USA*, **2005**, *102*, 11179

[71] K. H. Esbensen, *Multivariate Data Analysis in Practice: an Introduction to Multivariate Data Analysis and Experimental Design*, 5th ed., Camo Software, Oslo, Norway, 2010, 597, ISBN-10: 8299333032

[72] a) F. K. Ogasawara, Y. Wang, V. L. McGuffin, *Appl. Spectrosc.*, **1995**, *49*, 1; b) D. B. Papkovsky, G. J. Mohr, O. S. Wolfbeis, *Anal. Chim. Acta*, **1997**, *337*, 201

[73] The initial two emission bands can be assigned to the prevalent formation of the 2:1 ligand-to-metal complex (band at λ = 380 nm) in the presence also of a certain amount of the 1:1 complex (band at λ = 414 nm). Upon increase of the analyte concentration, the 1:1 complex becomes the prevalent species in the membrane phase, resulting in the prevalence of the band at λ = 414 nm.

[74] WHO, *Inorganic Mercury*, Vol. 118, Distribution and Sales Service, International Programme on Chemical Safety, Geneva (Switzerland), **1991**

[75] a) U.S. Environmental Protection Agency, *Drinking Water Criteria Document for Inorganic Mercury* (Final). PB 89-19A 2207. Environmental Criteria and Assessment Office, Cincinnati, OH 1988; b) U. S. Environmental Protection Agency, National Primary Drinking Water Regulations, EPA 816-F-09-004, **2009**

[76] E. Lindner, Y. Umezawa, *Pure Appl. Chem.*, **2008**, *80*, 85

Fra notti e giorni il sole farà
le mille stagioni
E ancora il mondo percorrerà
gli spazi di sempre
per mille secoli almeno,
ma noi non ci saremo, noi non ci saremo,
noi non ci saremo.

Noi non ci saremo

Francesco Guccini

Chapter 5: Conclusions

The results obtained in this PhD thesis provided precious information about the development of new fluorescent chemosensors - both molecular and nanoparticle-based - for metal ion sensing which are important from biological and environmental point of view: heavy metal pollution has become one of the most serious environmental problems and a fast and reliable detection of ions such as Hg^{2+} is one of the most important goals in analytical chemistry; in biomedical field it is necessary to synthesize new chemosensors able to "visualize" in real time and real space the presence of relevant metal ions such as Mg^{2+}, Zn^{2+}, Cu^{+}, which are involved in vital cellular processes and whose concentration variations can be harmful.
In this context the work if this PhD thesis brought useful information to proceed on this goal. In particular we demonstrated that:

1- it is possible to create efficient chemosensors able to complex different ions (see *Chapter 3*) by changing the position of substituents of the same 8-hydroxiquinoline skeleton. The optimization of the synthesis of DCHQ compounds allowed a more flexible approach to generate a panel of substituted derivatives with improved fluorescence, uptake and selective localization. Our results show the potential of these new fluorescent compounds in providing a versatile approach to the study of total intracellular Mg distribution and homeostasis in whole cells;
2- the results obtained with the phenyl derivative DCHQ5 in the detection of total intracellular Mg^{2+} are comparable to those obtained using routine techniques, such as AAS (see *Paragraph 3.2*); we showed the possibility to use DCHQ5 to accurately quantify the intracellular total Mg with comparable performance than the reference species DCHQ1, to assess intracellular total Mg in much lower number of cells by loading a smaller amount of chemosensor in comparison with DCHQ1, the progenitor chemosensor, in cytofluorimetric assays by loading a smaller amount of it, with the advantage of displaying a more stable intracellular staining after washing than DCHQ1;
3- another compound of the DCHQ series, the one with a methoxy group in position 4 (DCHQ9) of the 8-hydroxyquinoline, is a promising candidate for intracellular Zn^{2+} sensing, presenting a very low toxicity, Zn^{2+}/Mg^{2+} selectivity and a very large fluorescence enhancement upon complexation (see *Paragraph 3.3*). Cytofluorimetric analyses of HL60-stained cells clearly indicate that DCHQ9 is able to permeate cell membranes without significantly affecting their mortality. All these aspects were confirmed by microscopy experiments performed on living cells, which also evidenced its ability to follow Zn(II) concentration variations;
4- by loading chemosensors in the PEG shell of silica nanoparticles (both doped and not doped) it is possible to completely change their complexation properties, as in the case of **L1**-**L3** (see *Paragraph 4.2.2.1*), and solubilise otherwise insoluble organic molecules in water;
5- by using membranes prepared with ligand **L3** we could fluorimetrically determine the mercury(II) content in natural water samples in concentrations that lay well below the maximal presence recommended respectively by WHO and EPA, and even under the limit of detection of the standard DMA method. Moreover, devices obtained with the same membranes and the very convenient CSPT can be also applied to efficiently measure the mercury(II) ion content in real samples presenting a linear response in a concentration range compatible with the current regulation;
6- it is possible to sensitize the emission of fluorophores/chemosensors loaded in the PEG shell of dye-doped silica nanoparticles, as shown for **1** (see *Paragraph 4.1.2*), and use this system for the assessment of intracellular Cu^{+} (in our case) in physiological conditions, with higher selectivity and sensibility;

7- the systems consisting of dye-doped silica nanoparticles loaded with fluorescent chemosensors are ratiometric and present the advantage of the double emission signal, which allows the determination of the analyte concentration without further calibration, and are characterized by higher Stokes shifts, which minimizes the effects of scattered excitation light, thus improving signal-to-noise ratio.

These results allow to say that the studied systems have very promising characteristics and represent a starting point for the creation of more efficient chemical sensors based on luminescence for biomedical and environmental applications.

Appendix

A.1 Principles of photophysics

Electromagnetic radiation and matter can interact in different ways. Photochemistry is interested in the conversion of the energy (hν) of a photon absorbed by a chemical species in electronic energy, causing the transfer of an electron toward an orbital possessing higher energy. The species turns from its electronic ground state A to an electronic excited state A*, which possesses a different electronic configuration:

$$A + h\nu \rightarrow A^*$$

This different electronic distribution causes the excited states of a chemical species to have physico-chemical properties so different from those of the ground state that they can be considered different chemical species. For this reason it is possible to define photochemistry as the chemistry of excited states.
A photon can be absorbed and provoke the formation of an electronic excited state only if its energy hν exactly corresponds to the energy difference between the excited and the ground state.
Absorption electronic transitions occur in a time scale of the order of femtoseconds (10^{-15} s), creating excited states which are transient and can deactivare in different ways, shown in the Jablonski diagram (*Figure A.1*). In this diagram electronic states (the singlets S_0, S_1 and the triplets T_1 and T_2) are represented by thicker lines. The distinction between states with different spin multiplicity is due to the fact that transitions between these states are partially not allowed. Thinner lines represent the vibrational levels of the electronic states.
After the energy absorption and reaching an excited vibrational level of an S_2 electronic excited state, the molecule goes rapidly (< 10^{-12} s) to the ground vibrational level of that excited state (*vibrational relaxation*); then *internal conversion* occurs, passing from the ground vibrational level of S_2 to the isoenergetic vibrational level of S_1, the electronic state at lower energy (< 10^{-12} s). Another vibrational relaxation is then observed toward the ground vibrational state of S_1, and at this stage the excited molecule can deactivate in two ways:

1- *Non-radiative deactivation*: the energy is released as vibrational energy generating heat. If this process occurs between two states with the same spin multiplicity we speak about *internal conversion* (10^{-12}-10^{-6} s), while if the states have different spin multiplicity we have intersystem crossing (10^{-11}-10^{-6} s). The successive vibrational relaxation leads in the first case to the ground vibrational level of S_0, in the second case to that of T_1;
2- *Radiative deactivation*: it is a processe that generates luminescence and it is defined *fluorescence* if it occurs between states with the same spin multiplicity, phosphorescence if it occurs between states with different spin multiplicity.

Similarly to S_1, T_1 can deactivate to S_0 by radiative deactivation (phosphorescence, 10^{-4}-10^{2} s) or by non-radiative deactivation (intersystem crossing, 10^{-3}-10 s, and successive vibrational relaxation to S_0). Long-lived states such as T_1 can undergo photochemical reactions, for example with oxygen, producing other chemical species. Generally speaking, since the time scale to decay to S_1 and T_1 are shorter than that necessary to pass from S_1 and T_1 to S_0, only lowest energetic states of each spin multiplicity (that is S_1 and T_1) live enough to undergo luminescence (*Kasha's rule*) or photochemical reactions.[1]

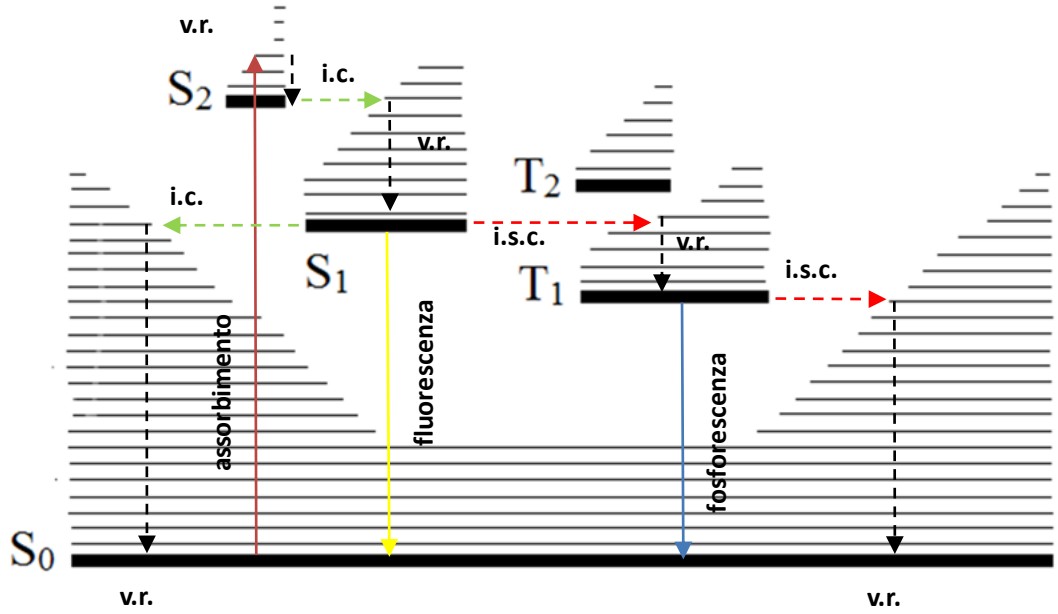

Figure A.1: Jablonski diagram for a generic organic molecule: v.r. = vibrational relaxation; i.c. = internal conversion; i.s.c. = intersystem crossing

A.2 Electronic Excitation Energy Transfer

With the term electronic excitation energy transfer we indicate the process in which an excited molecule of a donor D* decays to its ground state D with the simultaneous transfer of its excitation energy to a molecule of acceptor A, which is thus led to an excited state A*:

$$D^* + A \rightarrow D + A^*$$

it is possible to observe this phenomenon exciting D in a spectral region in which it absorbs but A does not: if energy transfer occurs, D* emission is quenched and at the same time the appearance of the emission of A* is observed, which is called sensitized emission. In the case in which D and A are different molecules of the same chemical species we speak about homo energy transfer.
It is possible to observe also intramolecular energy transfer in the case of a (super)molecule containing a donor and an acceptor, separated by a spacer B:

$$D^* - B - A \rightarrow D - B - A^*$$

Two possible mechanisms of energy transfer exist, radiative one and non-radiative one.

The *radiative mechanism* (also called trivial energy transfer) does not require the diect interaction of D and A, but it occurs via the electromagnetic field produced form the photons emitted by D, which can be absorbed by A, provided that an overlap between the emission spectrum of D and the absorption one of A exists.
This mechanism consist of two different steps:

$D^* \rightarrow D + h\nu'$ (emission of the donor)

$$A + h\nu' \rightarrow A^* \text{ (absorption of the acceptor)}$$

It is possible to correlate the probability of absorption of A of a photon emitted by D*, that is the probability of energy transfer ($a_{D^*\rightarrow A}$), with the overlap between the emission spectrum of D and the absorption one of A. In particular a relation stands between $a_{D^*\rightarrow A}$ and the overlap integral J, defined as

$$J = \int_0^\infty F_D(\lambda)\varepsilon_A(\lambda)\lambda^4 d\lambda$$

where $F_D(\lambda)$ is the normalized emission spectrum of D (the area under the spectrum is equal to 1) and $\varepsilon_A(\lambda)$ is the absorption spectrum of A in $dm^3 \cdot mol^{-1} \cdot cm^{-1}$. So as J increases, the probability of radiative energy transfer linearly increases. This probability is also directly proportional to the concentration of A, to the optical path length and inversely proportional to the luminescence quantum yield of D.
The radiative energy transfer can occur over extremely long distances: solar irradiation on Earth is a striking example.
It is necessary that the transition of absorption in the acceptor is spin-allowed so that the radiative energy transfer can occur: thus singlet(D*)-singlet(A*) and triplet(D*)-singlet(A*) transfers are allowed, while singlet(D*)-tripletto(A*) and tripletto(D*)-tripletto(A*) transfers are not allowed.

The *non-radiative mechanism*, on the other hand, requires an intermolecular interaction between D and A mediated by the electromagnetic field. The energy transfer between the partners occurs in resonance conditions, involving isoenergetic non-radiative transitions between D* and A. Also in this case the probability of energy transfer is directly proportional to J. The theoretical description of the process leads to obtain that the interaction between D* and A consists of a Coulombic term (Förster mechanism) and of an exchange term (Dexter mechanism) (*Figure A.2*).

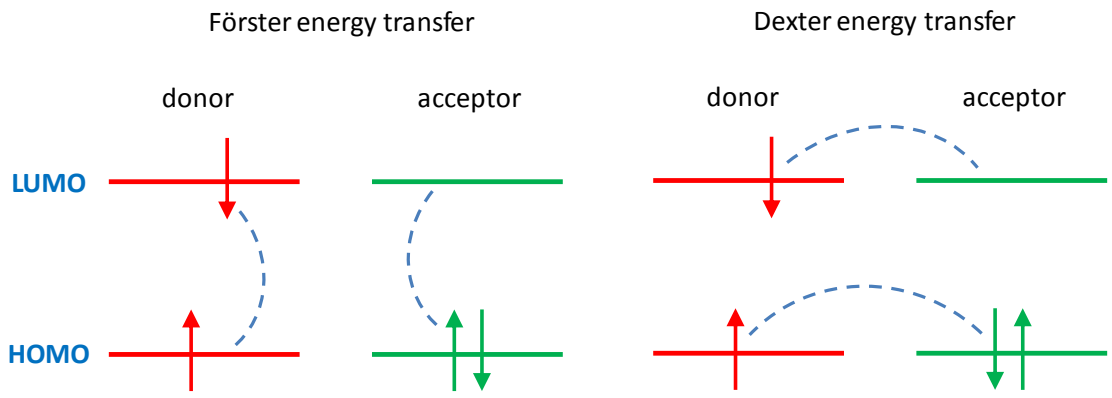

Figure A.2: energy transfer via Coulombic mechanism (left) and with exchange mechanism (right)

The Coulombic mechanism arises from the coupling of the electronic transition moments of electric dipole of the transitions $D^* \rightarrow D$ and $A \rightarrow A^*$. This interaction is governed by Förster's equation, which correlates the energy transfer kinetic constant with the distance R_{DA}:

$$k_{ET} = \frac{1}{\tau_D}\left(\frac{R_0}{R_{DA}}\right)^6$$

Where τ_D is the lifetime of the donor in the absence of the acceptor and R_0 is the *Förster distance*, that is the distance between D and A at which the energy transfer rate (k_{ET}) is equal to the decay rate of the donor in the absence of the acceptor ($k_D = \frac{1}{\tau_D}$). At this distance half of the molecules of D decay via energy transfer. Förster distance is correlated to the overlap between the emission spectrum of D and the absorption spectrum of A by means of the following relation:

$$\mathrm{R_0}^6 = 2.303\ \frac{9000 \cdot \chi^2 \cdot \Phi_\mathrm{D}}{\mathrm{n}^4 \cdot \mathrm{N_A} \cdot 128\pi^5} \int F_D(\lambda)\varepsilon_A(\lambda)\lambda^4 d\lambda$$

where χ is the orientational factor which describes the relative orientation of the electric dipole moment of D and A (it is assumed to be equal to 2/3 in the case of freely rotating D and A), Φ_D is the fluorescence quantum yield of D in the absence of A, n is the refractive index of the solvent, $\mathrm{N_A}$ is the Avogadro's constant, $F_D(\lambda)$ is the luminescence spectrum of D normalized to 1, $\varepsilon_A(\lambda)$ is tha absorption spectrum of A expressed in $dm^3 \cdot mol^{-1} \cdot cm^{-1}$. The higher the overlap between the emission spectrum of A and the absorption spectrum of A, the higher the value of $\mathrm{R_0}$. Typical values are about 20-100 Å.

It is possible to define an efficiency of energy transfer

$$\eta = \frac{k_{ET}}{k_{ET} + k_D}$$

which is linked to R_{DA} by means of the following relation

$$\eta = \frac{{R_0}^6}{{R_0}^6 + {R_{DA}}^6}$$

which highlights that the efficiency of the energy transfer process is equal to 0.5 when $R_{DA} = R_0$.
It is possible to experimentally obtain η from the fluorescence quantum yield of D in the presence of A (Φ_{DA}) and in its absence (Φ_D), or from lifetimes in the two conditions (τ_{DA},τ_D):

$$\eta = 1 - \frac{\Phi_{DA}}{\Phi_D}$$
$$\eta = 1 - \frac{\tau_{DA}}{\tau_D}$$

The processes of Förster type energy transfer are generally allowed if the transition in D and in A does not involve spin changes of the single species. On the contrary Dexter type energy transfer dominates.
The exchange interaction requires a simultaneous double electronic exchange involving the LUMO of D and the HOMO of A (*Figure A.2*) and it is a short-range interaction, becoming important when R_{DA} is ≤ 5 Å. According to Dexter model, the kinetic constant for the exchange mechanism decays exponentially with R_{DA}:

$${k_{ET}}^{ex} = \frac{2\pi}{\hbar} K J^{ex} e^{-\frac{2R_{DA}}{L}}$$

where K is a factor related to the specific orbitalic interaction, J^{ex} is the normalized overlap integral and L is an average Van der Waals radius which simulates molecular dimensions[2].

A.3 Nanoparticles synthesis and morphological characterization

Core-shell silica-PEG (polyethyleneglycole) nanoparticles were synthesized adapting previously reported procedures[3]. In a typical preparation 100 mg of Pluronic F127 and 1.9 mg of the silanized dye (0.004 mmol) were carefully solubilized with 1.5 mL of dichloromethane in a 20 mL glass scintillation vial. The solvent was evaporated from the homogeneous solution by means of a gently nitrogen flow and subsequently under vacuum at room temperature. NaCl (68.6 mg) was added to the solid residue and the mixture was solubilized at 25°C under magnetic stirring with 1565 µL of acetic acid 1 M. Tetraethyl orthosilicate (TEOS, 179 µL, 0.8 mmol) was then added to the resulting aqueous homogeneous solution followed by TMSCl (10 µL, 0.08 mmol) after 180 min.

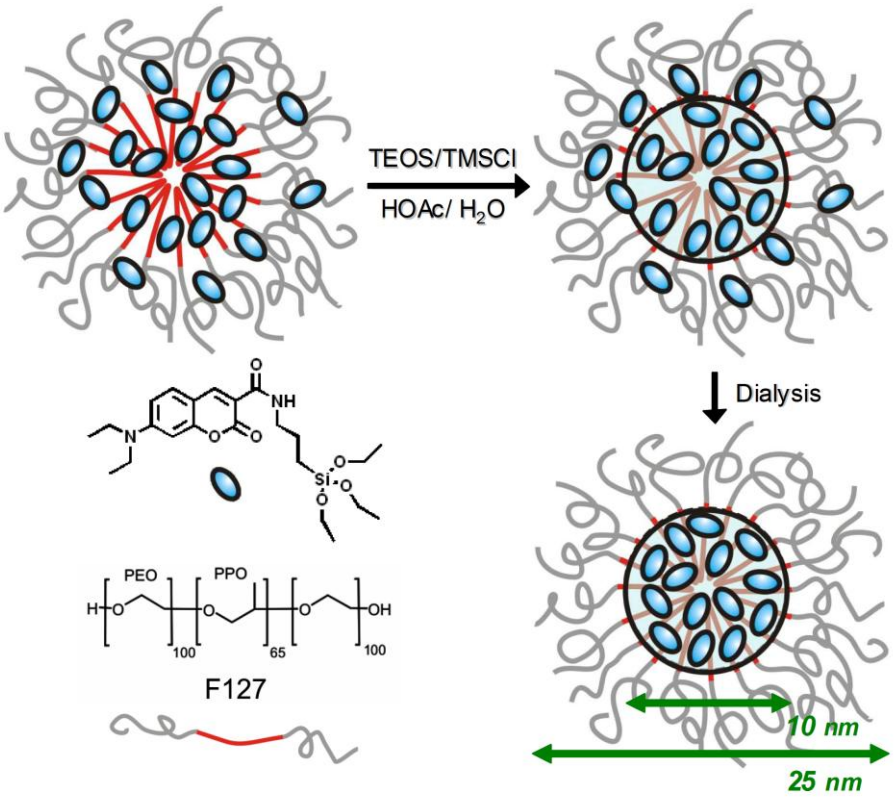

Figure A.3: synthesis of dye doped core-shell silica-PEG nanoparticles.

The mixture was kept under stirring for 48 h at 25°C before dialysis treatments. The dialysis purification steps were carried out versus water on a precise amount of nanoparticles solution (1500 µL) finally diluted to a total volume of 5 mL with water.

The determination of the nanoparticles hydrodynamic diameter distributions was carried out through Dynamic Light Scattering measurements employing a Malvern Nano ZS instrument equipped with a 633 nm laser diode. Samples were housed in disposable polystyrene cuvettes of 1 cm optical path length, using water as solvent. The width of DLS hydrodynamic diameter distribution is indicated by PdI (Polydispersion Index). In case of a mono-modal distribution (gaussian) calculated by means of cumulant analysis,

$PdI=(\sigma/Z_{avg})^2$, where σ is the width of the distribution and Z_{avg} is average diameter of the particles population respectively.

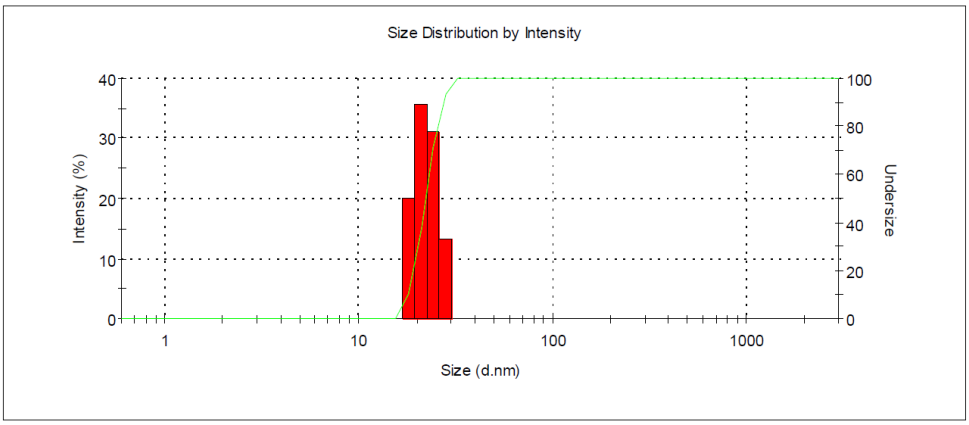

Figure A.4: typical Dynamic light scattering diameter distribution of Core-shell silica-PEG nanoparticles (d = 23 nm, PdI = 0.09).

For TEM investigastions a Philips CM 100 transmission electron microscope operating at 80 kV was used and a 3.05 mm copper grid (400 mesh) covered by a Formvar support film was dried up under vacuum after deposition of a drop of nanoparticles solution diluted with water (1:50).

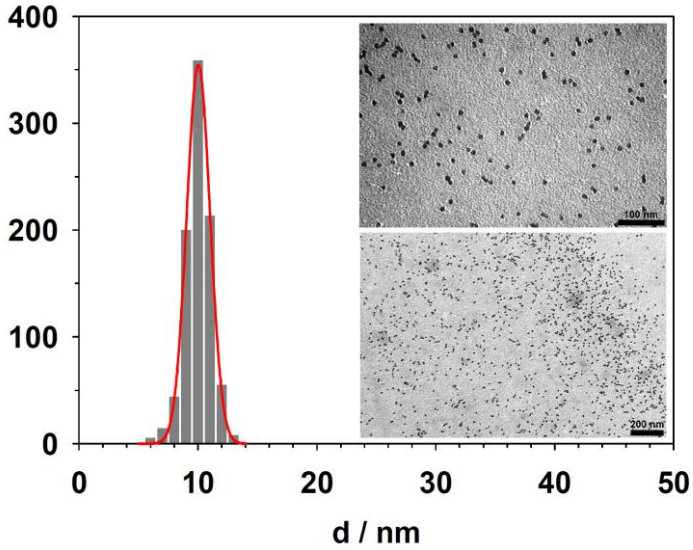

Figure A.5: TEM images of core-shell silica-PEG nanoparticles, and silica core size distribution, d = (11±3) nm, (scale bars 100 nm and 200 nm).

The NPs TEM images show that only the silica cores present sufficient contrast to appear in the images. The size distribution was obtained analyzing images with a block of several hundred nanoparticles (Figure A.5, left). The obtained histogram was fitted according to a Gaussian distribution obtaining an average diameter of (11±3) nm for the silica nanoparticles core.

References

[1] L. Moggi, A. Juris, M. T. Gandolfi, *Manuale del Fotochimico, Tecniche e metodologie*, Bononia University Press, Bologna, **2006**

[2] I. Baraldi, *La Luminescenza, Elementi di fotofisica molecolare*, Bononia University Press, Bologna, **2007**

[3] S. Zanarini, E. Rampazzo, S. Bonacchi, R. Juris, M. Marcaccio, M. Montalti, F. Paolucci, L. Prodi, *J. Am. Chem. Soc.*, **2009**, *131*, 14208

List of publications

1- G. Farruggia, S. Iotti, M. Lombardo, C. Marraccini, D. Petruzziello, L. Prodi, M. Sgarzi, C. Trombini, N. Zaccheroni, Microwave Assisted Synthesis of a Small Library of Substituted N,N'-Bis((8-hydroxy-7-quinolinyl)methyl)-1,10-diaza-18-crown-6 Ethers, *J. Org. Chem.*, **2010**, *75*, 6275 – 6278

2- S. Bonacchi, D. Genovese, R. Juris, M. Montalti, L. Prodi, E. Rampazzo, M. Sgarzi, N.Zaccheroni, Luminescent chemosensors based on silica nanoparticles, *Top. Curr. Chem.*, **2011**, *300*, 93-138

3- E. Rampazzo, S. Bonacchi, D. Genovese, R. Juris, M. Sgarzi, M. Montalti, L. Prodi, N. Zaccheroni, G. Tomaselli, S. Gentile, C. Satriano, E. Rizzarelli, A versatile strategy for signal amplification based on Core/Shell Silica Nanoparticles, *Chem. Eur. J.*, **2011**, *17*, 13429-13432

4- C. Marraccini, G. Farruggia, M. Lombardo, L. Prodi, M. Sgarzi, V. Trapani, C. Trombini, N. Zaccheroni, F.I. Wolf, S. Iotti, Diaza-18-crown-6 hydroxyquinoline derivatives as flexible tools for the assessment and imaging of total intracellular magnesium, *Chem. Sci.*, **2012**, *3*, 727-734

5- E. Rampazzo, S. Bonacchi, D. Genovese, R. Juris, M. Marcaccio, M. Montalti, F. Paolucci, M. Sgarzi, G. Valenti, N. Zaccheroni, L. Prodi, Nanoparticles in Metal Complexes-Based Electrogenerated Chemiluminescence for Highly Sensitive Applications, *Coord. Chem. Rev.*, **2012**, *256*, 1664-1681

6- M. Sgarzi, M. Lombardo, C. Trombini, N. Zaccheroni, G. Farruggia, L. Merolle, A. Sargenti, S. Iotti, C. Marraccini, L. Prodi, Expanding the targets of the diaza-18-crown-6 hydroxyquinoline derivatives family to Zn(II) ions for intracellular sensing, *Supramol. Chem.*, **2013**, *25*, 7-15

7- C. Bazzicalupi, C. Caltagirone, Z. Cao, Q. Chen, C. Di Natale, A. Garau, V. Lippolis, L. Lvova, H. Liu, I. Lundström, M. C. Mostallino, M. Nieddu, R. Paolesse, L. Prodi, M. Sgarzi, N. Zaccheroni, Multimodal use of new coumarin-based fluorescent chemosensors: towards highly selective optical sensors for Hg^{2+} probing, *Chem. Eur. J.*, **2013**, *19*, 14639–1465

8- G. I. Grasso, S. Gentile, M. L. Giuffrida, C. Satriano, C. Sgarlata, M. Sgarzi, G. Tomaselli, G. Arena, L. Prodi, Ratiometric fluorescence sensing and cellular imaging of Cu^{2+} by a new water soluble trehalose-naphthalimide based chemosensor, *RSC Adv.*, **2013**, *3*, 24288 – 24297

9- D. Braga, S. D'Agostino, E. D'Amen, F. Grepioni, D. Genovese, L. Prodi, M. Sgarzi, A quest for supramolecular gelators: silver(I) complexes with quinoline-urea derivatives, *Dalton Trans.*, **2013**, *42*, 16949-16960

10- A. Sargenti, G. Farruggia, E. Malucelli, C. Cappadone, L. Merolle, C. Marraccini, G. Andreani, L. Prodi, N. Zaccheroni, M. Sgarzi, C. Trombini, M. Lombardo, S. Iotti, A novel fluorescent chemosensor allows the assessment of intracellular total magnesium in small samples, *Analyst*, **2014**,*139*, 1201-1207